5-2021

Multiphysics Design and Sensitivity Analysis of Nuclear Heated Critical Heat Flux Pool Boiling Test Devices in TREAT.

Richard Hernandez
University of Tennessee, Knoxville, rhernan7@vols.utk.edu

To the Graduate Council:

I am submitting herewith a dissertation written by Richard Hernandez entitled "Multiphysics Design and Sensitivity Analysis of Nuclear Heated Critical Heat Flux Pool Boiling Test Devices in TREAT.." I have examined the final electronic copy of this dissertation for form and content and recommend that it be accepted in partial fulfillment of the requirements for the degree of Doctor of Philosophy, with a major in Nuclear Engineering.

Nicholas R. Brown, Major Professor

We have read this dissertation and recommend its acceptance:

Nicholas R. Brown, Guillermo I. Maldonado, Colby B. Jensen, Michael S. Greenwood

Accepted for the Council:

Dixie L. Thompson

Vice Provost and Dean of the Graduate School

(Original signatures are on file with official student records.)

Multiphysics Design and Sensitivity Analysis of Nuclear Heated Critical Heat Flux Pool Boiling Test Devices in TREAT

A Dissertation Presented for the

Doctor of Philosophy

Degree

The University of Tennessee, Knoxville

Richard Hernandez

May 2021

ACKNOWLEDGEMENTS

I would like to sincerely thank my Professor Dr. Nicholas R. Brown for his support and guidance. The work in this dissertation was accomplished with his continued technical expertise and his mentorship both in life and towards my graduate career. He provided me with all of the opportunities that have been presented to me, and has aided me in evolving into a knowledgeable nuclear engineer. He has continuously encouraged and has helped me evolve into a greater version of myself.

I also want to recognize the highly valuable support that my sponsors at the Idaho National Laboratory have provided me through years of collaboration. Specifically, Dr. Colby B. Jensen, Dr. Charles P. Folsom and Mr. Nicholas E. Woolstenhulme whom have provided me with technical help, and guidance in achieving all the work that is presented in this dissertation.

I would also like to thank Dr. J. Wesley Hines for giving me the opportunity to come to the University of Tennessee, Knoxville and accepting the expertise of our group. In addition, I would like to thank the members of my Ph.D. committee including Dr. G. Ivan Maldonado and Dr. Michael S. Greenwood. They both provided valuable feedback that greatly enhanced the value of this dissertation.

I want to also thank the several funding sources that made my graduate school journey a possibility. The work in this dissertation was fully supported through the INL Laboratory Directed Research and Development (LDRD) Program under the DOE Idaho Operations Office under Contract No. DE-AC07-05ID14517. Furthermore, additional funding was provided to me by the University of Tennessee Graduate School in the form of scholarships and awards. In addition, I would also like to thank the DOE Advanced Fuels Campaign and the DOE Fusion Energy Sciences for additional funding opportunities that allowed me to progress on this journey.

Lastly, I would like to extend a sincere thank you to my family and friends. Specifically, my mother Dalia, my father Ricardo and my brothers Landon and Daniel. They proved to be my number one fans and motivated me to continue working hard no matter the obstacles.

ABSTRACT

Following the events of the 2011 Fukushima Daiichi accident, there has been a drive to develop accident tolerant fuels (ATF) capable of enhancing safety margins provided by conventional light water reactor (LWR) materials, with a focus on the critical heat flux (CHF) behavior under fast transient heating irradiation conditions. Presented in this dissertation, is the modeling scope of a current effort aimed at elucidating the mechanisms of CHF under in-pile fast transient irradiation conditions using the Transient Reactor Test (TREAT) facility. A heater rodlet made from stainless steel type-304 with tailored natural boron content was held within experimental pool boiling capsules, to induce CHF in the surrounding coolant when submitted to a power pulse. The experimental aspect of this project is focused on studying the CHF impacts of radiation-induced surface activation (RISA), as well as rapid surface heating effects.

The initial unique contributions of the computational studies in this dissertation, depict the multiphysics design process of an experimental separate effects borated heater apparatus that was inserted into TREAT in December of 2019. Boron concentrations between 0.1-2.09 wt.% were considered. A self-shielding study determined that a borated tube could be used instead of a solid rod. Following, a thermal hydraulics study determined that the current borated tube configuration achieved a maximum CHF multiplier value of 7.8 using a 1400 MJ power pulse in TREAT.

Following, sensitivity studies analyzed the potential impacts of the CHF event on the heat transfer of more complex integral TREAT experiments under rapid heating conditions, utilizing the heat transfer time constant (HTTC) as the fundamental basis. The analysis showed the maximum fuel centerline temperature is independent of the CHF event, and the UO_2 volumetric heat capacity is the only significant HTTC parameter. For the peak outer cladding temperatures (POCTs), the occurrence of DNB was determined to be dominant on the heat transfer mechanisms

of these experimental fuel designs. For the cases where the DNB event manifested, the HTTC was resolved to have significant impacts on the predictions of the POCTs. Furthermore, when studying the time occurrence of the CHF, the variations in the gap thickness was dominant.

TABLE OF CONTENTS

LIST OF TABLES

LIST OF FIGURES

CHAPTER 1

INTRODUCTION

1.1 Reactor Safety and Postulated Accident Events

Following the events that led to the destruction of three containment buildings and three reactor core meltdowns in the Fukushima Daiichi nuclear power plant accident, there has been renewed interest to develop accident tolerant light water reactor (LWR) fuel/cladding materials. This severe accident was a result of a tsunami subsequent to a very powerful offshore earthquake that knocked off the backup power generators as a result of a station black out (SBO) event. The current drive to develop enhanced materials capable of buying time for reactor controllers in the event of such accidents, is being accomplished through the accident tolerant fuels (ATF) program [1]. Among these, iron-chromium-aluminum (FeCrAl) has emerged as a promising cladding candidate because of several advantages over conventional Zircaloy cladding, including excellent oxidation resistance at high temperatures [2,3], superior mechanical properties [2], and high resistivity to thermal and irradiation creep [4].

Design basis accidents (DBAs) and beyond design basis accidents (BDBAs) are used to evaluate the accident tolerant comparisons between ATF candidates and current Zircaloy based LWR fuel/cladding systems. Several postulated DBAs consist of power/cooling mismatching events in a reactor core. The Fukushima Daiichi accident is an example of an undercooling DBA event, during which the adequate amounts of water coolant need to maintain safe, operable temperatures that would prevent loss of integrity or melting of the core fuel components materials could not be supplied as a result of onsite power loss. In an overpowering DBA event, such as during a reactivity-initiated accident (RIA), there is a sudden increase in fission rates leading to a surge in power that causes a significant change in the heat load that could overwhelm the reactor

coolant systems, and could lead to the damage of the fuel systems in LWRs. For both of these, the efficiency of the heat removal system is limited by the critical heat flux (CHF) phenomenon. In a pressurized water reactor (PWR), it is referred to as a DNB event during which essentially the fuel rodlets experiencing it are engulfed by a layer of vapor which thermally insulates them.

In order to analytically predict both accident progression and fuel performance behavior of ATF candidates and current Zircaloy based fuel systems in the event of an RIA, modeling and experimental uncertainties of the CHF onset and duration of transition phenomena under fast transient irradiation conditions must be resolved. The work in this dissertation is focused on improving the understanding of the manifestation of the CHF phenomenon under RIA-like conditions. The computational modeling analyzes presented here, leverages the restart of the Transient Reactor Test (TREAT) facility to develop experimental heater apparatuses to study the CHF. The transient irradiation capabilities of the TREAT are needed to replicate RIA-like conditions in LWRs.

1.2 Overarching Project Discussion

1.2.1 Motivations and Goals

Highly relevant towards the scope of the work presented in this dissertation are RIAs in light water reactor systems. Since the occurrence of the Fukushima Daiichi nuclear accident, new cladding design options have been considered to enhance the safety of nuclear reactors. The challenge associated with this effort, is that these materials must be evaluated under normal operating, as well as accident conditions. These accident settings include overpowering and undercooling events, during which high temperatures can compromise the integrity of the fuel systems. In addition, current fundamental challenges in reactor safety involve understanding

cladding-to-coolant heat transfer characteristics, particularly involving predictions of the CHF phenomenon under these transient and accident scenarios.

The motivation of the Idaho National Laboratory (INL) project for which the work in this dissertation is a part of, involves a better understanding of the CHF under fast transient heating irradiation conditions because preventing or eliminating a DNB crisis during an RIA is arguably the most important safety concern when designing a PWR core or its fuel components. Fuel-to-coolant heat transfer during transient irradiation conditions remains a critical area of uncertainty in understanding reactor safety, as was demonstrated in a Nuclear Energy Agency (NEA) RIA fuel codes benchmark [5]. Eight fuel safety codes were used to model four different control rod ejection (CRE) reactivity insertion experiments. The results show that when modeling fuel temperature histories, all the codes were in relative agreement. However, when it came to the cladding temperature behavior, the results showed major discrepancies between codes simulating the same RIA, especially when nucleate boiling (NB) occurred in the coolant. The NEA carried out a subsequent uncertainty analysis in [6] of the results in [5], showing that the power pulse width, and thermophysical material and coolant properties had a strong impact on the calculations. The final recommendation of the work was centered around a better understanding of cladding-to-coolant heat transfer under fast transient conditions that can be accomplished through more separate effects experiments [5,6]. Currently, conservative limits put in place by the Nuclear Regulatory Commission (NRC) govern design and operational safety margins in PWRs.

The overarching project goals is to gain a better understanding of the most critical CHF-impacting parameters, and this will enable enhanced best-estimate fuel safety criteria. This could potentially also provide the opportunity for extending operating limits for LWRs or implementing an ATF candidate into the current LWR fleet or in future advanced reactor systems. Furthermore,

the data obtained from the efforts of this INL led project could potentially improve current CHF correlations used in present thermal-hydraulic computational tools. This could lead to better predictions of accident progression performance of accident tolerant and current LWR materials using current and future advanced modeling tools.

1.2.2 Project Tasks and Specific Contributions

The overarching approach of this INL led project leveraged the restart of the TREAT facility, covered in detail in section 2.2. This project consisted of the coupling of the advanced computational simulation tools discussed in section 1.3, to conduct parallel modeling work in support of experimental efforts conducted by the INL team at the TREAT facility. The specific project tasks, described in the flow chart shown in Figure 1, consisted of the development of initial technical requirements (task 1), experimental design and analysis (task 2), as well as experimental execution and post data analytics (task 3).

Under task 1, the INL was tasked with development of the initial functionalities of the test device that be used for CHF experimentation in TREAT. Whereas, the involvement of my work in this dissertation under task 1 was associated with developing representative models using the computational tools in section 1.3, as well as an initial informative matrix for the heater test device in TREAT. The contributions of this dissertation towards accomplishing the goals of tasks 1 are shown in Chapter 3. Following, task 2 was involved with the experimental design and analysis portion of the INL led project. The contributions of the INL towards accomplishing task 2, involved developing the vehicles that will hold the heater test device inside of the TREAT core, as well as out-of-pile transient experimental capabilities for comparison with in-pile results. Whereas, my unique contributions within this dissertation in support of task 2 can be found in Chapter 4, and was heavily involved in computer modeling associated with the development of

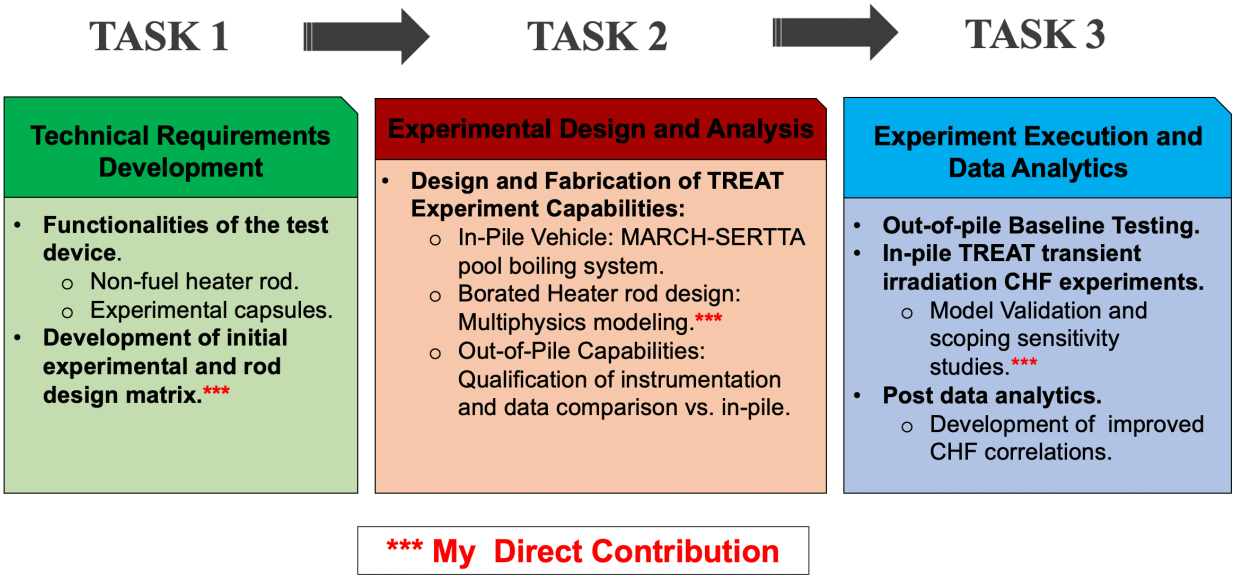

Figure 1. Flow chart describing specific tasks of the overall project associated with the work in this dissertation.

the heater device. Lastly, task 3 consisted of conducting the actual experimentation of the designed heater device within the TREAT facility. Under this task, INL was the main contributor on the experimental side. My specific contributions in this dissertation for task 3 can be found in Chapter 5, and involved validation of representative models used with experimental data originated experiments conducted at the TREAT facility in December of 2019.

Under task 1, the INL was tasked with development of the initial functionalities of the test device that be used for CHF experimentation in TREAT. Whereas, the involvement of my work in this dissertation under task 1 was associated with developing representative models using the computational tools in section 1.3, as well as an initial informative matrix for the heater test device in TREAT. The contributions of this dissertation towards accomplishing the goals of tasks 1 are shown in Chapter 3. Following, task 2 was involved with the experimental design and analysis portion of the INL led project. The contributions of the INL towards accomplishing task 2, involved developing the vehicles that will hold the heater test device inside of the TREAT core, as well as out-of-pile transient experimental capabilities for comparison with in-pile results. Whereas, my unique contributions within this dissertation in support of task 2 can be found in Chapter 4, and was heavily involved in computer modeling associated with the development of the heater device. Lastly, task 3 consisted of conducting the actual experimentation of the designed heater device within the TREAT facility. Under this task, INL was the main contributor on the experimental side. My specific contributions in this dissertation for task 3 can be found in Chapter 5, and involved validation of representative models used with experimental data originated experiments conducted at the TREAT facility in December of 2019. For the heater specimen, a separate effects sequential experimental method was used because it allows for a reduction in input variables and factors, to better isolate and understand the behavior of a single or multiple variables.

For this project, the variable behavior of interest was understanding CHF-influencing parameters and their associated uncertainties. Therefore, a separate effects heater was used to eliminate uncertainties introduced when conducting these TREAT test using integral fuel system heaters, similar to PWR rodlets, in order to decrease complexities in experimental principles as shown in Figure 2.

The separate effects in-pile novel heater device consisted of a boron-enriched stainless steel type-304 that generated heat through the ^{10}B (n, α) capture reaction with a thermal neutron cross section of ~3840 barns. Because this borated heater consisted of one material with no surrounding gap and cladding region, this device was capable of isolating the effects of the CHF-influencing parameters of interest to the study due to the reduced impact and uncertainties associated with thermomechanical behavior and thermophysical properties. Thus, the input variable of interest can be better studied. In addition to this in-pile novel heater device, out-of-pile separate effects were also conducted to further decreased the complexity in the experimentation approach.

Lastly, we will discuss the CHF-parameters that are highly relevant to the INL led project associated with the work in this dissertation and how the separate effects approach was utilized to study these. These parameters are rapid heating effects, as well as in-pile associated radiation induced surface activation (RISA), shown in Figure 3. These two are discussed in more detail in the literature portion of the dissertation found in Chapter 2. The separate effects approach shown in Figure 2, was used as follows to investigate these effects. The out-of-pile separate effects facility was used to conduct transient CHF experiments that would isolate the influence of these rapid heating effects. Furthermore, the in-pile borated heater was utilized so that the RISA activation effects can be included and when compared to the out-of-pile tests these effects could be isolated

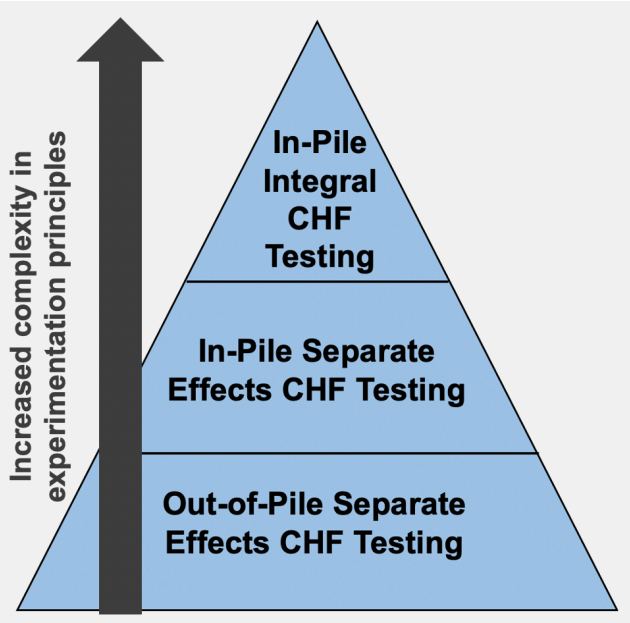

Figure 2. In-Pile TREAT CHF experimentation development tree used in the approach of the INL led project associated with the work in this dissertation.

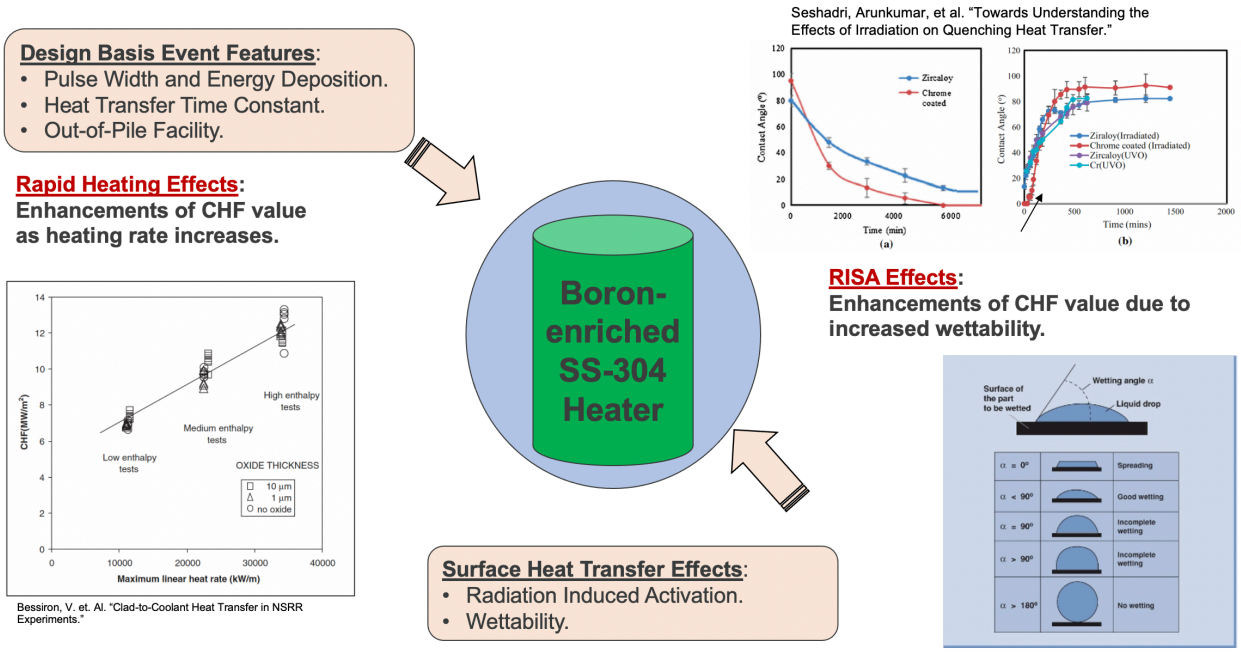

Figure 3. CHF-impacting parameters of interest to the work in this dissertation.

as well. Lastly, integral test at the top of the TREAT experimentation development tree for this project could then be developed so that the effects of thermophysical properties on the CHF phenomenon can be observed. Contributions of this dissertation towards understanding thermophysical property CHF effects can be found in the analysis conducted in Chapter 6.

1.2.3 Dissertation Hypothesis

Having discussed the overarching tasks and specific involvement of where the work in this dissertation contributed towards the overall project goals, several hypothetical questions were developed to aid in the development of the scientific method to achieve these goals. Experimentally, the hypothetical questions and reasoning behind developing the separate effects novel borated heater rodlet was to elucidate the impacts of the following parameters on the CHF:

1. What impacts does the surface activation in an irradiation environment play in predicting CHF?
2. What are the effects of rapid transient heating on CHF?
3. Fuel System Thermal Properties: How do the pellet-gap-cladding heat transfer time constants impact CHF?

These questions will be addressed by experimentally inserting the designed borated heater rodlets in TREAT and subjecting them to a power pulse, so that the CHF event is induced in the water surrounding the test device. The unique contributions provided by my work in this dissertation towards overall achieving project tasks, included the following:

1. Neutronics design analysis of heater apparatus to determine power generation response for different neutron content and the feasibility of utilizing a tube test device. (Chapter 3, section 3.2)

2. Thermal hydraulic design sensitivity study of heater apparatus to study the effects of rapid transient heating on the predicted CHF as well as boron content needed to cause CHF. (Chapter 3, section 3.3)
3. Multi-physics analysis elucidating the potential benefits of integrating axial and radial boron gradients to shape the power curve of the heater apparatus. (Chapter 4)
4. Validation of developed multiphysics modeling capabilities and advanced computational tools with experimental data from December 2019 TREAT experiments. (Chapter 5).
5. Development of best fit model with experimental results from December 2019 experiments. (Chapter 5, section 4.b)
6. Sensitivity studies of the thermal time constant of PWR fuel system experimental rodlets on the maximum fuel and outer cladding temperatures of under DNB and non-DNB conditions. (Chapter 6, sections 6.2.1)
7. Sensitivity study elucidating the thermomechanical effects of changing thickness of the gap region the during transient TREAT testing on the maximum fuel and outer cladding temperatures. (Chapter 6, section 6.2.3)
8. Sensitivity studies of the impacts of the thermal time constant of PWR fuel system experimental rodlets on the time of CHF. (Chapter 6, section 6.2.4)

The following hypothesis are theorized based on my unique contributions towards overall project tasks listed above and presented in this dissertation:

1. The strong self-shielding effects of the borated material of the test device will allow the utilization of a tube design, instead of a solid heater rodlet, with beneficial instrumentational capabilities at its center region.

2. The heating capabilities of the borated material coupled with the transient pulse capabilities in TREAT will provide a large margin that could potentially overcome the transient heating effects on the CHF manifestation.
3. The thermophysical properties of the experimental PWR fuel rodlet systems will be a significant contributing factor for the maximum outer cladding temperature under DNB conditions.
4. Due to numerous sources of uncertainties, large discrepancies between experimental data and modeling prediction will exist when validating the developed multiphysics capabilities.
5. The decreasing gap thickness that could be experienced during the application of a transient power pulse in TREAT, will result in an increased important in the fuel material properties of the TREAT experimental PWR fuel systems.
6. The time of CHF will be significantly impacted by the thermal time constant of the PWR fuel systems, as well as the thermomechanical effects of the changing gap region.

1.3 Computational Simulation Tools

Several modeling tools were used in the multi-physics work presented in this dissertation. The neutronics design aspect utilized a full core TREAT model that was developed using the Serpent Monte Carlo reactor physics code developed at the VTT Technical Research Centre of Finland [7]. Serpent is a probabilistic three-dimensional neutron transport code, with capabilities that include steady state reactor physics calculations, as well as burnup and reactivity coefficients analysis. The development of the second version of the Serpent code which is used in this dissertation started in 2010 and continues on today. The thermal hydraulics analysis in this dissertation was conducted using the deterministic finite differencing capabilities of the Reactor Excursion and Leak Analysis Program (RELAP5-3D), developed at the INL, which is a proven

computational tool with the multidimensional ability to model a wide variety of reactor components and transient situations [8]. The RELAP code was initially developed as a tool capable of modeling typical LWR accidents, to its current multidimensional capabilities that allow it to model a full range of reactor components and transient situations. Thus, it is highly applicable to the analyzes in this dissertation. Sensitivity studies were conducted through the coupling of the RELAP5-3D program with the Risk Analysis Virtual Environment (RAVEN) code [9] developed at INL, and the Design Analysis Kit for Optimization and Terascale Applications (DAKOTA) framework developed at the Sandia National Laboratory [10]. Examples of the coupling capabilities of these codes is found in the literature and are highlighted in this dissertation in sections 3.3 and 6.1.1.

CHAPTER 2

LITERATURE REVIEW

The chapter presents a literature review of topics that are relevant to the subsequent work in this dissertation. The purpose is to highlight important terminology that must be understood, as well as situating where the work presented in the follow-up chapters is situated with current knowledge. The unique contributions of the work presented in this dissertation to the overall scope of the project included developing the technical computational requirements, including models in support of experimental design efforts, as well as post experimental data analytics. Therefore, the contents of this literature review involves a throughout understanding of the critical knowledge needed to perform these contributions in support of this INL led project. Initially, this chapter covers the highly relevant topics of reactivity-initiated accidents (RIAs) and its relationship to consequently manifesting the departure from nucleate boiling (DNB) event. A historical background and the current capabilities of the Transient Reactor Test (TREAT) facility is included, as well as a comprehensive literature survey of experimentation of relevant pool and flow boiling CHF impacting parameters is also included. Further, the heat transfer time constant (HTTC) definition as well as its exploration including thermophysical material and coolant properties on the manifestation of CHF are covered.

2.1 Reactivity Initiated Accidents and the Departure from Nucleate Boiling Event

Nuclear reactors are designed with many inherent safety features to prevent the occurrence of accidents throughout their operational lifetime. RIAs are one type of postulated event governing the design of nuclear reactors. An RIA occurs when there is an abrupt and unexpected insertion of reactivity, due to a large increase in neutron fission rates, that results in an unwanted surge in reactor power during which fuel and core structural components can experience rapid temperature

increases. The RIA event is characterized by a nearly adiabatic instantaneous initial phase at time scales too short for heat transfer out of the fuel to occur, followed by a long-term high temperature phase during which the cladding component is highly affected by thermal behavior [11]. In PWRs, the most limiting RIA occurs during the accidental ejection of a control rod cluster [12,13]. Although this surge in reactor power is promptly mitigated by inherent negative feedback mechanism due to the Doppler broadening of uranium-238 capture cross sections [14], the core components experience large thermal effects that could result in structural and mechanical failure. The negative consequences of such an event on nuclear fuel and cladding integrity have been experimentally shown, using transient facilities around the world, to increase with an increment in the length of time that these materials have been exposed to an irradiation environment [15,16,17,18,19,20]. Therefore, the NRC has set safety limitations for fuel and cladding components for different stages of PWR fuel cycles. This includes fuel failure criteria of 170g/cal for fuel rods at hot zero power conditions with internal pressures lower than the system pressure of the reactor, and a peak radial fuel enthalpy limitation of 230 g/cal to meet coolability criteria [21].

One type of thermal failure behavior results from the pellet-to-cladding mechanical interactions (PCMI). During an RIA event, the fuel region will expand faster than the cladding components of the fuel/cladding system due to the ceramic properties of typical uranium dioxide (UO_2) and fission gas expansion. This type of failure usually occurs during the low temperature brittle cladding phase during which cracking can compromise this material, and may result in the limited release of fission gas into the primary coolant loop of a PWR [12,13,22]. High temperature fuel system failures can occur in the second phase of the RIA during which the overheated cladding temperatures can lead to the degradation of the coolability capabilities of the reactor design.

Consequences of this type of failures include cladding ballooning and bursting, cladding melting, and high oxidation rates which could result in the release of large amounts of hydrogen gas into the containment building which could result in an explosion exposing the core and dangerous highly-radioactive fission products to the environment [12,13]. Thus, understanding the cladding-to-coolant heat transfer characteristics under fast transient irradiation conditions is an important aspect of PWR operational safety.

The coolability capabilities of PWR primary loop systems is limited by the CHF phenomenon. The CHF is indicative of when the onset of DNB event occurs in a PWR system, also referred to as a boiling crisis. Under normal PWR operating conditions, nucleation of vapor bubbles in the subcooled water coolant occurs at the superheated cladding surface. This causes fluid mixing due to bubble formation and detachment, which enhances the heat transfer ability of the water coolant in contact with the cladding surface. Thus, a high heat transfer coefficient is achieved resulting in the cooling of the fuel and cladding materials. As with any heated solid surface in contact with a fluid, there is a maximum heat flux (MHF), the CHF, value at which the heat transfer begins to deteriorate and the onset of DNB is manifested. The DNB event is characterized by the sudden drop in the heat transfer coefficient at the cladding-to-coolant boundary, causing a rapid increase in cladding temperature. DNB occurs when the density of bubbles is considerable enough that a vapor film develops around the cladding surface, preventing direct contact with the subcooled water coolant [23]. Post-CHF behavior is characterized by a low heat flux film boiling phase during which elevated temperatures and embrittlement of the cladding can occur [13,22]. As the fuel pellets expand with increasing temperature, cladding embrittlement can lead to cladding failure and the subsequent release of highly radioactive fission products into the coolant as described above during the high cladding temperature phase.

The CHF phenomenon has been studied extensively in the literature under transient irradiation conditions, and several correlations have been developed to attempt to accurately predict its manifestation. Rosenthal [24] experimentally studied the effects of transient power ramps using vertically oriented ribbon-shaped heaters under pool boiling conditions. The study revealed the dominance of transient conduction on the predictions of heat transfer before the onset of NB, and motivated others to be aware of the importance of understanding the evolution of heat transfer during transient heating. Serizawa [25] analytically correlated the CHF in transient pool boiling systems, by building upon the visual and photographic observations of the vapor-liquid configuration near the maximum heat flux. He assumed that CHF occurs because of the consumption of a thin liquid layer that formed into a vapor blanket, between the heated surface and the supply of liquid during transient heating. Pasamehmetoglu [26] suggested a theoretical predictive model for transient CHF by accounting for the rate-of-change of the liquid layer thickness underneath the bubbly boundary layer on the heater surface. Chang [27] proposed a transient CHF map that considered upstream and local effects to classify the transient CHF mechanisms into four regions. He derived the transient CHF correction factors for each regime using a local-micro-layer-depletion factor and an upstream-effect factor. Kossolapov [28] experimentally investigated the transient flow boiling CHF under transient heating conditions. He reported contrasting transient CHF trends at different power escalation periods but couldn't provide a robust explanation about these results.

The 2006 Groeneveld look up table (LUT) is another method used to predict the CHF value [29]. LUTs are a large database that calculates the value of CHF based on local or inlet hydrodynamic parameter conditions, while applying a numerical factor that takes into account the diameter effect of water-cooled heated tubes. As described in the literature, the 2006 Groeneveld

CHF LUT [29] uses more than 30,000 data points to predict CHF values based on local flow conditions (e.g. X_{local}, P_{local}, G_{local}). Additionally, it can also use a constant inlet conditions method (e.g. G_{inlet}, $q''_{constant}$, T_{inlet}) to predict the quality from which the CHF is then predicted. This initially determined CHF value applies to an 8-mm diameter cylindrical geometry. The Groeneveld LUTs then apply a diameter factor, defined by $F = (\frac{D_e}{8})^{-0.5}$, where D_e is the diameter of the rod. The 2006 Groeneveld LUT is an improved version of the 1995 Groeneveld LUT [29,30]. Among these, the 2006 LUT more accurately predicts CHF under subcooling water conditions, and contains 20% more pressure and mass flux data points effectively extending the range of systematic conditions, to which this CHF databank can be applied [29]. The 2006 LUT covers pressure ranges between 0.1-21 MPa, mass flux values between 0-8000 Kg/m^2s and subcooling values of up to 50K. For the thermal-hydraulics modeling work presented in this dissertation, the 2006 CHF LUT is an important tool that was used to predict the value of CHF.

2.2 The Transient Reactor Test Facility

The experimental aspect of this project will take advantage of the transient capabilities of the TREAT facility. Therefore, this chapter includes a review into the historical aspect and characteristics of this test reactor. The TREAT is an air-cooled, graphite-moderated reactor, cross sectional view shown in Figure 4, located at the INL. Constructed in 1959, it was developed for transient experimental simulation testing of nuclear fuel rod samples under transient conditions. TREAT was operated for 35 years until April of 1994, during which it conducted 2884 transient irradiation tests over 6604 reactor startups and 720MWh of energy produced [31]. The transient testing experiments using this facility have made historical contributions to reactor fuel safety. It proved key in helping determine the NRC fuel enthalpy safety limitations of nuclear rods in LWRs,

as well as the capabilities of these rods to potentially reduce or eliminate the probability of accident occurrences [32].

The TREAT is one of four transient facilities available in the world today, along with the Nuclear Safety Research Reactor (NSRR), and is also one of the most practical due to its simple air-cooled design not requiring any coolant pumps to maintain operational safety [31]. The power pulse capabilities of the TREAT facility are achieved using the highly enriched uranium (HEU) dispersed in graphite blocks with an atomic ratio of 1 235U atom per 10000 12C [33]. The uranium fuel is contained within blocks encased in Zircaloy-3 to retain the fission products from being released into the environment [33]. The TREAT capabilities were also demonstrated during a transient experiment in which the reactor power rose exponentially from 0 to about 13,000 MW in just under 0.2 seconds [33]. The Fukushima Daiichi nuclear power plant accident in 2011 highlighted the need for continued transient testing in TREAT. In 2014, 21 years after being on standby, in-core fuel and control rod drive movements were allowed in support of a planned restart of the TREAT facility and reactor experiments [34]. By 2018 it was operational again with the experimental rodlet developed in this work being one of the first into the reactor. Due to the large graphite heat reservoir of the TREAT facility, it is capable of producing high energy power pulses with no consequential resulting core damage.

The cartridge core accommodates a 19x19 square pitch assembly, with an active core that is 1.2m in height and 361 fuel assembly locations, with capabilities to insert experiments at the center of the facility [33,35]. A thick radial graphite reflector and a concrete biological shield surround the assemblies of this facility. Although not capable of producing transient power pulse widths similar to those in light-water moderated reactors, due to the larger neutron generation time of graphite moderators, it is capable of replicating fuel rod energy depositions similar to those

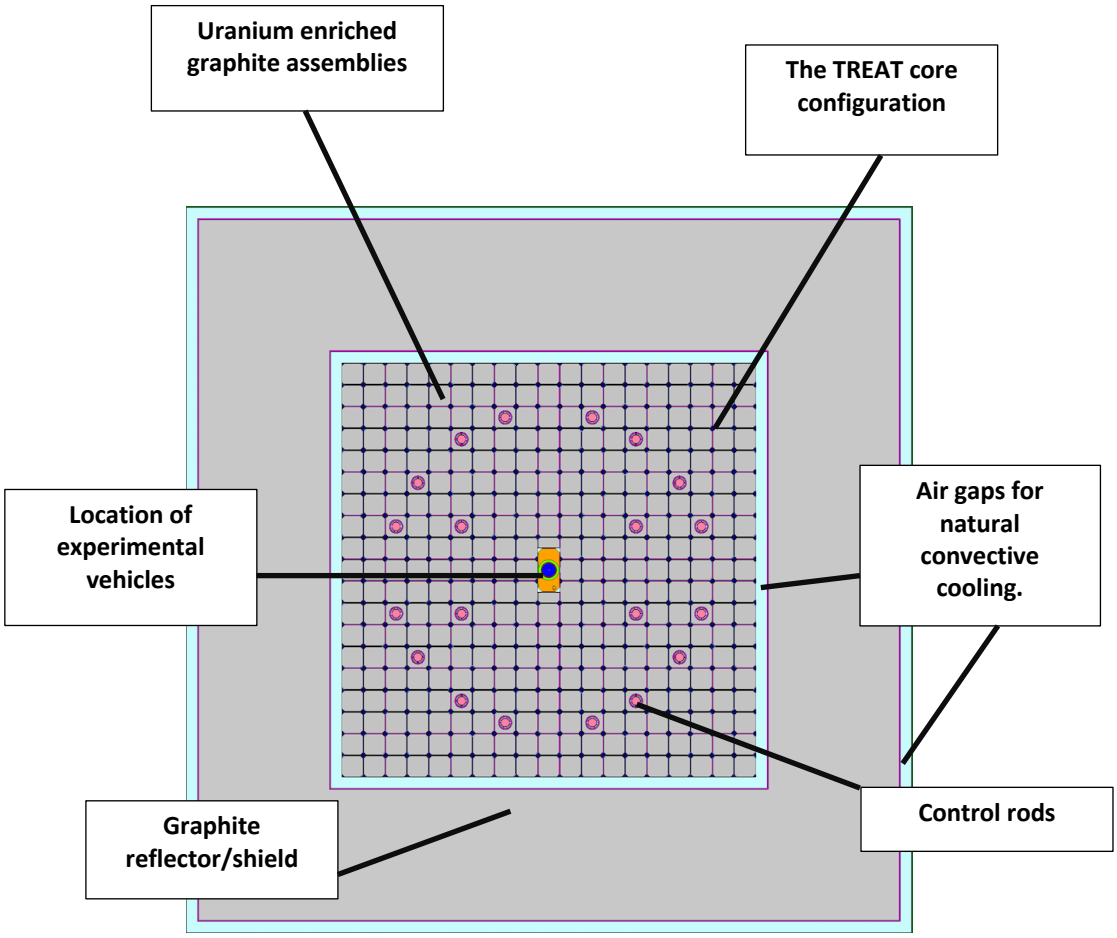

Figure 4. Top view of the TREAT core.

found in LWRs. Efforts are in progress to narrow the TREAT pulse width to be more representative of those in LWRs [36].

At the center of the TREAT core, modern experimental vehicles currently under development at INL can be inserted and subjected to in-pile transient irradiation testing [33,37]. Relevant to this work is the minimal activation retrievable capsule holder (MARCH) which is utilized to insert experimental capsules into the TREAT core [38]. The advantage of the MARCH system is its low-activation and low radioactivity build up capabilities during TREAT transient testing. It consists of several components including the BUSTER pipe like containment region, a heater module, and a capsule holder. Two configurations of the MARCH system of interest to this work utilize the Separate Effects Test Holder (SETH) [38] and the Static Environment Rodlet Transient Test Apparatus (Multi-SERTTA) [39] experimental capsules. The latter will be discussed here because this capsule was used in the first experiments carried out using the designed heater rodlet in this work.

The Multi-SERTTA capsule is made up of titanium super alloy material to allow for more experimentation space at its center. Extensive work has been done to show how other advantages of utilizing a thin super alloy structure include an increased energy response generation in fuel rodlet experiments and larger applied transient power pulses in TREAT, both of which would be beneficial for this work to ensure the manifestation of the CHF event [39]. When testing fuels, this will be especially important for previously irradiated fuel materials. It is capable of holding a variety of nuclear fuel rodlet experiments under inert gas, and water coolant conditions representative of those found in typical commercial PWRs [39]. A heater within the Multi-SERTTA capsule can be used to initialize the water coolant to various degrees of subcooling, and pressures under pool boiling conditions. In the occurrence of fuel melting during testing, a melt

catcher is included in the design to protect the capsule structural materials. Further, instrumentation such as thermocouples and pyrometers can be inserted near the top of the Multi-SERTTA for accurate data gathering during experimentation. Attached to the Multi-SERTTA is an Argon/Helium expansion tank that prevents bursting of the capsule due to over pressurization during an irradiation transient test in TREAT. The experimental approach will utilize the MARCH irradiation vehicle [109] to insert the Multi-SERTTA capsule [110] that will be holding the designed sample rodlets for in-pile pool boiling CHF testing. These capabilities will prove vital in creating experimental prototypic PWR pressure and temperature conditions for the subsequent CHF experiments. The TREAT Water-Environment Recirculating Loop (TWERL) concept is another relevant TREAT facility experimental capability that is of interest to the work presented here, shown in Figure 6. This self-contained flow boiling loop system is currently in the pre-design phase at the INL, with the objective of replicating coolant hydraulic conditions within PWR fuel channels [40] during RIAs and LOCAs. The TWERL components are expected to include a test section region, where the fuel experiments will be held, along with a heat exchanger, pressurizers, downcomers and coolant pumps. The test section is expected be capable of holding anywhere between single rodlets, up to 3x3 rod bundles to study fuel interactions during accident events, with mass flow rates that are representative of those found in typical PWRs [40].

2.3 Review of Pool Boiling CHF and Impacting Parameters

Here we review parameters deemed significant to influencing the CHF phenomenon and the empirical correlations used to predict its occurrence under pool boiling conditions. The means through which CHF occurs on a heated surface has been described through several different methods, but the main focus of this section of the literature review will be centered around the pioneering work done by Zuber [41,42] using the hydrodynamic instability approach. Zuber's

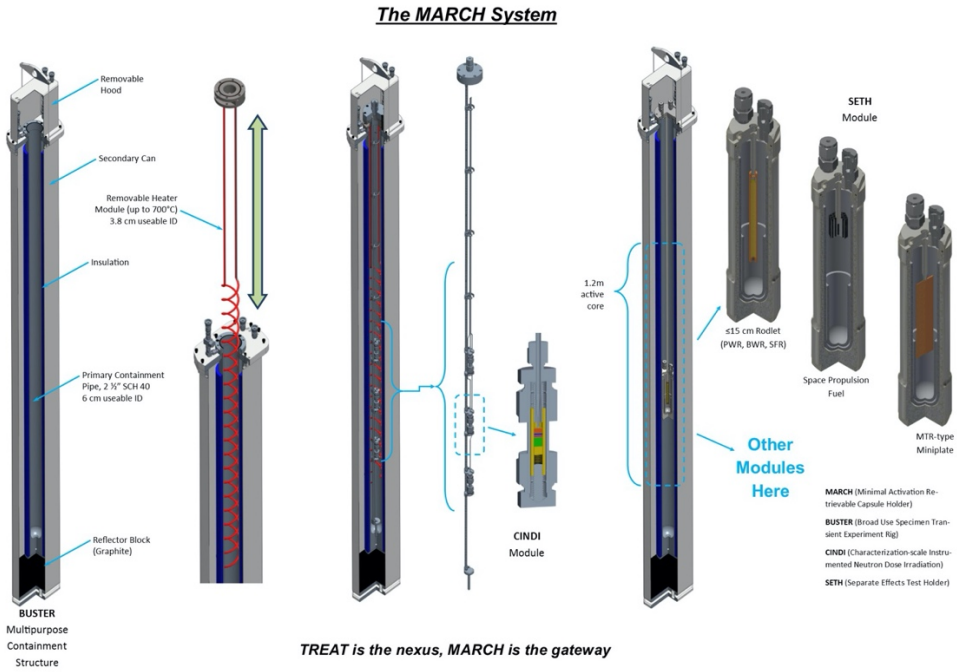

Figure 5. Overview of the MARCH system components taken from [38].

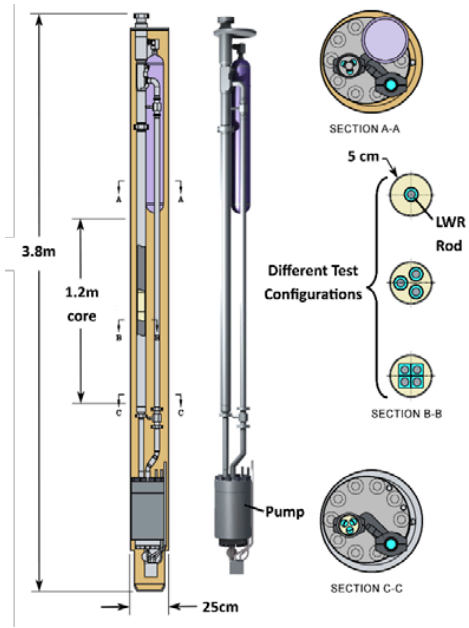

Figure 6. Overview of the TWERL loop system taken from [40].

correlation approach was built on the foundation of an early correlation developed by Kutateladze [43,44] in which dimensional analysis was applied to a model relating the pool boiling CHF in saturated water occurring due to the hydrodynamic effects of surface tension, vapor velocity, and the buoyant force as shown in equation 1

$$q_c^{"} = K\rho_v L_{lv}[\sigma g(\rho_l - \rho_v)\rho_v{}^2]^{0.25} \quad \text{Eq. 1}$$

where K is a constant, L_{lv} is the latent heat of vaporization, g is the gravity constant, and ρ_v and ρ_l are the vapor and liquid densities respectively. As described by Zuber [41], nucleation of bubbles occur at the heated surface when the latter exceeds the saturation temperature of the coolant liquid. Zuber [41,42] experimentally determined that bubble production was directly tied to the superheated degree of the heat transfer surface, and that the agitation motion of the nucleating bubbles detaching causes a reduction in the thermal resistance of the coolant at the thermal boundary due to fluid mixing. Zuber [41,42] also characterized a maximum NB heat transfer limit in which the efficiency begins to deteriorate because of the associated impacts of the Taylor and Helmholtz hydrodynamic instabilities that essentially impedes the coolant from reaching the heated surface. Zuber empirically determined the value of the constant K.

Another notable approach was that of Rohsenow [45], who employed the bubble interference method to describe the CHF phenomenon. Rohsenow described pool boiling through bubbles at the heated surface in contact with each other right before the CHF. Once the CHF is reached the bubbles begin to coalesce into large vapor bubbles that engulf the heated surface. Other mechanisms used to describe how CHF manifests are covered by Liang [46] including microlayer dry out and the interfacial liftoff approach.

Numerous modifications of Zuber's correlation have been developed throughout decades of research to account for the different effects of impacting parameters on pool boiling CHF, such as coolant subcooling and pressure as well as surface characteristics and rapid heating rates. Although many pool boiling CHF papers have been published, we focus on several important ones accounting for the effects of the above parameters on predicting the value of CHF. The identified parameters deemed important for the work in this dissertation and previous experimental work in the literature is discussed here.

2.3.1 Coolant Degree of Subcooling Effects

A quasi-linear relationship between the degree of subcooling and the value of pool boiling CHF has been described in the literature, with the latter generally increasing as subcooling is increased under different systematic conditions [41,44,47-52]. Kutateladze [44] observed this linear relationship in his early work on CHF for a horizontal plate submerged in water, iso-octane, and alcohol. Zuber [41,47] included a heat transfer convective factor in equation 1, resulting from the effects of the subcooled liquid, and developed a correlation that relates the CHF value at saturation with the CHF value at a particular degree of subcooling. Using experimental data of pool boiling in water and alcohol at pressures of 1 and 2 atm, the CHF was determined to linearly increase with subcooling regardless of the geometry of the heated surface, and it was shown that this correlation was fairly accurate.

Ponter [48] further studied the effects of subcooling, with values up to 60° C, on pool boiling CHF under pressures lower than 1 atm. His results concluded that regardless of the different bubble mechanisms at these pressure values, CHF was observed to increase with subcooling and the behavior can be accurately described by a linear relationship. Inoue [49] noticed that the influence of low subcooling on CHF increases with pressure. The work by Elkassabgi and

Lienhard [50] described three subcooling regions for saturated liquids. Region I at degrees of subcooling up to about 40K could be described by the linear relationship in equation 2, where $q''_{c,sub}$ and $q''_{c,sat}$ are the CHF values for the subcooling and saturation conditions respectively, ΔT_{sub} is the degree of subcooling and ΔT_{sat} is the wall superheat at CHF. In region III, found at high values of subcooling, CHF was less significantly impacted by this parameter. This conclusion was supported by Sakurai [51] who noticed similar trends in his results for degrees of subcooling up to 180K.

$$q''_{c,sub} = q''_{c,sat}(1 + \frac{\Delta T_{sub}}{\Delta T_{sat}})_{sub} \quad \text{Eq. 2}$$

More recent efforts by Jun [52] observed that for the same material and using two different methods of treating the surface, the value of CHF was observed to increase by about 60 kW/m^2 per degree of subcooling increment for both cases at atmospheric pressure. The main takeaway is that regardless of pressure or surface conditions, the pool boiling value of CHF is enhanced as the coolant subcooling is increased, and the parametric trend is a linear relationship.

2.3.2 Coolant Pressure Effects

The effects of pressure on the value of CHF were immediately recognized in Kutateladze's [43] and Zuber's [41,42] hydrodynamic correlations [see equation 1]. Zuber concluded with his pool boiling correlation that the CHF value will initially increase with pressure increments for saturated water at low values less than 2 MPa until a transitional range is reached where CHF becomes insensitive to pressure between values of about 2 and 7.85 MPa. At pressures higher than ~7.85 MPa the value of CHF then decreases [41]. Ponter [48] supported parts of the above conclusion when it was determined that his experimental CHF values increased as pressure was

raised between the low value ranges of 13.3 to 101.3 kPa. However, it was also noted that as pressure was decreased from atmospheric, Zuber's correlation, based on a boiling mechanisms approach, overpredicted the CHF values because bubble formation is dominant. Katto [53] agreed with Ponter that as the pressure is decreased to values lower than atmospheric, the vapor generated tends to remain around the heated surface due to a lack of significant boiling inertia and higher latent heat of vaporization causing a decrease in the CHF.

Sakurai [51] conducted pool boiling experiments on saturated and subcooled water with pressures varying between 101.3 and 2063 kPa. It was discovered that for subcooling values greater than 60K the CHF value decreased as pressure was increased up to values of 200 kPa and was insensitive to pressures higher than 500 kPa. However, for water subcooling values up to 40K, the CHF increased with a rise in pressure. Sakurai concluded that the hydrodynamic instability model is not an accurate method to predict CHF values at high pressures.

Pressure impacts on pool boiling CHF have also been known to vary depending on the type of coolant fluid used, surface characteristics, and the heating rate of the surface. Kirichenko [54] and Sakashita [55] noted that the Zuber correlation underestimates CHF because it doesn't take into account changes in the wettability of water resulting from pressure effects. The effect of pressure on the contact angle of water is specifically relevant to LWR systems, and it is taken into account in the correlation described in section 2.3.3 below. Stelute [56] suggested that the pressure effects could enhance the impacts of surface characteristics on CHF for certain materials.

Kunito [57], Dahariya [58] and Derewnicki [59] all experimentally demonstrated that the effects of pressure on CHF are also dependent on the heating rate of the transfer surface. Kunito [57] conducted an analysis using R113 refrigerant fluid and noticed that for pressures up to 1.5 MPa the transient heating CHF value was lower than the steady state heating case. At high

pressures, the opposite was true and both CHF values decreased with increasing pressure. Dahariya [58] conducted similar experiments using a copper wire submerged in a saturated pool of water at 101.3 kPa. The wire was heated at HF values of 100 W/m^2 and 25 W/m^2. The analysis showed a CHF enhancement of up to 175% when the pressure was increased by 413.7 kPa relative to atmospheric pressure in the faster heating case and no CHF improvement for the 25 W/m^2 heating case. Dahariya attribute this enhancement to the decrease in bubble size and increase in bubble detachment as a result of the rising pressure coupled with rapid heating effects that will be discussed later in section 2.3.7. However, there is a limit to this pressure enhancement effect during rapid heating as was described by Derewnicki [59].

The main takeaways are that the effects of pressure on CHF are dependent on the fluid properties, surface characteristics, and the heating rate of the heated surface. For pressures close to atmospheric, the Zuber hydrodynamic instability approach is accurate in predicting the value of pool boiling CHF, but in the case of low- and high-pressure conditions, the literature has shown that the accuracy of this approach deteriorates due to the complex nature of pressure effects. Further, modified Zuber correlations such as the Kirichenko [54] iteration more precisely predict the value of pool boiling CHF under different pressure conditions.

2.3.3 Contact Angle Effects

The initial hydrodynamic correlation derived by Zuber [41,42] did not include the impacts of surface characteristics on the value of pool boiling CHF. Stock [60] agreed with Zuber through observations made while experimenting on SS tube sections with different surface features, because it was determined that although changing surface features caused a change in the wall superheat at CHF, its value remained unchanged. Therefore, his analysis concluded that CHF

appeared to be solely a hydrodynamic phenomenon [60]. The effects of changes in the contact angle are considered in this section of this chapter.

Several studies have reported that a decrease in the contact angle shows a strong incremental response on the value of CHF due to an increased wettability of the surface [54, 61-65]. Chowdhury [61] determined through separate surface effects tests under pool boiling conditions that the contact angle had the most influential impact on the value of the CHF. Maracy [62] agreed with Chowdhury and noted that a decreasing contact angle causes a strong upward shift and delay of the CHF point essentially prolonging the NB phase of a heated surface. Maracy also observed that the CHF becomes less sensitive to the effects of contact angles at high values of the latter. Nevertheless, it is also important to include that some studies indicate exactly the opposite. For example, O'Hanley [63] concluded in his study of non-porous and porous smooth surfaces that, despite varying the contact angle from 0-100°, the value of CHF was not impacted by this parameter.

Several empirical correlations have been developed and show a typical decrease in CHF as the contact angle is increased. Kirichenko [54], Liaw [64] and Kandlikar [65] all developed correlations that incorporated the effects of contact angle and were based on the hydrodynamic instability model developed by Kutateladze [43] and Zuber [41,42]. Kirichenko [54] determined his correlation to be very accurate for contact angle values between 20° and 60° for saturated water, but overpredicted the CHF outside of this range. Liaw [64] used equilibrium contact angles to derive his correlation for CHF from experimental data. However, by far the best-known CHF correlation that incorporates the effects of contact angle is that of Kandlikar [65], which is given by equation 3 for saturated water

$$q_c^{"} = L_{lv}\,\rho_v^{0.5}\left(\frac{1+cos\,\beta}{16}\right)\left[\frac{2}{\pi}+\frac{\pi}{4}(1+cos\,\beta)\,cos\,\phi\right]^{0.5}[\sigma g(\rho_l-\rho_v)]^{0.25}$$ Eq. 3

where L_{lv} is the latent heat of vaporization and ϕ is the heated surface orientation with respect to horizontal. Kandlikar developed his correlation using the dynamic receding contact angle, β, of water and noted that for increasing β up to a value of 60° the CHF value minimally decreases. Further, for increasing β values higher than 60° the CHF significantly decreases. Sakashita [55] experimentally compared the Kandlikar and Kirichenko correlations and concluded that, although Kandlikar represents the trend qualitatively, the Kirichenko correlation most accurately predicted the CHF for contact angles between 20° and 60°. Lastly, Zuber [41,42] and Kutateladze [43] correlations overpredict CHF because they omit the effects of contact angle [54,55,64,65]. The main conclusion is that a decrease in the contact angle increases the wettability of the heated surface and therefore enhances the value of the CHF.

2.3.4 Surface Roughness and Porosity Effects

Roughness and porosity are two other surface parameters with some impacts on pool boiling CHF. How roughness impacts the value of CHF is dependent on whether it coincides with the generation of new active bubble cavitation sites on the heated surface [61,66,67]. Therefore, if the roughening is done using an adequate method, enhancements to the CHF value can be achieved. Chowdhury [61] used copper and aluminum cylinders submerged in water and methanol, and showed that by increasing the roughness of the surface, the CHF steadily improved. However, when he anodized the roughened surface of the aluminum tube, the CHF value was independent of the roughness [61]. Ferjancic [68] roughened the surfaces of SS304 and steel 1010 ribbon heaters using both a sanding and etching method and noted that the value of CHF increased relative to roughness for the two techniques. The analysis showed a 51% increase in the etched surface

relative to the sanded method. Stelute [56] studied brass, steel, and copper surfaces, and agreed with Ferjancic's conclusion. However, other studies conducted by O'Hanley [63] and Lienhard [69] argued that CHF is not very sensitivity to surface roughness.

CHF improvements due to an increase in roughness appear to also be confined to a range of values depending on the surface material [56,67,68]. Pioro [67] indicated a maximum roughness limit after which the CHF will decrease. Stelute [56] studied brass, copper, and SS tubes immersed in R-134a and R-123 refrigerant fluids and noticed a CHF reduction for the copper material after roughness values greater than 3 μm. For the brass and SS samples the roughness enhancement limit for CHF was even lower. Similarly, Ferjancic [68] noticed that the value of CHF was increased up to surface roughness values of 1.5 μm. When this limit was exceeded, he noted that the value of CHF decreased. Additionally, Kang [66] showed that roughness is also dependent on surface orientation, with horizontally oriented surfaces showing no sensitivity to surface roughness.

Surface porosity has also been shown to have a significant impact on CHF. O'Hanley [63] showed how porosity affects CHF is dependent on the wettability of the heated surface. Using hydrophilic and hydrophobic surface samples, porosity caused a 60% increase and a 97% reduction in the CHF value, respectively. O'Hanley suggested that this has to do with capillary wicking within the pores drawing and repelling water in the hydrophilic and hydrophobic surfaces, respectively. Jun [52] observed a two times higher CHF enhancement resulting from a sintered microporous coating on a copper surface, relative to a non-porous, for various water subcooling under pool conditions. Lee [70] and Rioux [71] also experimentally showed how nano-, micro-, and macro-scale structured porous metal surfaces hinders the hydrodynamic instability of the vapor columns on heated surfaces and improves nucleation heat transfer and thus CHF.

To summarize, whereas surface porosity generally increases the CHF value the potential for surface roughness to improve CHF lies on its ability to increase the number of nucleation sites on the heated surface. Therefore, the process of surface roughening is crucial in determining the effectiveness of CHF enhancement.

2.3.5 Oxide Layer Effects

The formation of an oxide layer is one type of surface chemical effect that has significant impacts on the CHF. The presence of an oxide layer has been found to decrease the contact angle and thus, increase the wettability of heated metal surfaces, such as Zircaloy-4 cladding in PWRs, thereby enhancing their heat transfer ability and thus the point at which CHF occurs [68,71-75]. Tachibana [72] studied several surfaces, including aluminum and SS samples, submerged in a pool of water at atmospheric pressure and noticed that oxidation occurred at high HF values and improved the CHF value. Lee [73] specifically studied the effects of an oxide layer on a zircaloy surface and noted a contact angle decrease of 40% compared to a non-oxidized zircaloy surface. Otsuka [74] explained that the presence of an oxide layer on a zircaloy material increases the surface energy, due to chemical changes in the surface, thus decreasing the contact angle with the coolant fluid. Ferjancic [68] used steel ribbon heaters with varying surface roughness and ran several measurements with several cases exceeding CHF. On the same ribbon heaters where CHF had been exceeded for the previous measurement, he observed that for subsequent measurements the value of CHF increased due to the formation of an oxide layer.

Ferjancic also pointed out that there appears to be a saturation effect during which the degree of oxidation no longer impacts the CHF [68]. Svanholm [75] agreed with this conclusion in experiments carried out using the Halden Boiling Heavy Water Reactor (HBWR). The oxide

layer was observed to increase the CHF and decrease the quenching time of test samples, up until a point during which a saturation effect was experienced [75].

Important work on the oxide layer effects on DNB was studied by Sugiyama [76] using the NSRR in Japan. Pool boiling experiments using three rods with different oxide layers were studied under three power pulses with peak fuel enthalpies of 335, 460 and 575 J/g. For the 335 J/g pulse, the no-oxide layer sample experienced DNB whereas the oxide layer rods did not. For the two higher energy pulses, all rod samples experienced DNB but quenching occurred much faster as the thickness of the oxide layer was increased. From these results, it was concluded that oxidation appears to increase rod coolability and this was most likely due to contact angle enhancements resulting from chemical potential changes due to the oxide layer [76]. Sugiyama [76] stated that the thermal conductivity of the oxide layer is most likely not the contributing factor to CHF enhancement. Results from the Halden and NSRR facilities appeared to also show that somehow the irradiation environment inside of the reactor appeared to enhanced the wettability effects of the oxide layer [75,76]. The main takeaway is that the presence of an oxide layer increases the wettability of the heated surface and thus results in an increase in the CHF value.

2.3.6 Radiation Induced Surface Activation

The effects of RISA have been fairly recently discovered, and it plays an important role in the manifestation of CHF. Sugiyama [76] observed that the irradiation environment of the NSRR enhanced the wettability of the oxide layer on rod surfaces. This was established through a comparison of oxidized and non-oxidized samples, submerged in water tubes, revealing no visual differences in the water meniscus surrounding the cladding in out-of-pile settings. Further, Svanholm [75] measured the quenching time between in-pile Halden reactor and out-of-pile electrically heated experiments with similar oxide layer thicknesses, and concluded that the

quenching time was twice as fast in the in-pile samples due to increased wettability. Lastly, Georgenthum [77] compared irradiation effects on different samples and determined that non-oxidized cases exceed CHF faster and their surface temperatures were higher.

Several studies investigating the effects of gamma and UV irradiation on the wettability of various cladding materials have been performed [74, 77-79]. Kano [78] examined RISA effects on PNC1520 and SS304 materials in pools of water with surface oxide layers present, and observed a decrease in the surface contact angle for both UV and gamma irradiation; but the latter caused a larger decrement. His work suggests irradiation effects are energy dependent and most likely due to a bending of the bandgap in the oxide layer causing the absorption of OH radicals from water, thus improving wettability. Takamasa [79] agreed with the above outcome after he noticed a linear decrease of the contact angle, relative to integrated radiation dose, under gamma and UV fields using titanium, Zircaloy-4, stainless steel 304, and copper surfaces and the increase in wettability was more significant under the gamma field. His analysis also agreed with data from Georgenthum [77] which notes that high HFs can be achieved with irradiation thus making reactor fuel elements less susceptible to DNB occurrences. Otsuka [74] carried out gamma irradiation experiments using two samples, one submerged in water and the other in open air, and concluded that the enhancement in wettability was more substantial in the water specimen and therefore mostly a result of water radiolysis.

More recently, Seshandri [80] also verified many of the above statements of the RISA effects in his study of Zircaloy-4 and chromium coated Zircaloy-4 oxidized surfaces. The samples were irradiated for a total of 96 hrs under UV and gamma fields and were checked every 24 hrs. The contact angle was determined to decrease every time [80]. The chromium sample also achieved “super hydrophility” with a contact angle of 0° due to their high surface conductivity. A

significant finding by Seshandri was made when it was observed that even non-oxidized surfaces experienced wettability enhancements due to irradiation effects [80]. Seshandri's analysis noted that RISA effects are dependent on the surface chemistry and material properties. Lastly, another important finding worth mentioning is that the wettability enhancement decreases once the samples were removed from the irradiation environments [74,77-79].

The takeaway is that RISA effects have significant impacts on the CHF because it increases the wettability of the surface. Thus, higher values of the CHF can be achieved under irradiation environments. Although its effects are enhanced because of the presence of an oxide layer, it appears to be a surface chemistry effect that also occurs on non-oxidized metallic materials. The improved wettability is also dependent on the energy of the incident radiation particles. Taking the effects of RISA into consideration can potentially result in improved best estimate limits on current operating LWRs.

2.3.7 Rapid Heating Effects

There are significant impacts on the CHF due to transient heat transfer effects. Zuber [42] initially indicated that an improved empirical correlation to calculate the peak NB HF would be needed due to different heat transfer mechanisms relative to steady-state heating. The value of CHF is generally known to increase as the heating rate of the surface increases [51,59, 83]. Sakurai [51] and Pasamehmetoglu [26] both developed improved Zuber-based correlations that agree with this trend. Sakurai's correlation used an exponential power rise period constant to relate steady state heating CHF to the transient CHF value.

Auracher [81] used the highly wetting FC-72 fluid to show that transient and steady state boiling curves are different. His analysis used heating rates up to 50 K/s and a heating method in which the nucleation sites were already active to negate perturbations due to spontaneous boiling.

His results showed that rapid heating enhancements on CHF were due to improved thermal boundary convection effects resulting from a highly turbulent two-phase boundary at the heated surface [81]. Derewnicki [59] agreed with these results in his experimentation of rapidly heated platinum wires. He concluded that fast heating of the surfaces creates more spontaneous nucleation sites. Further, forced convection due to the fast superheating of the liquid at the thermal boundary caused the agitation of bubbles that further enhanced the heat transfer out of the platinum wires [59].

Vincent Bessiron [82,83] carried out significant work on transient heating pool boiling CHF using the PATRICIA facility and results from NSRR. In the out-of-pile PATRICIA RIA simulated experiments, transient CHF values between 15.5 and 20.6 MW/m^2 were observed for cladding heating rates between 7,500-10,000 K/s [82]. Although a steady state case was not conducted, Bessiron indicated that typical values for those conditions vary between 1.5 and 4 MW/m^2. Further, Inconel material was used for the heater rod which has a lower wettability than typical zirconium-based rods, thus CHF enhancements could be higher. Bessiron indicated that the transient CHF behavior did not resemble the hydrodynamic instability models from Kutateladze [43] and Zuber [41,42] that occurs under fully developed nucleate boiling (FDNB) conditions as in steady state heating. Instead, the transient heating CHF occurred before FDNB was established and most closely corresponded to the bubble interference model derived by Rohsenow [45].

In the NSRR transient experiments, Bessiron [83] observed pool boiling CHF values that were up to 10 times higher than those found in steady state cases for cladding heating rates higher than 7000 K/s. Using a 250 frames/s camera, he observed that indeed FDNB does not occur under fast heating rates. Rather, more spontaneous nucleation sites and numerous small bubbles were observed at the surface [83]. The bubble mechanisms under fast heating conditions appears to be

homogeneous in nature, whereas heterogenous nucleation occurs under steady state heating [59]. In summary, rapid heating effects delay the point of CHF due to an increased number of spontaneous nucleation sites that results in greater induced turbulent flow when vapor bubbles are ejected from the heated surface.

2.4 Review of Flow Boiling CHF and Impacting Parameters

Historical effort has been dedicated to understanding the role of CHF-influencing parameters on the behavior of this phenomenon under flow boiling thermal-hydraulic conditions. Highly relevant flow boiling CHF-influencing parameters to the work in this dissertation include transient heating rate effects, as well as the impacts of thermophysical material properties. Hata et al. [84, 85] conducted flow boiling CHF experiments in short vertical tubes to explore the effects of exponential increases in heating rates, and used the results to derive CHF correlations dependent on local parameters, rather than inlet conditions, that described subcooled boiling heat transfer curves under turbulent flow conditions. Park et al. [86] studied the transient CHF phenomenon and determined two methods of manifestation for this event under flow boiling conditions. These CHF occurrence mechanisms were a result of hydrodynamic instabilities under steady state heating, and heterogeneous spontaneous nucleation; the latter which was determined to be mainly presented during transient heating CHF manifestation. The findings in Park et al. [86] also determined that the value of CHF increased relative to increments in heating rates. This was congruent with data from flow boiling PWR experiments conducted at the PATRICIA facility, which determined that faster heating rates increased the systematic CHF value, as well as the critical temperature, and that the manifestation of this phenomenon under transient heating conditions was not as a result of hydrodynamic instabilities [87]. Isao [88] has also related the effects of transient heating to the manifestation of CHF as a function of the heating time period.

2.5 Review of the Heat Transfer Time Constant and its Exploration in the Literature.

2.5.1 Heat Transfer Time Constant Definition

The heat transfer time constant (HTTC), given by $\lambda_H\ [s^{-1}]$ in equation 4 for a PWR fuel rodlet**,** is an important parameter that is used to quantify the time dependent exponential decay of the non-dimensionless ratio between the differential temperatures of the fuel centerline and the surrounding coolant for a specified time period

$$\frac{T_{fuel(t)}-T_{coolant(t)}}{T_{fuel(i)}-T_{coolant(i)}} = e^{-\lambda_H t} \quad \text{Eq. 4}$$

where, $T_{fuel(i)}$ and $T_{coolant(i)}$ are the initial fuel centerline and coolant temperatures, and $T_{fuel(t)}$ and $T_{coolant(t)}$ are those temperatures after some specified time represented by t. Typically, under flow boiling conditions found in PWRs the coolant temperature is assumed to be constant over time at a specific location, and increases relative to the axial height in the coolant channel. This is no longer true under the pool-boiling conditions of the environment for the considered CHF experiments. Fundamentally, the dimensionless exponential constituent of equation, $\lambda_H t$, is equivalent to the product of the Fourier and Biot numbers. The parameter for time, t, is part of the Fo number discussed in section 2.5.2. From equation 4, it can be mathematically observed that for a very large λ_H the thermal system will reach thermal equilibrium with its surroundings rather quickly. The opposite is true when the HTTC is small due to higher thermal resistances or a large fuel volumetric heat capacity, both reducing the heat transferred into the coolant over a time duration for an energy deposition. The HTTC is defined as follows in equation 5 and 6

$$\lambda_H = \frac{h_{equiv}}{\rho c_{p\ fuel} L_c} = \frac{h_{equiv}}{\pi \rho c_{p\ fuel} R^2} \quad \text{Eq. 5}$$

$$\frac{1}{h_{equiv}} = \frac{1}{4\pi k_{rod}} + \frac{1}{2\pi k_{gap}} + \frac{1}{2\pi k_{clad}} + \frac{1}{2\pi R\, h_{coolant}} \quad \text{Eq. 6}$$

where $\frac{1}{h_{equiv}}$, defined in equation 6 for a typical PWR fuel rodlet, is the summation of the combined thermal resistances of the rodlet materials and the coolant volume. In equation 5 L_c, the characteristic length, in fuel rod cylindrical geometry is equal to the product of pi and the squared radius of the outer cladding, R. The HTTC is dependent on the k and ρc_p properties of the components of the fuel/cladding designs and the h_{conv} at the cladding-to-coolant interface. Thus, these thermophysical parameters are important drivers in the evolution of the fuel centerline and outer cladding temperatures during a reactor power transient and are crucial in analyzing the heat transfer characteristics of nuclear fuel systems. Because the cladding temperature is the contact point between the energy transferred out of the fuel and into the coolant, the HTTC influences the manifestation of the DNB event in PWRs.

2.5.2 Other Important Heat Transfer Definitions

The Fourier number, given in equation 7, uses material thermal properties to describe the relationship between diffusive transport rate out of the fuel rodlet relative to the heat stored within its components

$$Fo = \frac{\alpha t}{L_c^2} = \frac{kt}{\rho c_p L^2} = \frac{Diffusive\ Transport\ Rate}{Heat\ Storage\ Rate} \quad \text{Eq. 7}$$

where α is thermal diffusivity [$\frac{m^2}{s}$] which describes the heat transfer rate within an object for a temperature gradient, k is thermal conductivity [$\frac{W}{m-K}$] which is a measure of the thermal resistance within a material, ρc_p is the volumetric heat capacity [$\frac{J}{m^3-K}$] which is the amount of energy needed to raise one unit volume of a material by one degree, and L_c is the characteristic length of the system which is defined as the total volume of the body divided by the total heat transfer surface area. Equation 8 gives the relationship for the Biot number, which represents the ratio of the relative importance of the thermal resistances within the volume over the ambient convection resistances for the temperature profile of a body being cooled or heated through convection processes.

$$Bi = \frac{h_{conv} L_c}{k} = \frac{Conductive\ Resistance}{Convective\ Resistance} \quad \text{Eq. 8}$$

In the case of a PWR fuel rod, h_{conv} is the convective heat transfer coefficient at the cladding-to-coolant heat transfer interface and k is the combined thermal conductivity of the fuel, gap and cladding materials. For a Biot number <0.1, the lumped capacitance method can usually be adopted because the significance of the conduction within the body is negligible. For a Biot number >0.1, this is no longer true and heat transport equations must be solved in order to accurately capture the temperature profile within the volume of the heated/cooled body. Equation 9 gives the thermal effusivity; another important parameter that was used to discuss the time constant effects of the two fuel/cladding systems.

$$e = \sqrt{k \rho c_p} \quad \text{Eq. 9}$$

Thermal effusivity is used to describe the thermal responsiveness, or thermal inertia. As the value of this parameter increases a body more rapidly exchanges heat with its surroundings

2.5.3 Review of Thermophysical Property Impacts on the CHF under Pool and Flow Conditions

After the initial contributions of Zuber [41,42] and Kutateladze [43,44], many researchers have dedicated their efforts to understanding the CHF behavior and the role of these influencing parameters. Coolant and material thermophysical properties are known to be key parameters which determine the CHF value. Tachibana et al. [72] conducted pool boiling burnout experiments using heating strips made out of different materials. They reported that the thermal diffusivity of the test section hardly affects the CHF, while the heat capacity per unit heat transfer area was well correlated. Unal et al. [89] investigated the occurrence of CHF using different heater materials and thicknesses, and reported a strong correlation between these and the size of the dry patch. Golobic and Bergles [90] conducted saturated pool boiling experimentation of different ribbon-shaped heaters in FC-72 liquid, and reported strong evidence of the effect of material properties on CHF. Saylor [91] introduced a new parameter referred to as the thermal activity, which was the product of the thermal effusivity and wall thickness, to describe the effects of heater material properties on CHF. Later, Arik and Bar-Cohen [92] developed pool boiling CHF correlations for horizontal square heaters with dielectric liquids, embodying an assumed dependence of CHF on this thermal activity parameter. Lee et al. [93] reported the delayed occurrence of CHF due to higher thermal activity in their pool boiling experiments using copper and graphite oxide coated heaters. However, the thermal activity-based correlations could not account for the pool boiling CHF of FC-72 liquid on aluminum-based heater surfaces conducted by Ho et al. [94]. Gogonin [95] summarized

previous CHF studies using thick-walled test sections regarding heat dissipation toward both the fluid and heater, and showed substantial dependence of CHF on both the wall thickness of the heater and its physical properties.

Raghupathi and Kandlikar [96] assessed comprehensive material effects on CHF with representative parameters. They reported an increased CHF value with a higher heater thermal effusivity, but concluded that CHF was not directly correlated to the thermal diffusivity of heater material. However, Staszel and Yarin [97] described the propagation of vaporization fronts leading to the CHF using thermal properties of heater materials including thermal diffusivity, in their pool boiling experiments with Novec 7300 liquid. Kam et al. [98] also emphasized the effects of material properties on CHF to support their pool boiling experiments using carbon steel-based samples. However, they could not clearly define the most influential parameter representing the effect of thermal properties on the CHF. Previous studies have reported the use of the thermal time constant in calculating transient fuel and cladding temperatures for RIA-like power transients [27,99,100,101]. Nevertheless, none of them attempted to characterize the effect of the transient CHF on the thermal time constant. Umekawa [102] stated the importance of the time constant for a tube with a relatively low heat capacity material and reported its effects on the transient CHF. However, the experiments were conducted under the oscillatory flow conditions and not under fast heating transient conditions.

Material thermophysical and coolant property effects predominantly have been studied under pool boiling conditions, and very sparingly, studies under transient flow boiling CHF have been investigated in the literature. Klandikar [103] developed an early two-phase saturated liquid correlation for flow boiling heat transfer coefficients that included a fluid-dependent parameter to account for the effects of different fluids on surface-to-coolant heating characteristics. Soon et al.

[104] conducted transient flow boiling experiments of several different materials– including Zircaloy-4, Inconel-600 and FeCrAl Alloys– to study the effects of thermophysical properties on the manifestation of the CHF phenomenon. Key findings in this study determined that material properties are primarily responsible for different observed CHF values between these materials. Soon used a "surface thermal economy" parameter, which described surface heat dissipation, to related observed transient flow boiling CHF variations between the different materials used in the experiments [104]. Nevertheless, these previous studies have not investigated the effects of the HTTC on the transient CHF under flow boiling conditions. Accurate prediction of transient CHF requires an exact characterization of the contribution of HTTC, including thermophysical material and coolant parameters, and such characterization is the ultimate goal of the work in chapter 6 for both flow and pool boiling conditions.

CHAPTER 3

EXPERIMENTAL HEATER FOR IN-PILE POOL BOILING TESTING USING THE TREAT FACILITY

This chapter covers preliminary neutronics and thermal hydraulics modeling analysis performed in support of the development of the initial experimental and design matrix for a non-nuclear heater rodlet apparatus that was inserted into the TREAT facility in December of 2019. This work is part of the INL led research project that coupled modeling capabilities, using advanced nuclear codes, with on-going experimental efforts at the TREAT facility. The unique contributions presented in this chapter involve a modeling effort that was used as an informative design matrix, that was part of task one of the overall project flow chart discussed in section 1.2.2. From this developed informative database, the design of the novel TREAT heater device was derived. Whereas, the overall experimental effort on the INL side, is aimed at better understanding the mechanisms of CHF manifestation under in-pile fast transient irradiation conditions using a separate-effects testing approach as well as the modeling design of the rodlet using the informative database developed here. Specifically, the long-term goals will be to experimentally investigate the impacts of the presence of an oxide layer, radiation-induced surface activation as well as heat transfer time constant and rapid surface heating effects on the CHF phenomenon. The generated experimental data will inform on the development of future CHF correlations that take into account these CHF-impacting parameters. The utilized heater apparatus is made out of tailored natural boron-enriched stainless steel 304 material, and is held within the TREAT facility using experimental capsules. When subjected to a TREAT power pulse, the heat generated within the test apparatus will induce CHF in the coolant surrounding it within the capsule holder.

3.1 Summary of Preliminary Design Study of Heater Rod Experiment

This modeling effort was utilized to develop an informative database for an initial experimental and design matrix of the non-nuclear borated heater apparatus. The overall modeling methodology consisted on an investigated effort with several advanced computational tools to inform on the design of the heater rodlet. To aid in this modeling approach, the energy deposition and occurrence of CHF were ultimately identified as the most crucial key Figures of Merit (FoMs). For the heater rod design, boron concentrations between 0.1-2.09 wt.% were considered. Further, a self-shielding study was performed using the Serpent code to determine whether an instrumented borated tube could be used in place of a solid borated rod. This study determined that the inner region of the rod can be excluded or instrumented without heat generation penalties, as well as helped develop several radial heating profiles for different rodlet boron content for decoupling with thermal hydraulics analysis. Lastly, a RELAP5-3D/RAVEN thermal-hydraulics sensitivity study determined the lowest limiting boron concentration needed to induce CHF in capsule coolant water with different degrees of subcooling. Additionally, the value of CHF is known to increase during a rapid transient. Therefore, a CHF multiplier sensitivity study determined what multipliers would inhibit CHF for varying degrees of subcooling of two chosen power coupling factors (PCFs). The current borated tube rodlet geometry configuration achieved a maximum CHF multiplier value of 7.8 using a 1400 MJ power pulse in TREAT. Although this was the power pulse with the greatest energy deposition considered for this study, the TREAT facility is capable of pulses up to ~2500 MJ. This provides a significant margin in energy capacity that was not included within the scope of the calculations in this chapter.

3.1.1 Assessment of Key FoMs for Heater Design Analysis

For the purpose of the preliminary neutronics and thermal-hydraulics analysis and design efforts, several important FoMs were identified to aid in the development of a test matrix that will be used to inform on the borated SS-304 rodlet design of the in-pile experiment to be inserted into the TREAT core. The FoMs selected for computer modeling of the power pulse transient cases were (1) the energy deposition into rodlet, (2) the heat transfer time constant, (3) the peak cladding temperature, and (4) the occurrence of CHF. FoMs (1-3) were selected because the in-depth fuel performance modeling and RIA codes benchmark analyses carried out in [105, 106, 107] identified these as the main sources of uncertainties in predicting the occurrence of CHF. The energy deposition FoM is of high priority because it directly influences the cladding temperature, the occurrence of CHF, as well as the post-CHF behavior. This FoM is also very important in determining the thermal and mechanical behaviors of the fuel and cladding materials [106, 107], and is dependent on the characteristics of the simulated TREAT power pulses as well as the various natural boron concentrations in the experimental steel rodlet. Further, the other FoM of high priority is the occurrence of CHF because predicting its manifestation is ultimately the goal. The peak cladding temperature FoM was determined to be of low priority for the work in this chapter because its behavior is mainly dependent on the energy deposition of the rodlet as described in the NEA RIA benchmark parametric sensitivity analysis [107]. Lastly, the heat transfer time constant FoM, λ_H, described in section 2.5.1 is also of low priority for the near-term design efforts covered in this chapter in support of the in-pile experiments, but was studied in detailed in the modeling analysis presented in chapter 6.

3.2 Neutronics Design of Heater Rod

3.2.1 Neutronics Model Description and Specifications

This study took advantage of a full-core Serpent model of the TREAT provided by INL [108]. Although the model utilized the SETH experimental capsule, its material constituents are similar from a neutronics point of view to the SERTTA capsule [109, 110], and thus was adequate for this preliminary neutronics study. For the investigation, the components of the model were kept the same with the exception of the placement of a solid borated SS-304 rodlet, instead of a Urania rodlet, and the addition of SS-304 cladding material in the model; see Figure 7. The modeled borated rodlet has a height of 10.16 cm and an outer radius of 0.41 cm, as found in typical PWRs, excluding the cladding and the helium gas gap. The neutronics analysis included rodlet boron concentrations between 0.1-2.09 wt.% (0.5-10.0 at.%) natural boron in a helium gas capsule.

The neutronics study consisted of two important tasks. First, a self-shielding study was performed to determine whether an instrumented borated tube could be used instead of a rodlet. Following this study, an investigation was conducted to determine coupling factors for the expected heat generation response of several different natural boron concentrations as a result of a transient power pulse in the TREAT. The subsequent neutronics calculations were carried out by initializing the neutron population in Serpent to 10,000 and setting the number of inactive and active cycles to 200 and 3000, respectively. The number of inactive cycles was determined to be more than enough to allow the Shannon entropy to converge, and 3000 active cycles achieved a k-effective statistical error of less than 20 pcm for all cases.

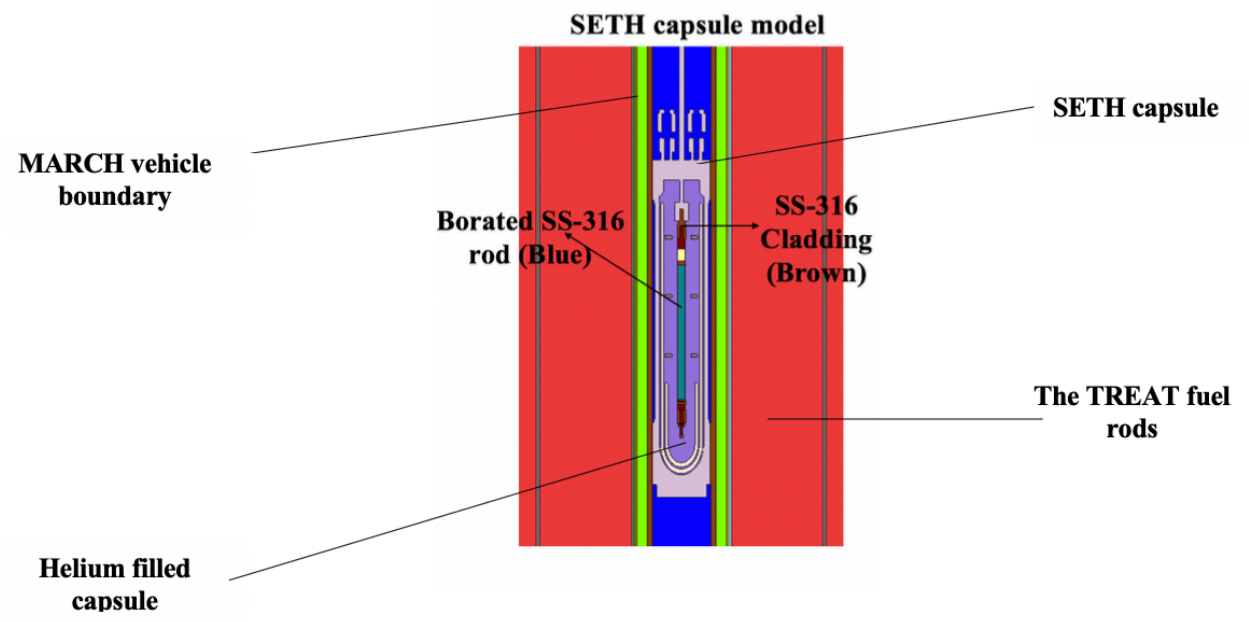

Figure 7. Serpent image depicting the borated steel rodlet within the SETH capsule inserted in the TREAT facility using MARCH.

3.2.2. Self-Shielding Study of Heater Rod

Self-shielding is a result of the majority of the neutrons being absorbed around the outer rim of the rodlet. Accordingly, the inner regions of the rodlet will experience considerably lower neutron flux levels [111]. This effect is also observed in oxide-based fuel rods, and in the borated rods this effect subsequently leads to an increase in the ^{10}B (n, α) capture reaction rate as you radially move away from the center of the rod. Using the Serpent code, six different rod boron atomic concentrations (0.5, 1.0, 2.5, 5.0, 7.5 and 10.0 at.%) were investigated by splitting the 0.41 cm radius of these cases into ten equal radial intervals. Heat detectors, a feature of Serpent, were used to tally the power generated in each cylinder [7]. The results shown in Figure 8, displays the radial power profiles of each of these chosen boron concentration cases.

The results of this self-shielding study for all the chosen cases show that less than 15% of the total heat generated was observed to occur in the inner 2 mm of the borated rodlet. Thus, the self-shielding effects of the boron enriched material is significant. Additionally, the self-shielding effects can be seen to increase as boron concentration increases. This is expected, because the ^{10}B atoms are more densely packed within the same rod volume. The main takeaway from this study is that a ~2-mm thick borated tube can be used in place of a solid borated rod with many possible benefits. A primary benefit is the possibility to utilize a tube geometry to allow additional thermometry instrumentation to measure the inner wall temperature in the heated tube, in an axial location corresponding to the first occurrence of CHF. This approach is not easily achieved with real fuel rods and eliminates problematic uncertainties found with surface mounted thermocouples at a water interface (on the rod outer diameter).

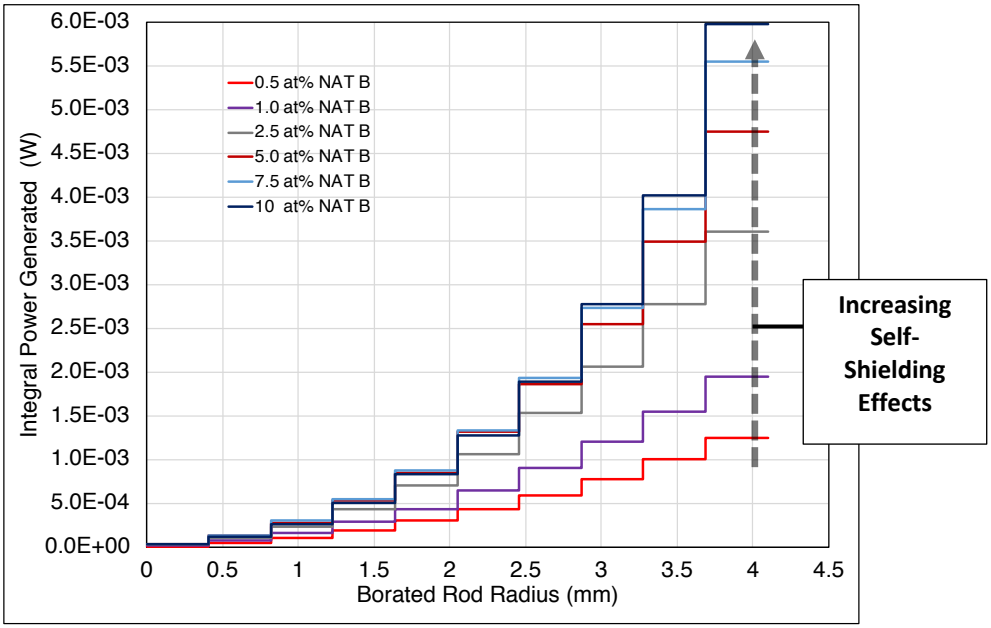

Figure 8. Integral heat generated as a function of radius for self-shielding study of the chosen boron cases.

3.2.3 Power Coupling Factors Neutronics Study

The purpose of this study was to determine the heat generation response of the borated steel rod placed in TREAT. Using Serpent [7], a power coupling factor (PCF) was calculated for each of the six chosen boron concentration candidates for the rod using equation 10. The PCF serves as a relation between how much heat, in Watts (W) per gram, is expected to be generated in the borated rodlet per Megawatt (MW) of reactor power produced in the TREAT facility resulting from a transient power prescription. A PCF was calculated for several known boron concentrations as shown in Table 1.

$$PCF\ \left[\frac{W}{g*MW_{reactor}}\right] = \frac{Detector\ Output\ (W)}{volume_{cell}*\rho_{ss304}*1000\ W_{reactor}} * \frac{10^6 W_{reactor}}{MW_{reactor}} \quad \text{Eq.10}$$

To determine the PCF values for boron concentrations between these cases, a continuous polynomial function was determined by plotting these values as a function of boron concentration as shown in Figure 9, and a database was formed. The slope of the line is seen to decrease due to the increasing effects of self-shielding as boron concentration increases. The advantage of these PCFs is that the heat generation can be scaled to different reactor power outputs or weight samples of the rodlet. These PCFs were used to provide a framework for the concurrent thermal-hydraulics analysis following this study.

3.2.4 Validation of Serpent Neutronics Study

A TREAT model using the Monte Carlo Neutron and Photon (MCNP) [112] transport code was used to carry out an independent study of the radial heat generation of a 1.50 % natural boron enriched steel tube rodlet with an inner and outer radius of 0.275 cm and 0.475 cm, respectively.

Table 1. PCFs results for the chosen natural boron concentration cases in the helium filled experimental capsule.

Natural Boron Concentration (at.%)	Natural Boron Concentration (wt.%)	Heat Generated in Rod (W)	Reactor Power (W)	Power Factor (W/g – MW)
0.50	0.10	8.62E-04	1000	0.0208
1.00	0.19	1.49E-03	1000	0.0369
2.50	0.49	2.94E-03	1000	0.0751
5.00	1.00	4.28E-03	1000	0.1131
7.50	1.54	5.06E-03	1000	0.1359
10.0	2.09	5.81E-03	1000	0.1612

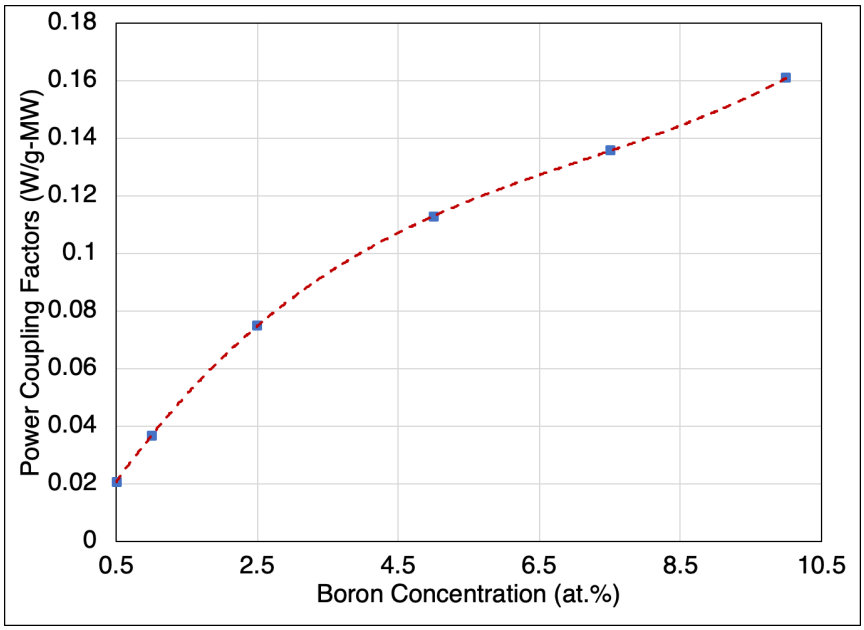

Figure 9. Polynomial fit used to determine PCFs as a function of natural boron concentration.

In this study, the radial PCFs for this 2-mm thick tube rodlet inside of the helium-filled MARCH-SERTTA capsule were generated. To independently verify the conclusion from the above Serpent results, a similar study of the heat generated in the outer 2 mm of the 0.41-cm outer radius of the solid SS304 rodlet with a boron concentration of 1.50 % was compared to these calculations. The radial PCF results for both of these cases are similar and are shown in Figure 10. At a midpoint value of about 0.3 cm, Serpent and MCNP calculations yielded similar PCFs of 0.118 and 0.116 respectively. At a midpoint range of around 0.35 cm, Serpent and MCNP values were also akin with PCFs of 0.130 and 0.120 respectively. The Serpent solid rodlet was split into smaller radii than those in the MCNP model, which, along with the different cross section libraries and model characteristics in both codes, could be the source of the minor discrepancies.

3.3 Thermal Hydraulics Design of Heater Rod

Thermal hydraulic sensitivity studies were conducted using the thermal-hydraulics RELAP5-3D code, coupled with the capabilities of the RAVEN program [8, 9]. RAVEN has the ability to act as a parametric input controller of the RELAP5-3D code, allowing the user to carry out uncertainty and sensitivity analyses and aids in identifying the most important impacting parameters for a specific scenario relating to reactor safety. Mandelli [113] demonstrated RAVEN's capabilities and other examples of the RELAP5-3D/RAVEN coupling for usage in sensitivity studies is discussed in section 6.1.1.

3.3.1 RELAP5-3D Model Description and Study Methodology

The thermal-hydraulics studies were started with the construction of a RELAP5-3D heater tube model, submerged in water within a simplified version of the SERTTA capsule. The characteristics of the model are shown in Figure 11. A pipe segment was used to represent the pool

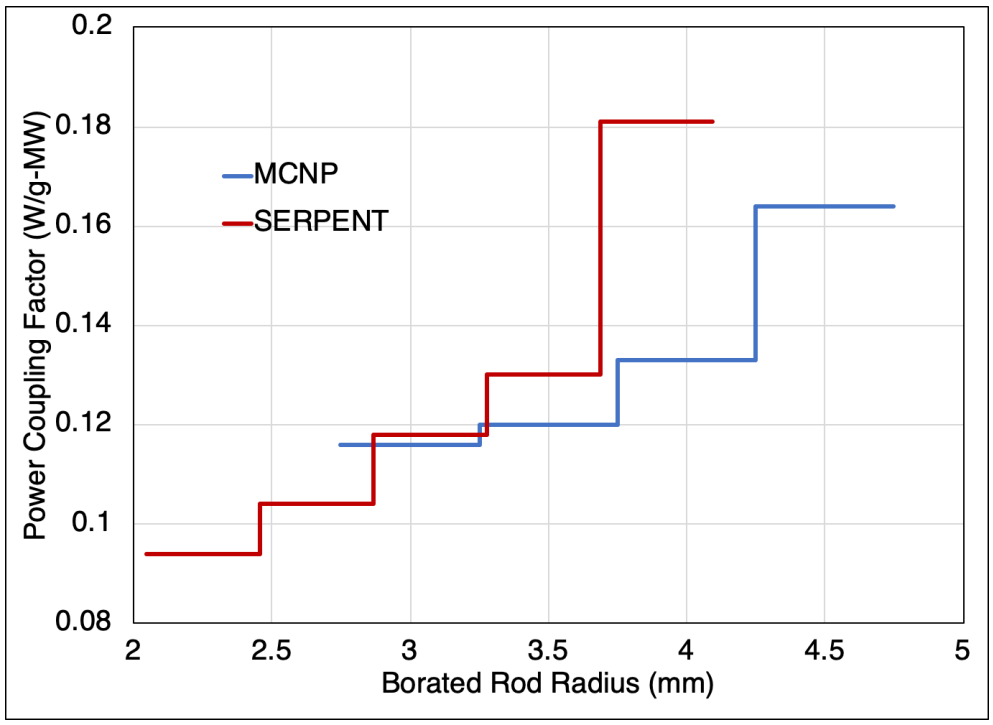

Figure 10. Comparison between the MCNP and Serpent PCFs neutronics analysis of the outer 2mm of two rodlet geometries.

of water surrounding the SS rodlet in the experimental SERTTA capsule and the argon gas chamber connected above that prevents over-pressurization of the capsule. The vertical length of the argon and water segments were 26.67 and 24.78 cm, respectively. The flow areas (FAs) were calculated by dividing the volume of these components by their respective lengths. An 80 mesh volumes HT represented the borated SS heater rodlet geometry within the capsule. Because the self-shielding study above indicated that a 2-mm thick tube could be used in place of a solid rod, the HT represented a tube with an outer radius of about 0.48 cm and inner radius of about 0.28 cm. The exact dimensions of the components in the model are summarized in Table 2. Axial and radial mesh node sensitivity studies were conducted on the model to verify that the correct number of these input parameters was being used so as to not bias the results. For a power pulse, the HF and outer cladding temperatures were compared as the axial nodes and radial mesh points were varied to determine when the results converged. The studies concluded that a minimum of 15 radial mesh points is needed to accurately predict the maximum HF and cladding temperatures, as shown in Figure 12. The number of axial nodes had no significant impact on the results.

Transient power pulses typical of those expected in the TREAT facility were used along with the PCFs determined from the neutronic study to apply the power into the SS tube heater. To accurately represent the SERTTA capsule conditions, no time-dependent inlet/outlet volumes were attached to the HT to allow pressurization within the pipe model. Further, the coolant pressure was initialized to 3.447 MPa (500 psi) to represent the anticipated test pressure under experimental conditions. The sensitivity studies were carried out on five different prototypic PWR subcooling test condition cases (0, 10, 20 30 and 40 K) and three different TREAT representative transient power pulses, shown in Figure 13, with energy depositions of 920, 1157 and 1407 MJs. All the power profiles were modeled as Gaussian shapes. To verify that the time steps for the power pulses

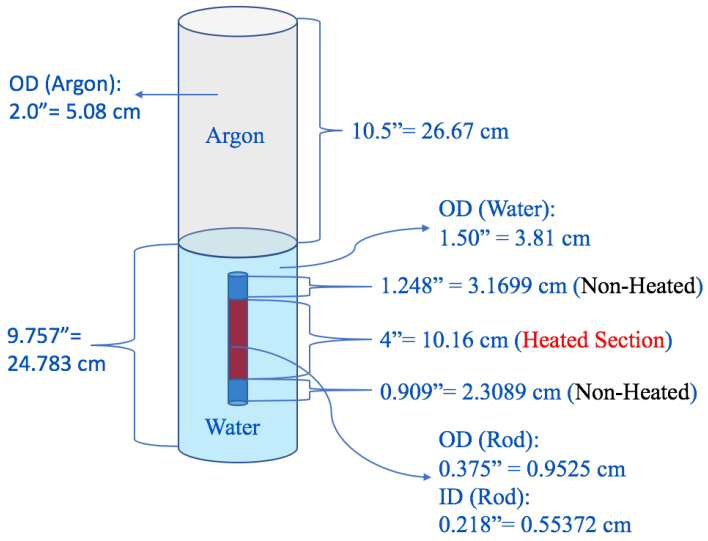

Figure 11. RELAP5-3D schematic of the simplified SERTTA capsule model.

Table 2. Summary of RELAP5-3D component geometries

Component	Component Value	Units
Length of Argon Chamber	26.67	Cm
FA of Argon Chamber	20.30	cm^2
Length of Water Segment	24.786	Cm
FA of Water Above/Below HT	11.40	cm^2
FA of Water surrounding HT	10.70	cm^2
HT Number of Axial Volumes	80	
HT Number of Radial Sections	15	
Inner Radius of HT	0.27686	cm
Outer Radius of HT	0.47625	Cm
Heat Structure Material	Type-304 Stainless Steel	

were accurately inserted into the input file, the trapezoid rule was used to estimate their energy depositions. The two thermal-hydraulic sensitivity studies covered below were conducted using the 2006 Groeneveld CHF LUT [114] to predict the value of CHF.

Transient power pulses typical of those expected in the TREAT facility were used along with the PCFs determined from the neutronic study to apply the power into the SS tube heater. To accurately represent the SERTTA capsule conditions, no time-dependent inlet/outlet volumes were attached to the HT to allow pressurization within the pipe model. Further, the coolant pressure was initialized to 3.447 MPa (500 psi) to represent the anticipated test pressure under experimental conditions. The sensitivity studies were carried out on five different prototypic PWR subcooling test condition cases (0, 10, 20 30 and 40 K) and three different TREAT representative transient power pulses, shown in Figure 13, with energy depositions of 920, 1157 and 1407 MJs. All the power profiles were modeled as Gaussian shapes. To verify that the time steps for the power pulses were accurately inserted into the input file, the trapezoid rule was used to estimate their energy depositions. The two thermal-hydraulic sensitivity studies covered below were conducted using the 2006 Groeneveld CHF LUT [115] to predict the value of CHF.

3.3.2 PCFs Thermal Hydraulics Sensitivity Study

The purpose of the PCF sensitivity study was to obtain a conservative estimate of the PCFs needed to induce the CHF phenomenon in different power pulse cases under varying water coolant conditions with different degrees of subcooling. Each of the PCFs corresponded to a rodlet boron concentration between 0.1-2.09 wt.% (0.5-10 at.%), that was determined through the neutronics study conducted in section 3.2.3. This study was conducted by utilizing the RAVEN code to parametrically vary the power factors in the power card feature of RELAP5-3D.

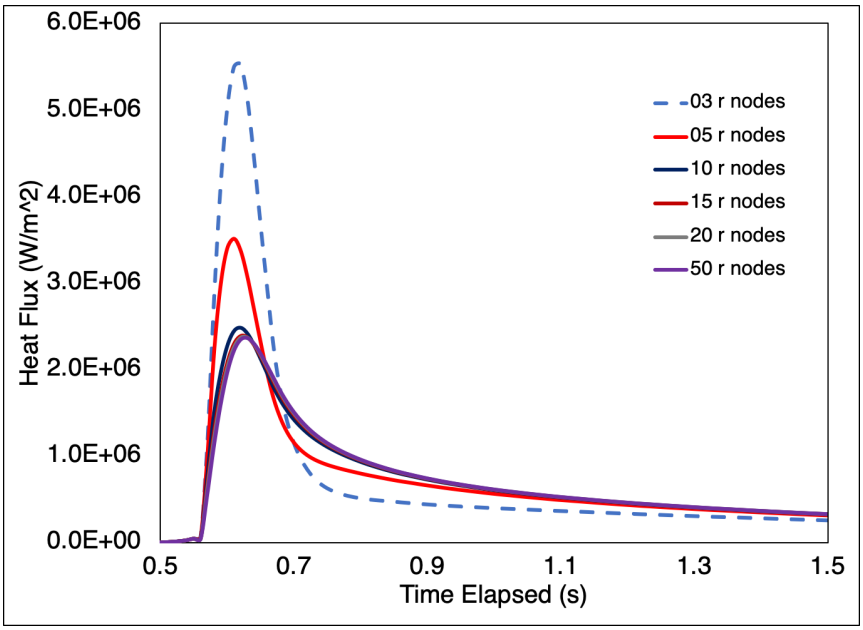

Figure 12. Radial mesh points sensitivity study showing convergence of results for input parameter values greater than 15.

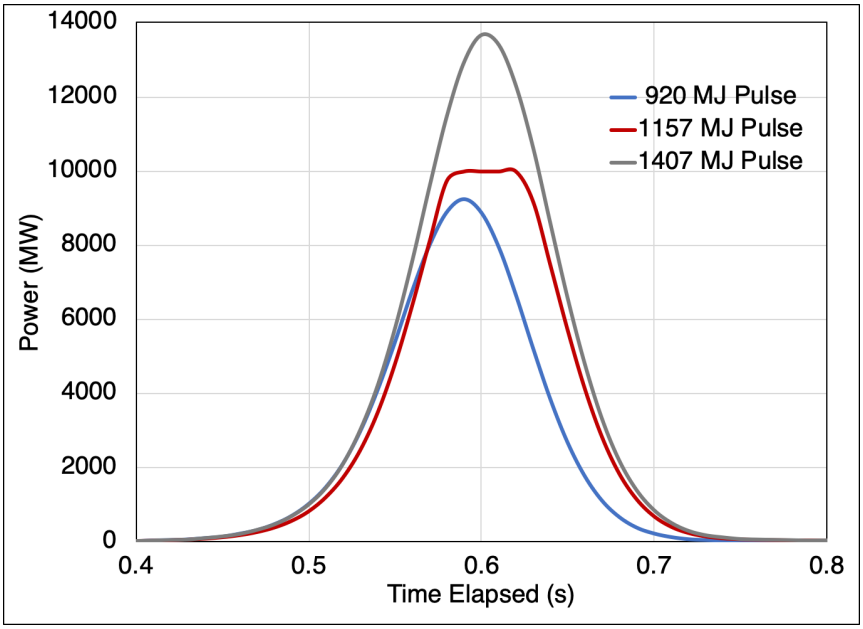

Figure 13. Representative TREAT power pulse transients used in the RELAP5-3D/RAVEN sensitivity studies.

Two methods were used to determine when the CHF occurred. First, the incidence of the CHF was verified through a code output to identify which boiling regime the heat transfer is currently under as a function of time. Second, characteristics of the post-CHF behavior was used as described by Bessiron [82]. After the CHF is exceeded, a transition boiling phase and subsequent establishment of a film boiling (FB) phase during which the cladding-to-coolant heat transfer drops significantly. The peak cladding temperature is determined by the HF during this established FB phase [82]. The duration of the FB phase is extended as the rodlet energy deposition is increased and therefore resulted in higher cladding temperatures. Further, a rewetting HF peak is observed that terminates the establishment of the film boiling phase and indicates that CHF was exceeded. This rewetting peak results in an enhanced heat transfer coefficient and the cladding temperature is reduced to near the saturated temperature of the liquid [82].

The methodology of the PCF sensitivity study is shown below for the 20K subcooling and 1157 MJ energy deposition power pulse combination. An initial broad sweep (Figure 14) of PCFs was conducted with RAVEN for each subcooling and power pulse case. Following, a more defined sweep (Figure 15) was conducted to better pinpoint what PCF first induced CHF.

The presence of a rewetting peak indicated the first occurrence of CHF. PCFs with energy depositions higher than this case resulted in the manifestations of post-CHF behavior and longer duration of the rewetting peak appearance. As shown in the defined sweep in Figure 14, the analysis indicated that the CHF is exceeded for a PCF higher than 0.0529 W/g-MW. The closest matching PCF value from the neutronics database is 0.0539 W/g-MW and corresponds to a natural boron concentration of 0.31 wt.% (1.6 at.%). In this case, the cladding temperature is seen to increase substantially relative to the non-CHF cases due to the insulating effects of the FB phase. This is when mechanical and thermal behavior can lead to fuel and cladding damage.

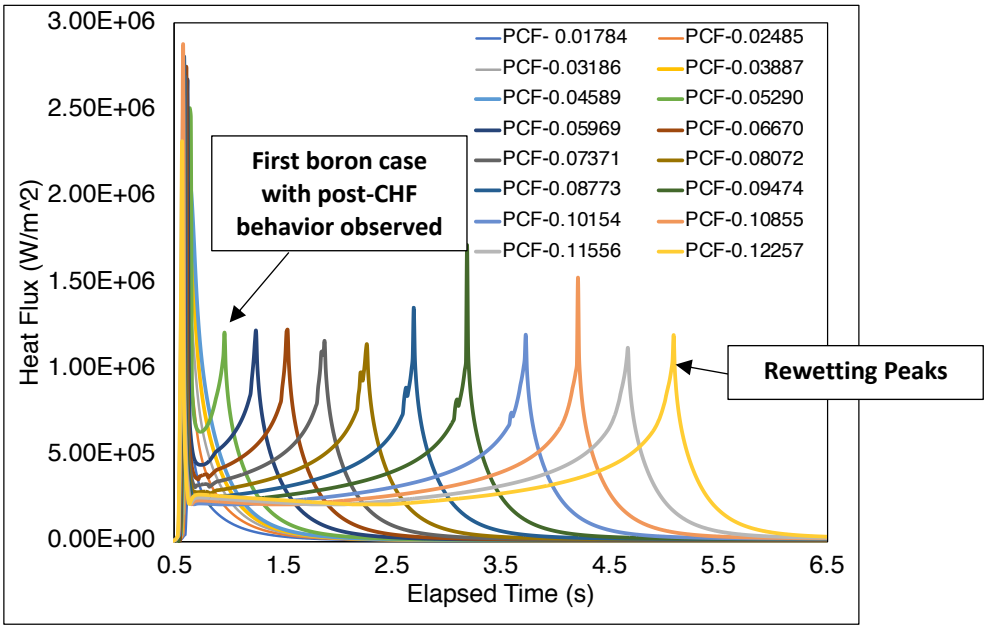

Figure 14. PCF sensitivity study broad sweep for the 20K subcooling and 1157-MJ power pulse case.

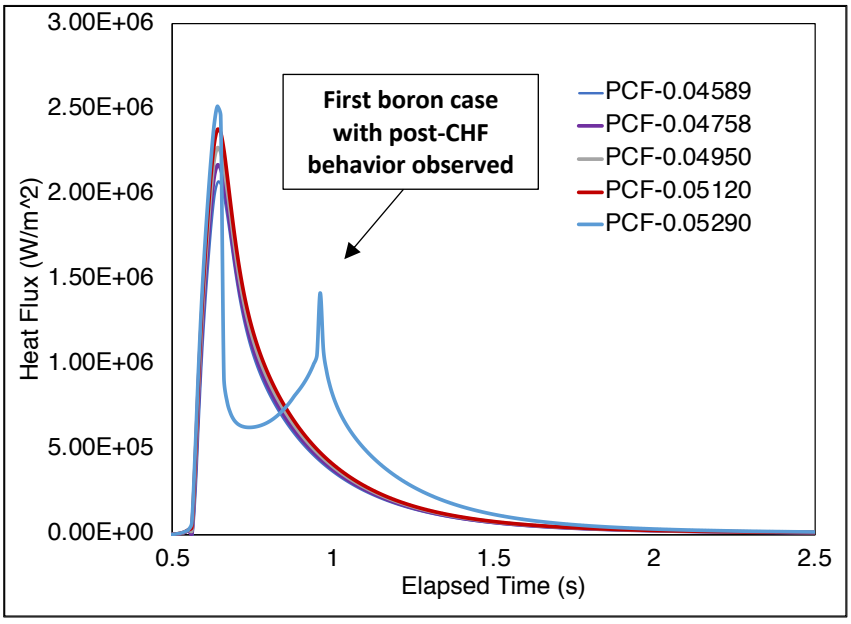

Figure 15. PCF sensitivity study defined sweep for the 20K subcooling and 1157-MJ power pulse case.

The results of the PCF sensitivity study are displayed in Table 3, and as expected the PCF needed to cause CHF increases as the subcooling is increased. These results, taken from the axial volume located at the center of the HT, are conservative because a uniform radial power profile was used in all cases, where the results in Figure 8 show a very large radial power distribution. Further, the 2006 Groeneveld LUTs do not take the effects of rapid heating into account. As Bessiron [82, 83] described in his experiments the value of pool boiling CHF is expected to increase under fast transient heating rates as experienced during these pulses. Since this effect exceeds the capabilities of the 2006 LUTs correlation used in the RELAP model, a follow up CHF multiplier sensitivity study was carried out below to investigate the influence of rapid heating.

3.3.3 CHF Multiplier Sensitivity Study

RELAP5-3D has a CHF multiplier parametric feature that allows the user to change the transition to film boiling point by increasing/decreasing the CHF value at which this occurs [8]. Therefore, the goal of this sensitivity study was to determine what multiplier value would inhibit the occurrence of CHF under specified conditions. NSRR pool boiling transient heat experiments have shown that during these fast energy deposition rates, such as those found under RIA conditions, higher HF can be achieved due to higher nucleation sites and increased forced convection resulting from bubble agitation as explained in section 2.3.7. Bessiron [82, 83] also determined that transient CHF values can be up to about 10 times higher than those found in steady state heating. This forms the basis behind the analysis carried out in this section.

Over 550 CHF multiplier cases were conducted for two different PCFs corresponding to natural boron concentrations of 1.5 wt.% (7.4 at.%) and 2.0 wt.% (9.6 at.%). The tube averaged PCFs were 0.135 and 0.156 W/g-MW, respectively, for these two boron concentrations, which were chosen because borated steel can be procured with these concentrations. The RELAP model

Table 3. PCF sensitivity study results for all cases studied taken from the center axial HT volume.

Coolant Subcooling (°C)	920 MJ Pulse PCFs (W/g-MW)	Boron Conc (wt.%)	1157 MJ Pulse PCFs (W/g-MW)	Boron Conc (wt.%)	1407 MJ Pulse PCFs (W/g-MW)	Boron Conc (wt.%)
0	0.0565	0.33	0.0457	0.25	0.0369	0.19
10	0.0615	0.37	0.0512	0.29	0.0428	0.23
20	0.0663	0.41	0.0539	0.31	0.0457	0.25
30	0.0708	0.45	0.0565	0.33	0.0485	0.27
40	0.0730	0.47	0.0615	0.37	0.0512	0.29

model incorporated radial power profiles for these two cases, which were determined using the same approach described in self-shielding study in section 3.2.2. This radial profile distributed the heat generation from the PCFs above within the tube geometry of the HT.

The investigated degrees of subcooling were 40, 30, 20, 10 and 0K. Further, power pulses with total energy depositions of 920, 1157 and 1407 MJ were used. Using RAVEN, the RELAP5-3D CHF multiplier parameter was varied between the default value of 1.0 and increased up to 10.0 times the CHF value. To demonstrate the approach of the CHF multiplier study, the combination of a 2.0 wt.% boron case, a power pulse energy deposition of 1407 MJ, and a coolant degree of subcooling of 30K was selected. The broad sweep shown in Figure 16 indicates that CHF is inhibited when the CHF multiplier exceeds a value of 5.0. Further, Figure 17 shows the defined sweep of CHF values between 5.0 and 6.0. After a value of 5.8, a rewetting peak is no longer observed, and thus CHF was no longer exceeded. The results of the CHF multiplier study are shown in Table 4 and Table 5 below. As expected, the CHF multiplier value is observed to increase as the degree of subcooling decreases. This is because as the subcooling increases the value of CHF increases and thus, keeping the energy deposition constant, the CHF multiplier would be smaller for higher degrees of subcooling. A maximum CHF multiplier value of 7.8 was achieved using a 1407-MJ pulse and 0° subcooling conditions for the current borated tube rodlet geometrical configuration.

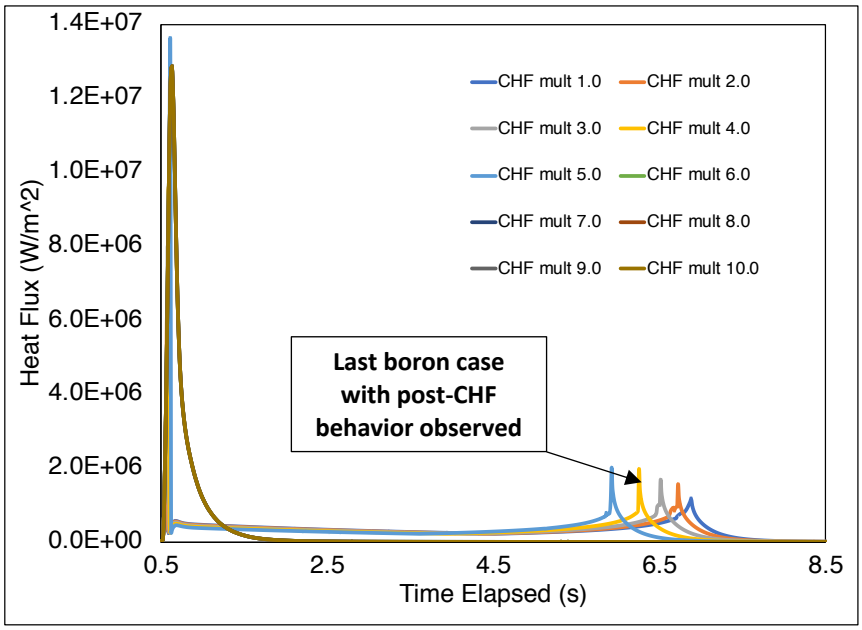

Figure 16. HF Broad Sweep of the 1407MJ Pulse, 2.0 wt.% Boron, 30°K Subcooling Case.

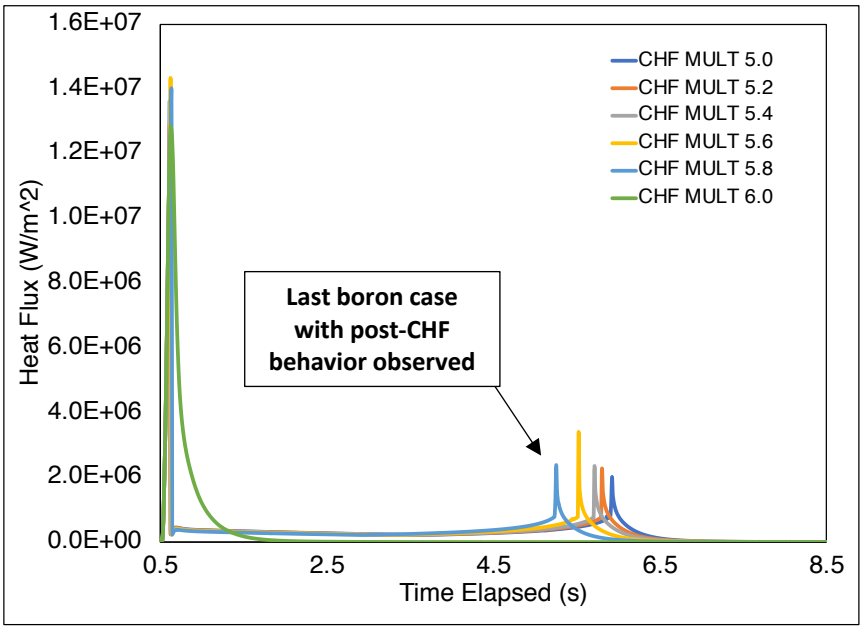

Figure 17. HF Defined Sweep of the 1407MJ Pulse, 2.0 wt.% Boron, 30°C Subcooling Case.

Table 4. CHF multipliers for the Tube Rodlet with 1.5 wt.% Natural Boron Concentration.

Subcooling Case (°C)	920 MJ Power Pulse	1157 MJ Power Pulse	1407 MJ Power Pulse
40	2.8	3.6	4.6
30	3.0	3.6	4.8
20	3.0	4.0	5.0
10	3.2	4.2	5.4
0	3.8	4.8	6.2
Total Rod Energy deposition:	**4635.6 J**	**5829.8 J**	**7089.5 J**

Table 5. CHF multipliers for the Tube Rodlet with 2.0 wt.% Natural Boron Concentration.

Subcooling Case (°C)	920 MJ Power Pulse	1157 MJ Power Pulse	1407 MJ Power Pulse
40	3.4	4.4	5.6
30	3.6	4.6	5.8
20	3.8	4.8	6.2
10	4.0	5.2	6.8
0	4.8	6.0	7.8
Total Rod Energy deposition:	**5349.4 J**	**6727.4 J**	**8181.1 J**

CHAPTER 4

INCORPORATING BORON GRADIENTS INTO HEATER ROD EXPERIMENT

The unique contributions of the work in this chapter investigated the potential to shape both the axial and radial power profiles of the borated heater tube designed at INL, through additive manufacturing of axial and radial boron gradients. The motivation of this was to provide an alternative approach to fabrication of these heater specimens. The analysis in this chapter was involved with the multiphysics modeling work under task two of the specific project flow chart discussed in section 1.2.2. Having developed the initial design of the borated heater rodlet, it is desired to shape the power curve so that the CHF phenomenon occurs at the optimal observation location during experiments. Therefore, the objective of such approach is to provide a method that can ensure that the peak PCFs, and thus heating, upon the application of a TREAT power pulse on the borated test specimen occurs at the center region of heater test device through incorporation of axial boron gradients. Furthermore, the manufacturing of radial boron gradients was analyzed to study the potential of flattening the radial power profile of the borated heater to address potential melting at the surface of this material as a result of power peaking due to self-shielding effects. During the first TREAT experiments carried out in December of 2019, an hourglass tube geometry was utilized to shape the axial profile and achieve the maximum heat flux at the center of the borated experiment [116]; the investigation presented here provides an alternative approach.

In this chapter, axial and radial boron gradients cases were studied separately through neutronics and thermal hydraulics computational analyzes. First, a neutronics analysis of a homogeneous content borated rodlet were compared to those of a rodlet containing axial and radial boron gradients. Following, the expected shape of these two borated tube rodlets was analyzed using a thermal hydraulics RELAP5-3D model that incorporated decoupled data from the

neutronics analysis in this chapter. The axial shape of the generic curve was analyzed for three different power pulses, as well as investigate how the DNB event affects the axial power profile with emphasis on the behavior of the power curve over time.

4.1 Neutronics Study

4.1.1 Axial Boron Gradient Performance

The neutronics study in this chapter was conducted using the full core Serpent model of the TREAT facility that was provided by INL [108]. The components of the TREAT in the model were kept the same, with the exception of the insertion of a borated heater geometry used to represent the borated heater tube specimen with a total height of 10.16 cm. Two cases were modeled using this approach; a homogeneous (2.0 wt.%) boron tube, and a borated heater tube with incorporated axial boron gradients to shape the PCFs (~2.0 wt.% for center 2.54 cm region, decreasing to 0.19 wt.% at top/bottom end regions). The objective of this neutronics study was to shape the HF power shape using axial boron gradients. Benefits included enhancing the power peaking near the axial center of the rodlet so that CHF occurs at this region where the instrumentation is located. Further, this effort also addressed the prevention of considerable heat transfer that may lead to melting of welding near the top/bottom edges of the borated tube.

For both cases, the borated tube within the model was discretized into 16 equal height axial regions each 0.635 cm in height, with each being split into 4 equal volume areas (total of 64 equal volume cells for the heater tube), as shown in Figure 18. The heat detectors feature of Serpent was used to determine the heat generation within these 64 regions. This was then used to develop a heat generation map of the two considered boron tube cases, using PCFs to characterize each volume cell within the borated heater rodlet model. These PCFs were calculated using equation 10 in section 3.2.3. To achieve convergence of the heat generations calculated using Serpent for each

of the considered regions within the borated rodlets, a neutron population of 2,000,000 was used, along with 30 inactive and 100 active cycles to achieve Shannon entropy convergence and less than +/- 20 pcm statistical inaccuracy.

The resulting PCFs for the axial boron gradients study, displayed in Figure 19, shows how the shaping of the axial power curve can be achieved through additive manufacturing. The homogeneous boron gradient tube rodlet shows high peaking PCFs along the entire outer radial region of its axial length. In the case of the rodlet with axial boron gradients these relative high peaking PCFs have been confined to the outer radial region of the center of the rodlet, and thus, this is where the highest heating rates will occur. Another important observation in the homogeneous case, is that there appears to be an axial self-shielding effect as well as the expected radial self-shielding for which higher PCFs are observed in all of the radial segments of the outer most axial regions. These PCFs are higher on the edge axial regions due to the larger surface exposure through which moderated neutrons can enter, and could lead to melting of the welding holding the borated rodlet to the experimental capsule holder during TREAT testing. Using axial boron gradients, this axial self-shielding effect observed in the homogeneous case can be eliminated as shown in Figure 19, highlighting another advantage of the axial boron gradients tube.

4.1.2 Radial Boron Gradients Performance

Following the axial boron gradient study, shaping the radial profile of the boron tube specimens for TREAT experimentation was also analyzed. For this specific study, the reason behind flattening the radial HF power shape (which natural peaks towards the outside due to self-shielding) using boron gradients, is to possibly prevent melting at the outer edges of the heater tube during transient CHF power pulse testing in TREAT. The Serpent Monte Carlo code was used to determine PCFs for a case for which the flattening of the radial power profile is the objective.

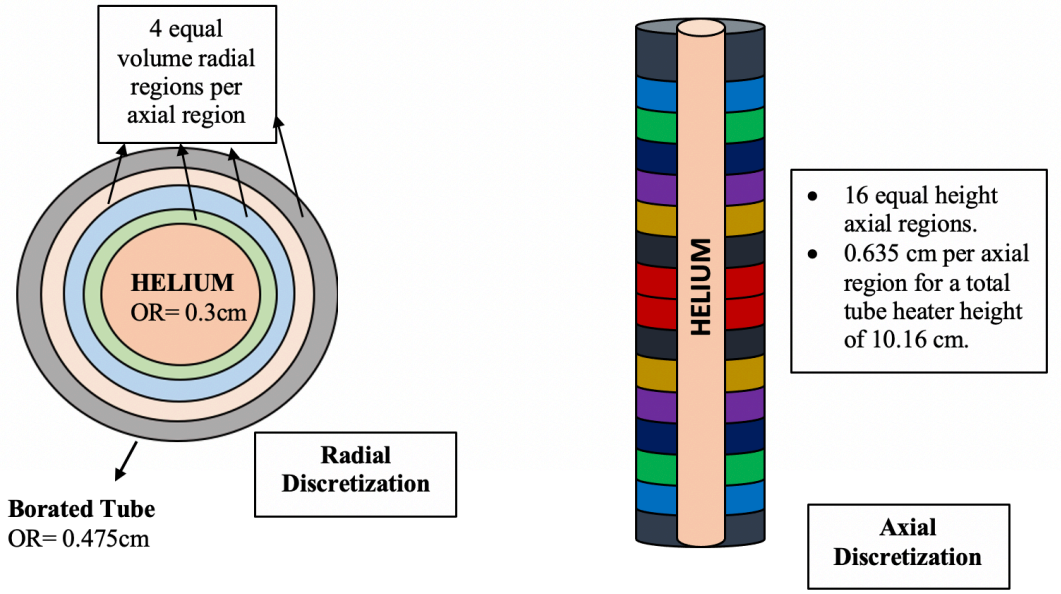

Figure 18. Serpent model axial and radial discretization of the borated tube geometry for boron gradients neutronics analysis.

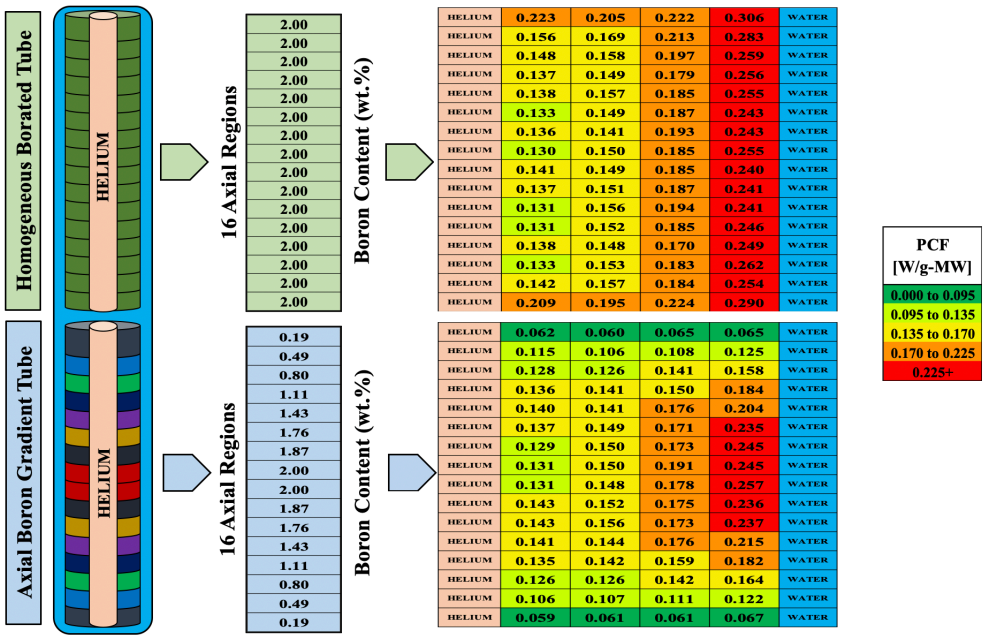

Figure 19. PCFs comparison between the homogeneous content borated tube and the chosen axial boron gradients case. boron content in wt.% for both of these cases is shown.

A homogenous boron heater tube case was compared to a case that had radial boron gradients incorporated, and radial power profiles were generated for both. The goal of this study was to show what radial boron concentrations are needed to generated a uniform radial power profile relative to the homogeneous case. To achieve convergence of the heat generations calculated using Serpent for each of the considered regions within the borated rodlets, a neutron population of 100,000 was used, along with 30 inactive and 100 active cycles to achieve Shannon entropy convergence and less than +/- 20 pcm statistical inaccuracy. Reactor power in the TREAT model was set to 1000 W to normalize the heat generation rates.

The radial boron content distribution of the homogeneous and chosen radial boron gradient cases is shown in Table 6, as a function of radial length. As shown, the chosen radial gradient case had a boron content of around 1.00 wt.% on the outside, increasing to 2.00 wt.% in the center region. The radial PCFs were compared to that of the homogeneous 2.0 wt.% natural boron case and shown in Figure 20. These PCFs are averaged axially for the tube thickness of the respective radius, and show how the power curve can be flattened to eliminate the effects of self-shielding observed in the homogeneous borated case.

4.2 Thermal Hydraulics Study

4.2.1 Methodology

The goal of the thermal hydraulics analysis in this section was to investigate the heat transfer behavior of the axial boron gradient rodlet for applications of power pulses in TREAT. Furthermore, characterizing how the CHF phenomenon affects the shape of the power curve of the borated axial gradient heater device was also investigated. The basis of the TH study was the neutronics data from the axial boron gradient study in section 4.1.1. The PCFs that were determined during this neutronics study were decoupled into a RELAP5-3D simplified model of

Table 6. Comparison of the radial boron content distribution between the homogeneous case and the radial BG case chosen.

Radial Cylinders (cm)	Homogeneous Tube Boron Content (wt.%)	Radial Gradient Tube Boron Content (wt.%)
0.000 to 0.300	None	None
0.300 to 0.352	2.00	2.00
0.352 to 0.397	2.00	1.76
0.397 to 0.438	2.00	1.43
0.438 to 0.475	2.00	1.00

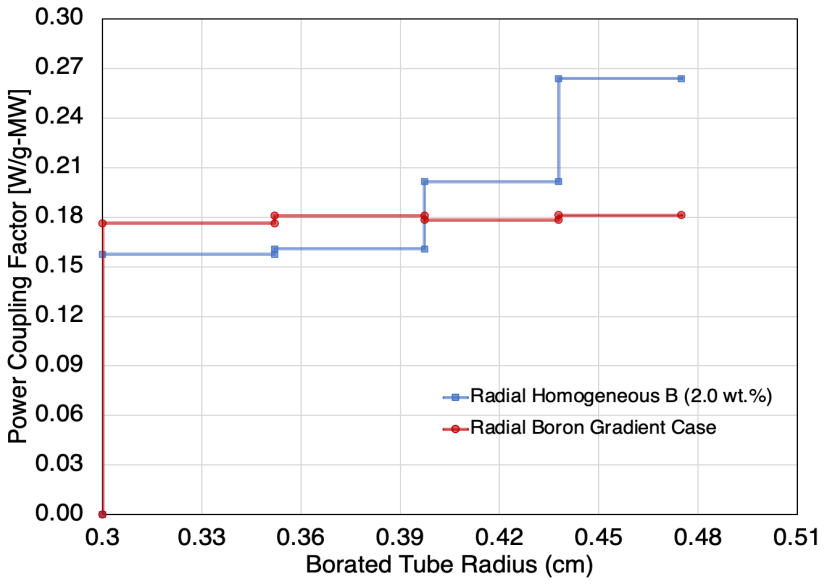

Figure 20. Radial PCFs of the comparison between homogeneous and radial boron gradient case.

the SERTTA capsule that held this borated heater tube within the water capsule. Essentially, the neutronics data indicated the amount of axial and radial hear generation for the HT used to represent the heater tube in the RELAP5-3D model. The tube geometry was modeled according to that of the borated tube with a constant radial thickness throughout its 10.16 cm height, and inner and outer diameters of 0.60 cm and 0.975 cm respectively. Once the PCFs were integrated into the RELAP5-3D model, shown in Figure 21 along with model specifications, the CHF multiplier was set to a value of 100 to inhibit the occurrence of the CHF phenomenon for the purpose of studying the influence of increasing energy depositions on the HF power curve of the axial BG heater tube. Following, the occurrence of CHF was included to study its effects on the shape of the HF power curve. To predict the CHF value, the 2006 Groeneveld LUT feature of RELAP5-3D was used. For all of these analyses, 20 degrees of subcooling was provided to the system. At 500 psi, this means that the system was initialized to 493°C.

4.2.2 Influence of Energy Deposition on the HF power curve

The thermal hydraulics analysis in this chapter began with studying the influence of the energy deposition of different transient power pulses on the shape of the heat flux power curve of the axial boron gradient borated rodlets. For this study, three gaussian shaped TREAT power pulses were considered with energy depositions, peak power and full width half maximums (FWHMs) shown in Table 7. This study was done to demonstrate how the HF power curve of the axial boron gradient heater would be influence during experiments in TREAT that utilized different power curves. One drawback is that RELAP5-3D is not capable of capturing the transient heating CHF value enhancements. The heating rate would increase (and thus this enhancement) as a result of an increase in power pulse energy deposition rate. The results of the effects of energy deposition on axial heat flux curve of the borated gradient heater is shown in Figure 22. The

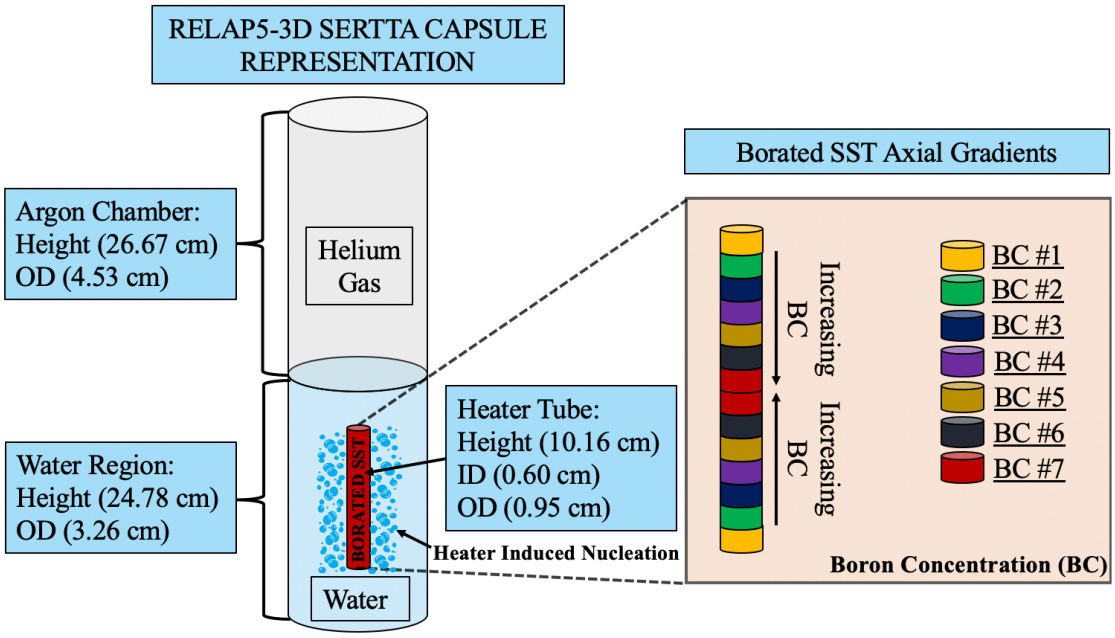

Figure 21. RELAP5-3D model consisting of the axial boron gradient tube rodlet held within the SERTTA capsule.

RELAP5-3D heat transfer prediction results show that the shape of the power curves is not impacted by the total TREAT power pulse energy deposition. Nevertheless, the effect of increasing the power pulse energy results in a higher magnitude of the values of the HF for the power curve of the borated rodlet. These cases involved a high CHF multiplier in RELAP5-3D to inhibit the occurrence of this phenomenon. The HF power curves have a larger curvature than that of the radial averaged PCFs comparison, as a result of self-shielding effects enhance the power peaking near the center.

4.2.3 Influence of the CHF Phenomenon on the Shape of the Power Curve

The focus of the thermal hydraulics analysis was now to investigate how the CHF phenomenon impacts the shape of the power curve. To study the influence of the CHF phenomenon on the shape of the power curve over time, a case for which the CHF was exceeded in the center region was analyzed. This case was chosen because this is the region where CHF occurrence is preferred during TREAT testing. The 920 MJ power pulse from Table 7, was chosen for this analysis. The analysis shows that before CHF is exceeded the shape of the HF power curve doesn't not change as you would expect during this nucleate boiling heat transfer dominated regime; remains same as that prescribed initially. When CHF is exceeded in the center axial length of the heater rod, because of the higher boron concentration and thus enhanced heating in this region, the heat flux immediately drops, as modeled by RELAP5-3D, due to a decreased heat transfer efficiency, see Figure 23. This results in an increased surface temperature of the borated heater rodlet within this region, see Figure 24. As we can see from the analysis of this specific case, the shape of the power curve permanently changes for the remainder of the TREAT experiment following the application of the power pulse. Therefore, this study determined that the CHF location along the axial height of the borated heater strongly influences the shape of the power curve over time.

Table 7. Characteristics of the TREAT transient pulses used in this study.

Power Pulse Case	TREAT Peak Power (MW)	FWHM (msec)	Total TREAT Energy Deposition (MJ)
Power Pulse 1	9,243.0	92.5	920.0
Power Pulse 2	9.998.0	102.2	1,157.0
Power Pulse 3	13,661.0	90.0	1,407.0

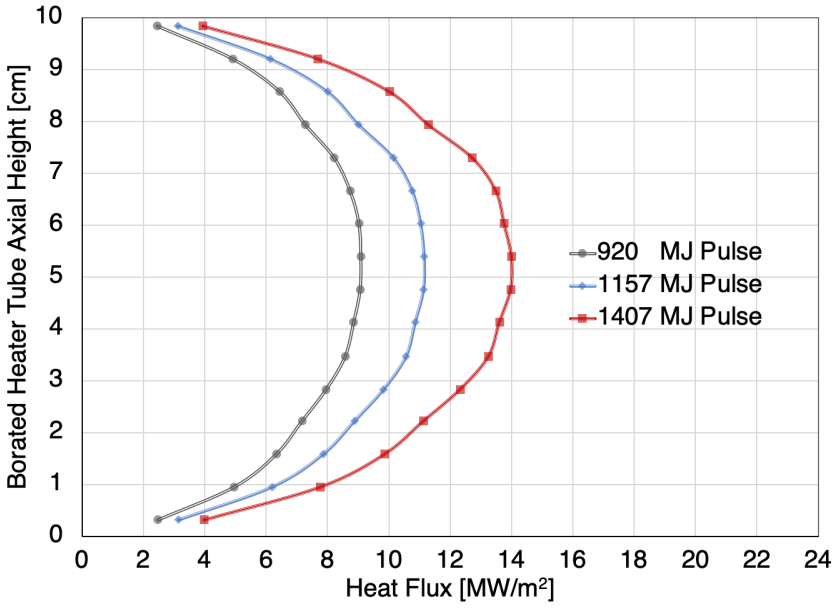

Figure 22. Heat flux power profiles of the axial boron gradient case for the three considered power pulses.

4.2.4 Influence of the CHF Phenomenon on the Shape of the Power Curve

The focus of the thermal hydraulics analysis was now to investigate how the CHF phenomenon impacts the shape of the power curve. To study the influence of the CHF phenomenon on the shape of the power curve over time, a case for which the CHF was exceeded in the center region was analyzed. This case was chosen because this is the region where CHF occurrence is preferred during TREAT testing. The 920 MJ power pulse from Table 7, was chosen for this analysis. The analysis shows that before CHF is exceeded the shape of the HF power curve doesn't not change as you would expect during this nucleate boiling heat transfer dominated regime; remains same as that prescribed initially. When CHF is exceeded in the center axial length of the heater rod, because of the higher boron concentration and thus enhanced heating in this region, the heat flux immediately drops, as modeled by RELAP5-3D, due to a decreased heat transfer efficiency, see Figure 23. This results in an increased surface temperature of the borated heater rodlet within this region, see Figure 24. As we can see from the analysis of this specific case, the shape of the power curve permanently changes for the remainder of the TREAT experiment following the application of the power pulse. Therefore, this study determined that where along the axial height of the borated heater the occurrence of the CHF manifests, strongly influences the shape of the power curve over time.

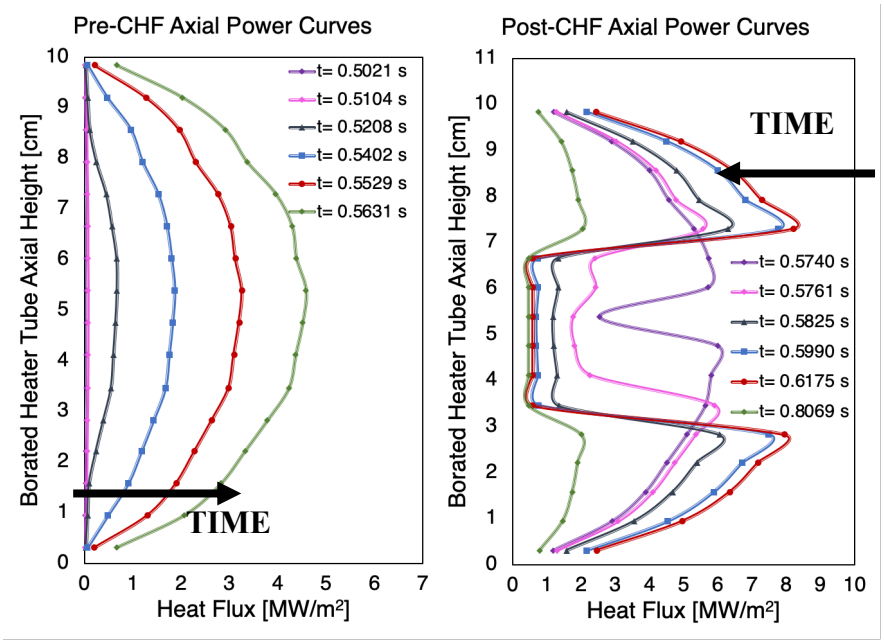

Figure 23. Pre-and-post CHF axial HF profiles for the borated heater tube as a result of application of power pulse in TREAT.

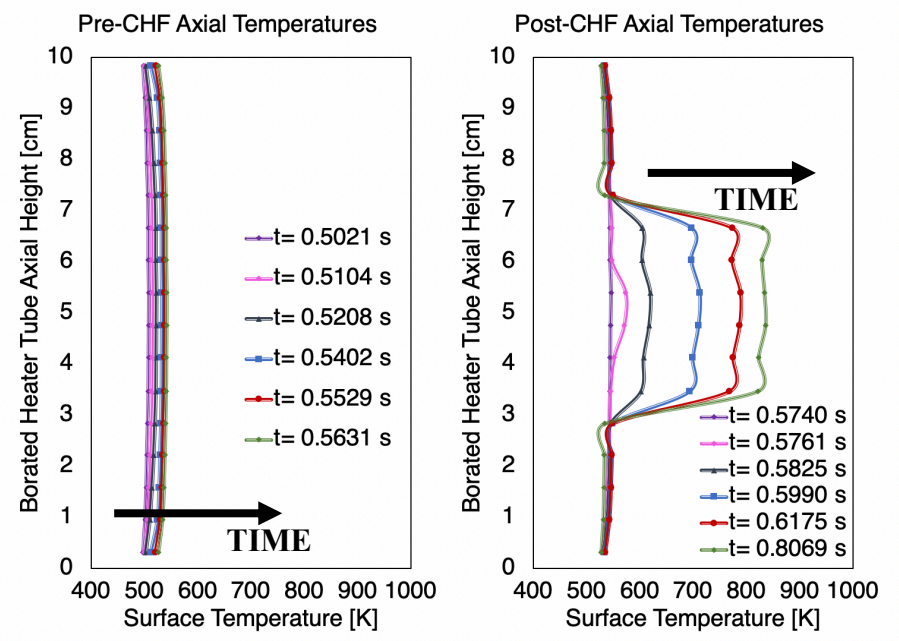

Figure 24. Pre-and-post CHF axial cladding temperatures for the borated heater tube as a result of application of power pulse in TREAT.

CHAPTER 5

VALIDATION OF MULTIPHYSICS MODELING CAPABILITIES

The contribution of the work presented in this chapter fall under task 3 of the overall project flow chart discussed in section 1.2.2. This work involved utilizing the data extracted from the INL conducted TREAT experiments, to validated the models that led to the analysis discussed in Chapter 6. Having developed the multiphysics capabilities needed to develop the initial informative design matrix for the separate effects borated heater experiments, the next step in the hierarchy of the computational approach is to validate the developed models being used to represent these CHF experimental rodlets in TREAT. Therefore, the work in this chapter presents a study that provides validation of the RELAP5-3D program and models that are being/were used for the associated work related to this laboratory directed research project. The objective was to build a RELAP5-3D model of the hourglass borated (2.0 wt.%) stainless steel type-304 tube heater experiment that was inserted into TREAT for the December 2019 tests, and compare experimental data to those of RELAP5-3D predictions. The data provided by INL consisted of TC temperature histories for four different transients with very similar energy depositions. For this study, the peak surface temperature and capsule water temperature histories of two of the transients were compared to predictions from RELAP5-3D, as well as other parameters, simulating the same conditions. Furthermore, having compared the results, the scope of the study also consisted of discussing where the major sources of uncertainties originated from. Lastly, a best fit model was developed using sensitivity study methods that generated a more accurate model prediction of the maximum peak surface temperature.

5.1 Methodology and RELAP5-3D Model Description

The overall methodology approach of this multiphysics validation study consisted of developing the RELAP5-3D models neccesary and decoupling these with neutronics results, comparing the RELAP5-3D predictions with those results from the December 2019 TREAT runs, followed by identifying the sources of uncertainties and development of a best fit model. Figure 25 and Table 8, summarize the overall specifications of the developed RELAP5-3D model, which consisted of an hourglass rodlet because this was the configuration used in the TREAT experimental runs. The RELAP5-3D model represented a simplified version of the SERTTA capsule with a Helium chamber and a water segment represented by a pipe structure. The helium and water sections had a height of 27.43 cm and 25.61 cm respectively. To represent the hourglass tube heater within the SERTTA capsule, 18 SS-304 heat structures (HTs) were utilized with different axial heights and outer radial lengths. The outermost HTs had an outer radius of 0.4826 cm, decreasing to an outer radius of 0.3658 cm for the center region HTs. The combined HTs had a total axial height of 10.16 cm, and all of the heat structures had an inner radius of 0.2769 cm. Further, the water region was split into 6 different sections including one above and below the hourglass HT and four sections surrounding the HTs representing the hourglass heater each with a height of 2.54 cm. The model was then initialized to atmospheric pressure and room temperature (293K) to replicate the systematic experimental conditions of the TREAT runs. To represent characteristic TREAT pulses applied during the TREAT experiments, a general table was introduced into the model that presented MW of reactor power as a function of time. Neutronics analysis of the 2.0 wt.% borated SS-304 hourglass tube heater was conducted using the Monte Carlo N-Particle (MCNP) code, and the data was coupled into the RELAP5-3D model.

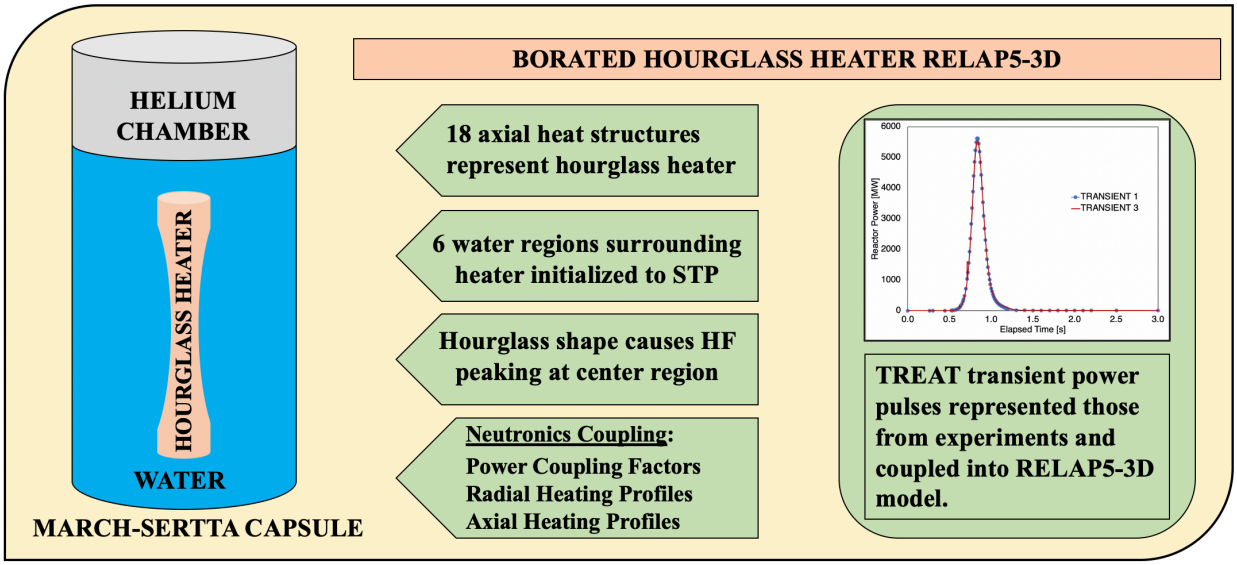

Figure 25. Characteristics and methodology of the RELAP5-3D model used for validation with experimental TREAT testing data.

Table 8. Geometric Specifications of the RELAP5-3D Borated Hourglass Heater Model.

Component	Component Value	Units
Length of Helium Chamber	2.743 e-01	m
FA of Helium Chamber	1.830 e-03	m^2
Length of Water Segments	2.561 e-01	m
FA of Water Above HTs	1.303 e-03	m^2
FA of Water surrounding HTs	1.149 e-03	m^2
FA of Water Below HTs	7.809 e-04	m^2
Number of Axial HTs	18	
Inner Radius of HTs	2.769 e-03	m
Outer Radius of Top/Bot HTs	4.826 e-03	m
Outer Radius of Center HTs	3.658 e-03	m
Heat Structure Material	Type-304 Stainless Steel	

5.2 Comparison of RELAP5-3D Results with Provided TREAT Experimental Data

Following the development of the RELAP5-3D model, comparisons were made between several RELAP5-3D predictions and the results of two of the four (transients 1 and 3) of the December 2019 TREAT transient experimental runs. The compared metrics included:

- Comparison of peak surface temperatures of the hourglass rodlet and time occurrence of these temperatures resulting from transient power pulses.
- Comparison of wall superheat duration between RELAP5-3D and TREAT experimental runs.
- The capsule system thermal equilibrium and the change in the system's thermal equilibrium temperatures after the application of the TREAT power pulse.
- Comparison of the overall transient pulse capsule system thermal behavior response of the RELAP5-3D model and the experimental runs.

The results of the metric comparisons between RELAP5-3D predictions and transients 1 and 3, shown in Figure 26 with TREAT energy depositions equal to about 1062 MJ and 1054 MJ respectively, is shown in Figure 27 and Table 2. These are discussed in detail in this section. For the experimental data, transient 1 is believed to be on the cusp of CHF but post-CHF behavior doesn't fully manifest. Whereas in transient 3, it is a bit clearer that post-CHF behavior was briefly experienced as can be seen from the rise in surface temperature. The data from the third thermocouple (TC3), which is located just above the center of the hourglass rod, and the RELAP5-3D predictions for the HT just above the center was chosen to conduct this comparison analysis.

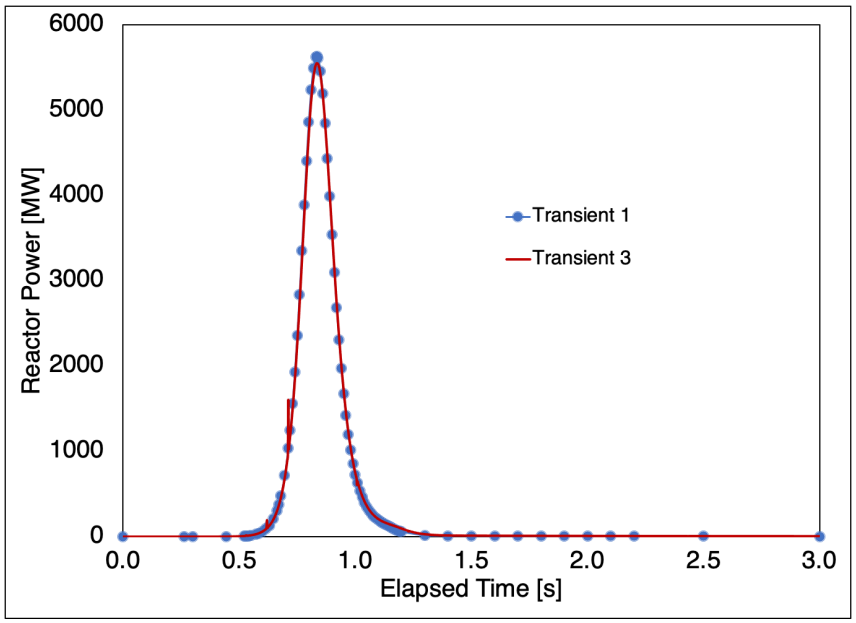

Figure 26. Characteristic TREAT power pulses used in the validation of the RELAP5-3D model.

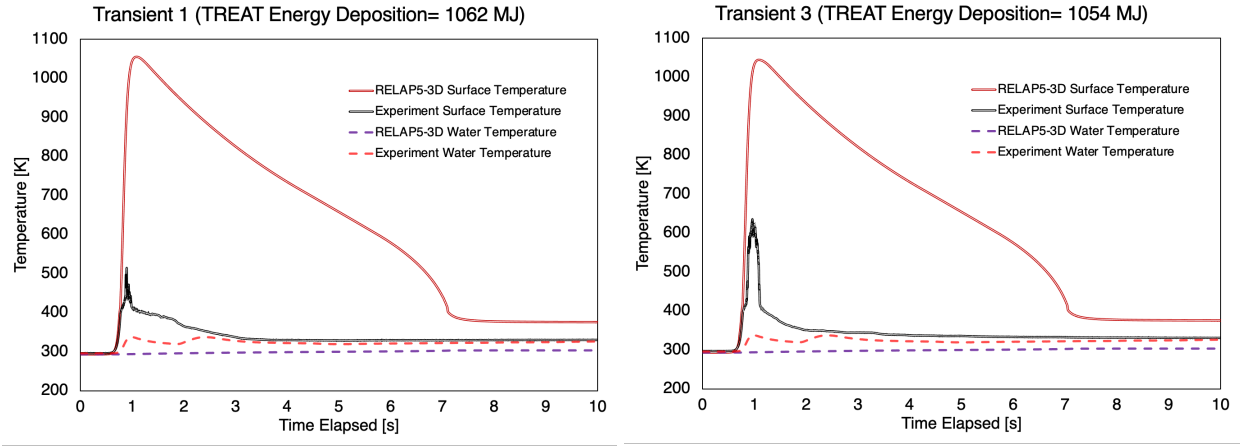

Figure 27. Borated heater surface and water capsule temperatures comparison between experimental data and RELAP5-3D predictions.

Table 9. Comparison of chosen metrics of experimental results and RELAP5-3D predictions for both transients.

Parameter	Transient 1			Transient 3		
	Experiment	**RELAP5-3D**	**Difference**	**Experiment**	**RELAP5-3D**	**Difference**
Peak Surface Temperature	514.1K	1055.5K	105.4 %	634.9K	1044.4K	64.5 %
Time of Peak Surface Temperature	0.893 secs	1.084 secs	21.4 %	0.961 secs	1.084 secs	11.4%
System Thermal Equilibrium Temperature (*post transient*)	~328.0K	~373.0K	13.7 %	~334.0K	~373K	11.7 %
Thermal Equilibrium Temperature Change	35.0K	80.0K	128.6 %	41.0K	80.0K	95.1%

1. **Comparison of peak surface temperatures of the hourglass rodlet and time occurrence of these temperatures resulting from transient power pulse application.**

As shown in Figure 3, RELAP5-3D greatly overpredicts the surface temperature for both experimental transient runs. From Table 1, the peak surface temperature for the experiment in transients 1 and 3 was indicated to be 514.1K and 634.9K respectively. Whereas, RELAP5-3D predicted a clear manifestation of post-CHF behavior with maximum surface temperatures of 1055.5K and 1044.4K for transients 1 and 3 respectively. Shown in Table 1 are also the time occurrence of the peak surface temperatures, which are overpredicted in the RELAP5-3D model for both transients. The resulting difference in values between model and experimental data that are also shown in Table 1 for both transients. RELAP5-3D provides a better fit to experimental data for transient 3 because of the more pronounced post-CHF manifestation experienced during this experimental run.

2. **Comparison of wall superheat duration between RELAP5-3D and TREAT experimental runs.**

The RELAP5-3D model also overpredicted the duration of superheated surface temperatures, as shown in Figure 3. Superheat was characterized by the surface temperature exceeding the saturated temperature of the liquid, ~373K, assuming no significant pressurization of the experimental capsule since the tests were conducted at atmospheric pressure for a relatively low power pulse energy insertion. During the experiment the surface temperature was measured to be superheated by about less than 2 seconds for both transients. Whereas in RELAP5-3D, both transient resulted in surface superheat temperature durations of around 7 seconds.

3. **Comparison of the capsule system thermal equilibrium and the change in the systems thermal equilibrium temperatures after the application of the TREAT power pulse.**

Comparisons between the TREAT runs and RELAP5-3D can also be made for the thermal response of the SERTTA capsule system due to the applied transients, shown in Table 1. Both the experimental and the model were initialized to room temperature (~293K). The experimental and RELAP5-3D thermal equilibrium of the capsule system after the application of the pulse were about 328K and 373K respectively for transient 1, and about 334K and 373K respectively for the transient 3. This constituted a higher increase in capsule temperature in the RELAP5-3D model than in the experimental data, with the percent differences displayed in Table 1.

4. **Comparison of the overall transient pulse capsule system thermal behavior response of the RELAP5-3D model and the experimental runs.**

The last step of the validation study comparison and discuss the overall system response to the applied TREAT power pulses for both the model and experimental runs. For both transients, RELAP5-3D underpredicts the value of CHF which results in an overprediction of the surface temperatures as well as the duration of post-CHF behavior including the wall superheat duration, and heat transfer into the coolant. The RELAP5-3D model also underpredicts the heating rate of the coolant surrounding the capsule. In the TREAT experimental runs, the coolant temperature quickly rises, between 1-3 secs, as thermal energy is transferred from the borated heater and the system is very close to reaching its new post-transient thermal equilibrium within 10 seconds after power pulse application. Whereas, RELAP5-3D models the heat transfer at the boundary condition between the coolant and the surface of the borated heater differently. The initial thermal response of the coolant in the RELAP5-3D model, due to the application of power pulse transients, results in an initial jump in temperature that is about 5K. Following, RELAP5-3D models a very slow increase (upwards of 20,000 seconds) in coolant temperature up to the saturation point (~373K) for both transients as a result of the initial post-CHF film boiling phase and the subsequent

modeling of the surface-to-coolant heat transfer under natural convection conditions once the heater surface has reached the saturation temperature (lack of nucleation heat transfer enhancement). Note that the fluid temperature provided by RELAP5-3D is that of the bulk coolant volume and that of the experiment is at a specified location.

a. Discussion of Sources of Uncertainty of Comparison between Experimental and RELAP5-3D Model Predictions

Having conducted a thorough comparison of the RELAP5-3D models and the TREAT experimental runs for the hourglass rodlet, a discussion of the major sources of uncertainties causing discrepancies between these two is included in this section. These sources of uncertainties included differences in predicted values of CHF and post-CHF behavior by the RELAP5-3D program and what is actually observed in the TREAT experiments, uncertainties in the multiphysics modeling decoupling, as well as experimental instrumentation uncertainties.

1. CHF Value Predictions:

The main source of discrepancies originates from the predictions of the value of CHF. RELAP5-3D only takes into account local or inlet hydrodynamic parameter conditions (e.g. X_{local}, P_{local}, G_{local}). But it has been shown that both rapid transient heating and in-pile radiation-induced surface activation (RISA) can enhance surface-to-coolant heat transfer. Because RELAP5-3D does not take these effects into account, it underpredicts the value of CHF and thus overpredicts the peak surface temperatures and wall superheat duration. This is probably the reason why RELAP5-3D predicted CHF conditions in both runs, whereas in the experiments CHF was briefly exceeded in transient 3 and, if any, in transient 1.

2. **Post-CHF behavior predictions by RELAP5-3D:**

Another source of uncertainties in the peak surface and duration of wall superheat between model and experimental is how RELAP5-3D characterizes post-CHF behavior. Gorton [117] has shown that there are major differences post-CHF behavior between actual experimental post-CHF behavior and RELAP5-3D; the main takeaway is that the latter is more conservative and this explains why the time of wall superheat temperature predicted by RELAP5-3D is much larger.

3. **Uncertainty in the neutronics and TH models as well as coupling:**

The uncertainty in calculated PCFs from the neutronics data can also cause sources of discrepancies as this propagates on the RELAP5-3D model. This includes statistical deviations using the MCNP code, and the lack of validation with experimental data to determine whether the experiment is actually generating somewhat similar PCFs as those predicted by the neutronics. Other sources of uncertainties include the simplifications that were assumed when representing the SERTTA capsule in the RELAP5-3D model, and the limitations of RELAP to only have the capability of 1-D conduction. These uncertainties could impact the maximum surface temperature because of their influence on the energy deposition inserted in the RELAP5-3D model.

4. **Uncertainties in the experimental data arising from the instrumentation and thermophysical properties uncertainties:**

The last major source of discrepancies between model and experimental results originate from uncertainties in the experimental instrumentation. Thermocouples (TCs) are known to be sources of major uncertainties when collecting data as shown in transients 1 and 3. Both included very similar transients and the same TC, but had two different surface temperature history results. Another source of uncertainty is the “fin effect” which hasn’t been taken into account in the provided data. This effect occurs when TCs are mounted directly onto the heated surface, and can

result in heat conduction/convection into the TC wire changing the surface temperature. Thus, the correct temperature measurements of the heated surface are not taken. Lastly, these also include uncertainties in the literature resulting from measurement of thermophysical properties which could result in different values of thermal conductivity and volumetric heat capacity for the rodlet. This could influence comparison parameters such as the time of wall superheat, and the maximum surface temperature.

b. Development of a RELAP5-3D Best-Fit Models for Comparison with TREAT Experimental Results

Having compared the initial RELAP5-3D model and discussed the different sources of uncertainties, the next step in the computational methodology approach towards validation of models with actual results is the development of best fit models that best match the results from the TREAT experimental runs in December of 2019. These best fit models can be developed through sensitivity studies, in order to generate either best match cases for a specific point within the TREAT experiments such as peak surface temperature, time of CHF or time of rewetting point, as well as being best fit models of surface-to-coolant heat transfer phases or averaged over the entire experimental run. Therefore, determining what these best fit models are intended to be a best match of is important in determining for what time period or event, the best fit case will be optimized for when simulating real life experiments. Furthermore, understanding the sources of uncertainties when developing best fit models is important in order to really understand the input parameters that will be of importance when conducting sensitivity studies to generate a best fit case. The scope of this section is then to provide an example of generating a best fit model to better represent a characteristic result from the TREAT experiment runs of December 2019.

For the scope of this section, the example best fit provided is intended to better match the peak surface temperature calculations of the RELAP5-3D hourglass model, relative to actual TREAT results for transient 3. For this example, the different sources of uncertainties impacting the RELAP5-3D model used to determine the considered parameters were discussed above, and can better help elucidate the discrepancies shown in Figure 27. To achieve developing this example best fit model, a sensitivity study of these uncertainty sources was conducted to understand how uncertainties in the material properties of the borated rodlet, clad-to-coolant heat transfer coefficients, predictions of the systematic value of CHF, as well as calculations of the rodlet PCFs are involved in deviations of the surface temperature in the RELAP5-3D model relatively to measured TREAT experimental results. The volumetric heat capacity and thermal conductivity of the borated simulator rod were varied ±20 %, to study uncertainties in the measurement data from the literature sources for which these values were taken, as well as geometrical discrepancies when utilizing assumptions to simplify the modeling representation of the hourglass rodlet and the SERTTA capsule. Further, the clad-to-coolant heat transfer coefficients natural convection factor, NC_F, the nucleate boiling factor, NB_F, the transition boiling factor, TB_F, as well as the film boiling factor, FB_F, were all varied ±20 % to account for uncertainties involved in clad-to-coolant heat transfer characteristics between RELAP5-3D modeling and TREAT experimental thermal behavior. The CHF multiplier, CHF_F, was also varied by up to a 500% increase to account for CHF influencing parameters experienced during TREAT testing that are not accounted for during the RELAP5-3D computational results. These include CHF enhancements resulting from transient CHF effects, as discussed by Bessiron [82], and RISA effects [79]. Lastly, the multiplier for energy deposition was arbitrarily varied by ±15 %, to account for uncertainties involved in the neutronics calculations of the PCFs data that was decoupled into the RELAP5-3D model. A summary of the

considered input parameters and range of value variations is shown in Table 10, along with the objective behind including the parameters in the sensitivity study.

A Latin Hypercubic Sampling (LHS) scheme was used to conduct the sensitivity study with the chosen FoM output being the peak surface temperature of the borated rodlet. To randomly pick values for these parameters within their respective ranges, a uniform distribution was utilized for these with 3000 different RELAP5-3D cases performed. The results of the sensitivity study involving the considered input parameters shown in Table 10, were then used to generate a best match parameter set for the peak surface temperature of the third transient TREAT experimental run during the December 2019 tests. To develop this best fit model, the peak surface temperature was compared to that of the TREAT experiment, and the model configuration that yielded the lowest relatively error between the two was deemed to be the best fit model. The results of the parameter multipliers that yielded the best fit model and a comparison between this configuration and the TREAT experimental results are shown in Tables 11 and 12. The best fit model has achieved a peak surface temperature prediction that has a 2.81% differential error relative to the TREAT experimental results, which is much more improved than the 64.5% observed in the comparison found in section 5.2. But as shown in Table 11 and Figure 28, this best fit model still overpredicts the duration of the post-CHF surface temperature behavior, the system's thermal equilibrium following the application of the transient pulse, as well as the time occurrences of CHF and the rewetting points. Therefore, although this best fit model has achieved a better prediction of the maximum surface temperature, there are still major different with how RELAP5-3D represents pre-and-post-CHF clad-to-coolant heat transfer characteristics. The trendline behavior the eight considered parameters in developing this best fit model relative to the peak surface temperature key FoM can be found in Figure 29.

Table 10. Summary of the range of value variations for the considered input parameters to develop the best fit RELAP5-3D model for the experimental results.

Parameter Multipliers	**Range of Variation**		**Sources of Uncertainties**
	Lower Bound	Upper Bound	
Volumetric Heat Capacity of Rod $\rho c_{p_{ss304}}$	0.8	1.2	Thermophysical properties data measurements and geometrical discrepancies.
Thermal Conductivity of Rod k_{ss304}	0.8	1.2	
Natural Convection Multiplier (NC_F)	0.8	1.2	Uncertainties involved with computational clad-to-coolant heat transfer characteristics when comparing RELAP5-3D vs. TREAT experimental.
Nucleate Boiling Multiplier (NB_F)	0.8	1.2	
Transition Boiling Multiplier (TB_F)	0.8	1.2	
Film Boiling Multiplier (FB_F)	0.8	1.2	
CHF Multiplier (CHF_F)	0.5	5.0	Uncertainties in predictions of the value of CHF comparing RELAP5-3D vs. TREAT experimental.
Energy Deposition (E_{dep})	0.85	1.15	Uncertainties in neutronics decoupled calculation of the PCFs characterizing the heat generation response in the borated rodlet resulting from a TREAT pulse application.

Table 11. Comparison of the peak surface temperature between the best fit model and the TREAT experimental results from Transient #3.

Parameter	**Transient 3**		
	Experiment	**RELAP5-3D**	**Difference**
Peak Surface Temperature	634.9K	652.77K	2.81 %
Time of Peak Surface Temperature	0.961 secs	1.147 secs	19.4 %
System Thermal Equilibrium Temperature (*post transient*)	~334.0K	~373K	11.7 %
Thermal Equilibrium Temperature Change	41.0K	80.0K	95.1 %
Time of CHF	0.841 secs	0.9135 secs	7.3 %
Rewetting Point	1.113 secs	3.079 secs	176.6 %

Table 12. Generated best fit model parameter configuration from the sensitivity study.

Parameter	Best Fit Value
Volumetric Heat Capacity of Rod $\rho c_{p_{ss304}}$	1.046
Thermal Conductivity of Rod k_{ss304}	1.031
Natural Convection Multiplier (NC_F)	1.190
Nucleate Boiling Multiplier (NB_F)	0.813
Transition Boiling Multiplier (TB_F)	1.115
Film Boiling Multiplier (FB_F)	1.138
CHF Multiplier (CHF_F)	4.496
Energy Deposition (E_{dep})	0.931

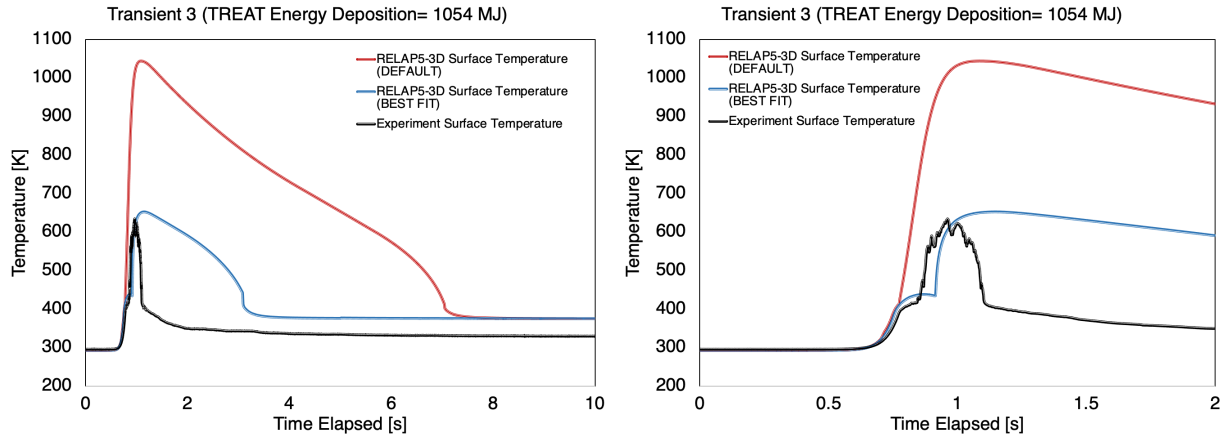

Figure 28. Comparison of TREAT borated heater experimental results with the best fit configuration for the RELAP5-3D model using the peak surface temperature as the key FoM.

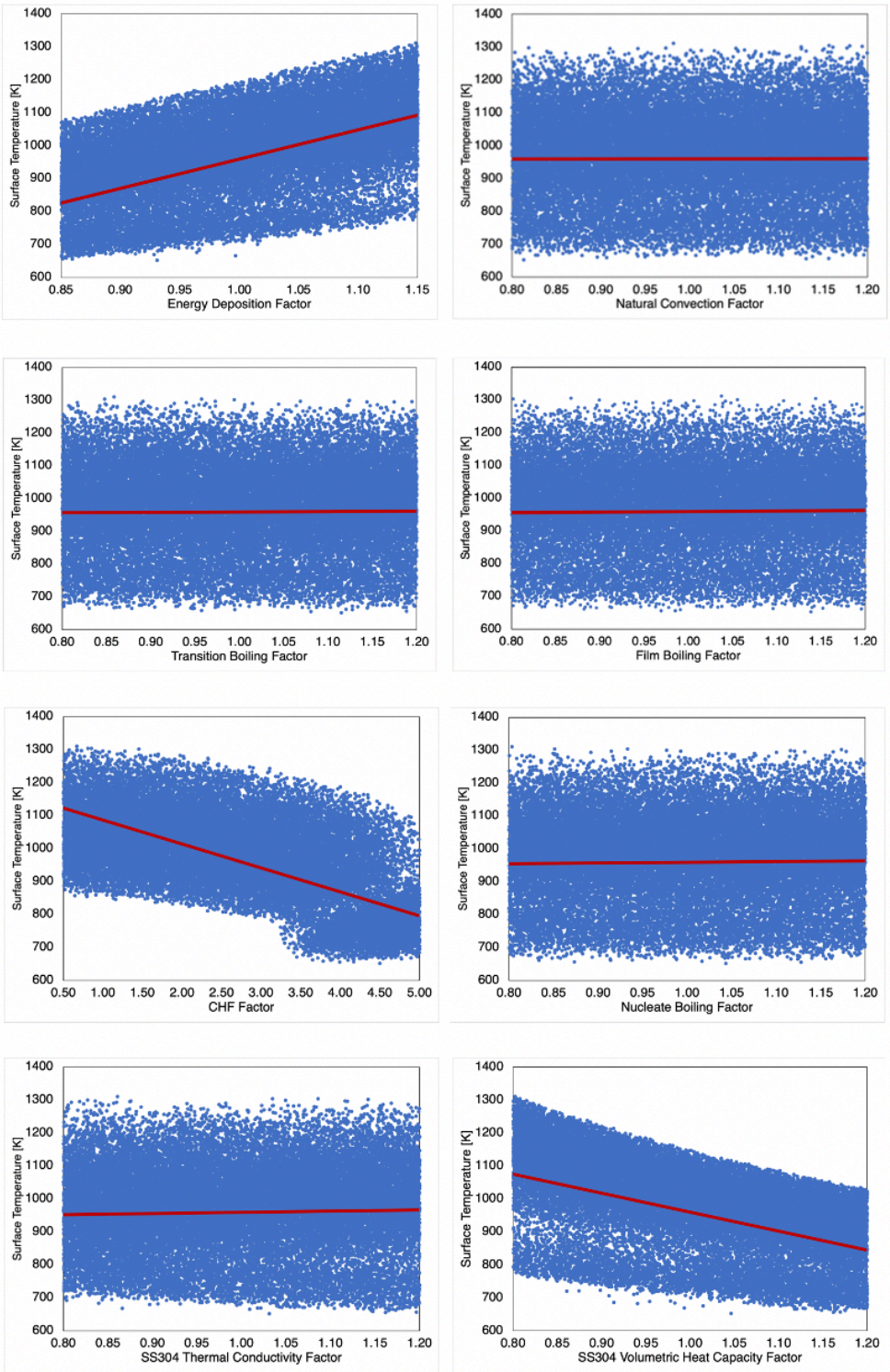

Figure 29. Trendline behavior of the considered eight input parameters in the development of the best fit model relative to the peak surface temperature.

To further elucidate on the limitations of the developed example best fit model used to better match the surface temperature, a detailed interpretation of the comparison between this model and the actual experimental results in Figure 28, will be discussed here using the time-dependent behavior of the peak surface temperature. The surface-to-coolant heat transfer behavior in Figure 28, can be described by several time periods including pre-CHF and post-CHF as well as the time occurrence of the rewetting and CHF point.

1. Pre-CHF time period:

The pre-CHF time period occurs up to just before 0.841 secs in the actual TREAT experiments, and up to 0.935 secs in the example best fit model as shown in Figure 28. Thus, although this model better predicts surface temperature, it still overpredicts the time duration of the pre-CHF time period by about 7.3%. This also means that the model overpredicts the time duration of the nucleate boiling surface-to-coolant heat transfer phase of the boiling curve, as can be seen from the duration of the pre-CHF exponential temperature increase at the surface. One positive observation in this pre-CHF time period comparison between the example best fit model of the peak surface temperature and the actual experiments is that the time-dependent surface temperature behavior of the experiment is closely matched by the RELAP5-3D model up until 0.841 secs which when CHF is detected in the TREAT experiments. Thus, this shows that the RELAP5-3D model is capable of capturing the nucleate boiling regime exponential behavior of the experiment, while not being capable of accurately capturing the timing duration of this heat transfer mode. Thus, an important takeaway is that although the example best fit model better matches the peak surface temperature, it is not a valid best fit capable of capturing the time of CHF leading to differences in pre-CHF behavior relative to actual TREAT experimental results.

2. Post-CHF time period:

Next a discussion of the comparison surface temperature behavior in the actual experiment and predictions by the RELAP5-3D best fit model optimized for the peak surface temperature is included here. The most noticeable observation during the post-CHF time period shown in Figure 28, is the discrepancies between the rewetting time period of the RELAP5-3D best fit model, versus that from the actual TREAT experiment. This is a result of differences between the correlations used to predict surface-to-coolant heat flux transfer in the models, as well as the exclusion of several impacting parameters fail to capture the enhanced heat transfer at the surface, such as, in-pile RISA which increase the wettability of the surface. Furthermore, there are other experimental instrument impacting factors that could create these discrepancies such as the enhanced heat transfer removal due to the localization of the thermocouples on the surface of the borated heater device creating an additional heat sink. These enhanced heat removal efficiency effects are capture with the example best fit model and thus overpredict the duration of elevated surface temperatures during the post-CHF time period. Another limitation of this best fit model for the peak surface temperature towards comparison with the overall experiment is its failure to accurately capture the long-term change in thermal equilibrium of the entire experimental capsule system.

3. Discussion of Developing Best Fit Models:

The purpose of interpretating in a detailed manner a comparison of the developed best fit model and the actual TREAT experimental results is to show its limitations due to its intended purpose. Because the scope of the best fit modeled developed here was to better capture the peak surface temperature, this model is not the optimized to best capture the time-dependent behavior of the surface temperature at other time periods relative to the actual TREAT experiments. In the

pre-CHF time period, the model less accurately captures the time of CHF which results in differences in the behavior of the surface temperature during this time period phase. Furthermore, in the post-CHF phase the model does not accurately capture the time of rewetting and thus overpredicts the duration of the post-CHF film boiling phase during which elevated surface temperatures are experienced. Thus, if the interest is to develop a best fit model that better predicts the pre-CHF surface temperature, a best fit model that best fits the time of CHF is needed to be developed. Likewise, if the intended target is to better predict post-CHF behavior, a best fit model that best fits the rewetting point can be developed. Lastly, in order to develop an overall best fit model sensitivity studies must be conducted in a methodological way so that an averaged optimized case that best fits the surface temperature behavior during all heat transfer modes of the boiling curve, as well as the peak surface, time occurrence of CHF and the rewetting point is needed.

CHAPTER 6

IMPACTS OF EXPERIMENTAL INTEGRAL PWR HEATER FUEL SYSTEM THERMOPHYSICAL PROPERTIES

6.1 Heat Transfer Time Constant Effects of TREAT Experimental Fuel/Cladding Fuel System Designs.

The work presented in this chapter aims at elucidating the potential impacts of the CHF event on the fuel-to-coolant heat transfer mechanisms of integral PWR fuel systems under rapid heating conditions, such as during an RIA, utilizing the thermal transfer time constant definition discussed in section 2.5.1 as the fundamental basis of the analysis. Having completed the computational analysis related to the design of the separate effects testing using the novel borated heater, this chapter investigates the uncertainties in heat transfer behavior of integral nuclear fuel rodlet experiments in TREAT. The accurate prediction of the transient CHF requires the exact characterization of the contribution of the HTTC. Therefore, the scope of this study investigates the heat transfer characteristics of experimental rodlets in TREAT during pool and flow boiling transient heating for both DNB and non-DNB conditions. The approach established a set of thermophysical material and heat transfer coolant properties that represented the HTTC for two TREAT experimental fuel/cladding fuel designs consisting of UO_2/FeCrAl and UO_2/Zircaloy. Specifically, the Zircaloy-2 and Fe-13Cr-5Al variants were considered for this investigation. The modeling methodology utilized in these studies consisted of creating representative TREAT testing rodlets, held within experimental capsules, under pool boiling heating conditions for which a transient power pulse was applied. The RELAP5-3D model used represented the pool boiling conditions of these fuel systems held within the SERTTA experimental capsule, and flow boiling conditions were used to represent these fuel systems in future TREAT experimental capabilities

such as the TWERL, and a power pulse was used to represent a transient insertion of energy in TREAT. The Groeneveld LUT feature was used to calculate the systematic value of the CHF in RELAP5-3D. Several Sobol sensitivity studies using thermal hydraulics analysis were conducted to identify the most important HTTC parameters towards the output of three key Figures of Merit (FoM); the peak outer cladding temperature (POCT), the maximum fuel centerline temperature, and the time occurrence of CHF. The latter FoM was only investigated for cases during which the CHF was exceeded. During a TREAT transient power pulse, the UO_2 fuel material is expected to thermally expand faster than both the FeCrAl and Zircaloy cladding materials. Therefore, how the thermomechanical effects of a changing gap thickness impacts the most influential HTTC parameters towards these three key FoMs was also analyzed in this chapter.

The contents within this chapter describes the RELAP5-3D model and the investigative methodology utilized, as well as the highlighting of all parameters that were a part of this analysis. Furthermore, the results of the ensuing sensitivity studies will be presented and discussed.

6.1.1 Methodology and RELAP5-3D Model Description

The thermal hydraulics analysis in this study was conducted using the deterministic finite differencing capabilities of the Idaho-National-Laboratory-developed Reactor Excursion and Leak Analysis Program (RELAP5-3D), a proven computational tool with the multidimensional ability to model a wide variety of reactor components and transient situations [8]. One advantage of the RELAP5-3D code is that it allows users to vary the boiling curve convective heat transfer coefficient (HTC) multipliers of the coolant surrounding the fuel rodlets [8]. Along with these HTCs, RELAP5-3D has a CHF multiplier feature that essentially moves the transition to the film boiling point. RELAP5-3D was coupled with the Risk Analysis Virtual Environment (RAVEN) [9] code, also developed at Idaho National Laboratory, and the Design Analysis Kit for

Optimization and Terascale Applications (DAKOTA) framework developed at Sandia National Laboratory [10]. Both have the capability to act as a controller of the RELAP5-3D input parameters in order to conduct optimization methods, uncertainty quantification, (UQ) and variance-based global sensitivity analysis. RELAP5-3D/RAVEN coupling capabilities were demonstrated by Gorton et al. [117] whose best-fit parameter estimates most closely matched the experimental steady state vs. transient heating CHF work carried out by Lee et al. [118]. DAKOTA's sensitivity analysis capabilities were demonstrated by Folsom [105] who conducted a Monte-Carlo-based sensitivity analysis on RIA experimental models in TREAT to estimate the variance of an output resulting from 21 different input variables.

For the work presented here, these codes were coupled with the RELAP5-3D models to conduct variance-based sensitivity studies, using Sobol decomposition methods, in order to rank the relative importance of considered input parameters pertaining to a desired key figure of merit (FoM) output. One advantage of RAVEN is that it utilizes a high-density reduced-order model (ROM) that considers several functions with a small number of polynomial cardinality, enabling accurate approximation of linear/highly-continuous system responses by using a relatively small number of computational samples to achieve convergence [9]. For input spaces in which discontinuity or non-linear behavior was encountered in this study, the DAKOTA framework generated more accurate results, and these instances required a much larger number of samples to achieve convergence [10, 119].

The investigation started with the development of RELAP5-3D models to represent the UO_2/Zircaloy and UO_2/FeCrAl rodlets contained in the SERTTA experimental capsule held within the SERTTA experimental capsule [110] under pool-boiling conditions, shown in Figure 30, and the test section of the TWERL system under flow boiling conditions, shown in Figure 31 [40]. The

solid rodlets in both models have fuel and cladding outer radii of 0.41 cm and 0.475 cm, respectively, and its 10.16-cm height was divided into 16 axial heat structures of equal radii and height dimensions. Fifteen radial mesh points were utilized in accordance with a previously conducted mesh study on this same model, which showed convergence of heat flux and outer cladding temperatures for this number of mesh points [120].

The model of the pool boiling SERTTA capsule, Figure 30, consists of a vertical hydrodynamic pipe component filled with water to a height of about 24.8 cm—engulfing the experimental rodlet—and topped by a helium gas chamber approximately 26.7 cm high, both of which are held at an initial temperature and pressure of 493 K and 3.45 MPa, respectively. This temperature value affords a degree of subcooling (about 20 K), and the pressure represents anticipated capsule testing conditions. Experimentally, the helium chamber serves to control over-pressurization of the capsule to prevent it from rupturing during a transient power pulse in TREAT [110]. In addition, flow areas within the model are representative of the SERTTA capsule and the gas chamber above, thereby fostering accurate modeling of the amount of water and helium gas used during experiments. No time dependent inlet/outlet volumes are included to accurately model the pressurization that is expected to occur within the SERTTA capsule during transient experimentation in TREAT. The RELAP5-3D flow boiling model water region and fuel/cladding system were represented using a pipe and a heat structure (HT) feature in RELAP5-3D respectively. The main difference is the addition of inlet/outlet time-dependent volumes, an inlet time-dependent junction and an outlet single junction to incorporate flow into the model and replicate the effects of the TWERL's pressurizer, as shown in Figure 31. The water section surrounding the HT has a height of 25.61 cm and a constant flow area of 0.0015 m^2. An entrance length is not needed, because RELAP5-3D assumes fully developed flow [8]. The HT representing

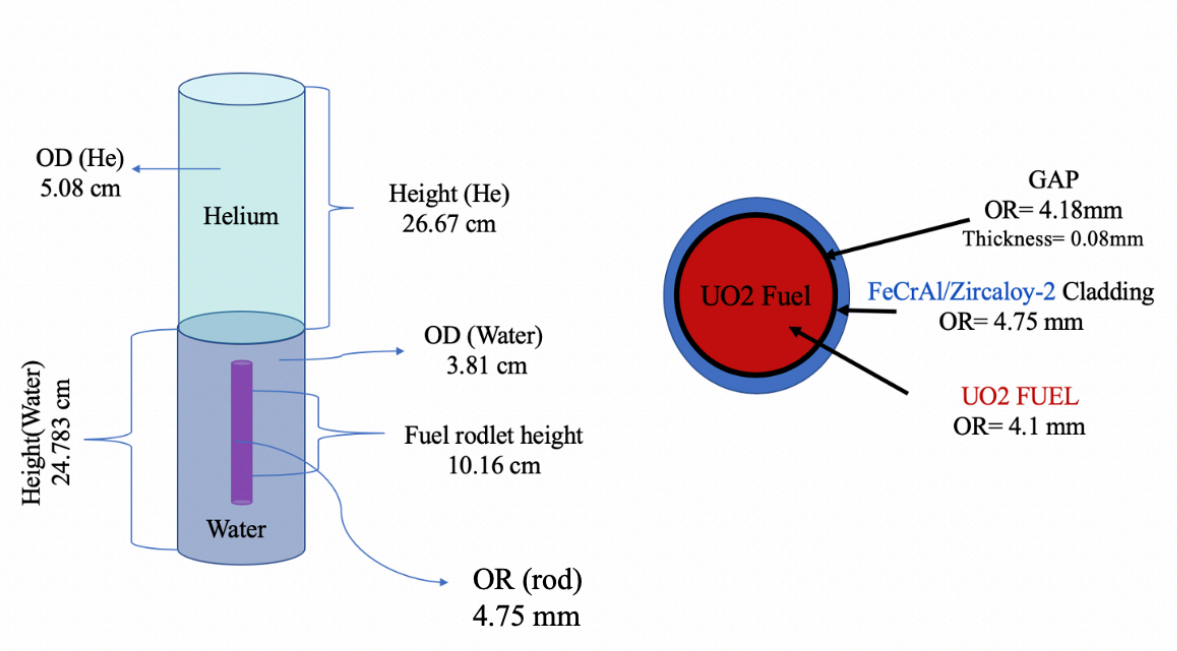

Figure 30. Schematic of the RELAP5-3D model used to represent the experimental PWR rodlets held in SERTTA capsule within TREAT.

the PWR fuel rodlet has a height of 10.16 cm and outer radius of 0.475 cm. The entire system was initialized to 3.45 MPa and 493K, as in the pool boiling model. Further, the time-dependent inlet junction was utilized to specify the MFR of the system. Essentially, this RELAP5-3D model was used to represent the test section of a recirculating fuel systems experimental loop in TREAT such as TWERL described in section 2.2.

For the scope of the study, a characteristic gaussian-shaped TREAT transient power pulse was considered with an energy generation in TREAT of about 920 MJ; estimated using the trapezoid rule method which integrates the energy in Joules deposited over the duration of all the time steps introduced in the model. The pulse has a full width at half maximum (FWHM) of about 92.5 ms, and a peak power of 9244 MW. This pulse is shown in Figure 13, and is representative of rapid heating conditions such as during an RIA in PWRs. The pulse was incorporated into the RELAP5-3D input file by using a data table that specified the applied power for a number of time steps [8]. Information about current TREAT pulse capabilities is discussed in section 2.2. The 2006 Groeneveld LUT was used to predict the manifestation of CHF in RELAP5-3D [8,115]. In summary, this LUT considers only hydrodynamic parameters such as pressure, thermodynamic quality and coolant mass flow when estimating the value of CHF [120].

6.1.2 Sobol Sensitivity Analysis Methods

Sensitivity analysis methods are used to determine an output's dependence on given input parameters. Sobol decomposition is a variance-based global sensitivity approach that became popular for reducing the computational requirements of conducting accurate sensitivity analyses of input spaces with a high number of dimensionalities [121]. Whereas other sensitivity methods are not applicable to non-linear output response curves, Sobol decomposition methods can rank

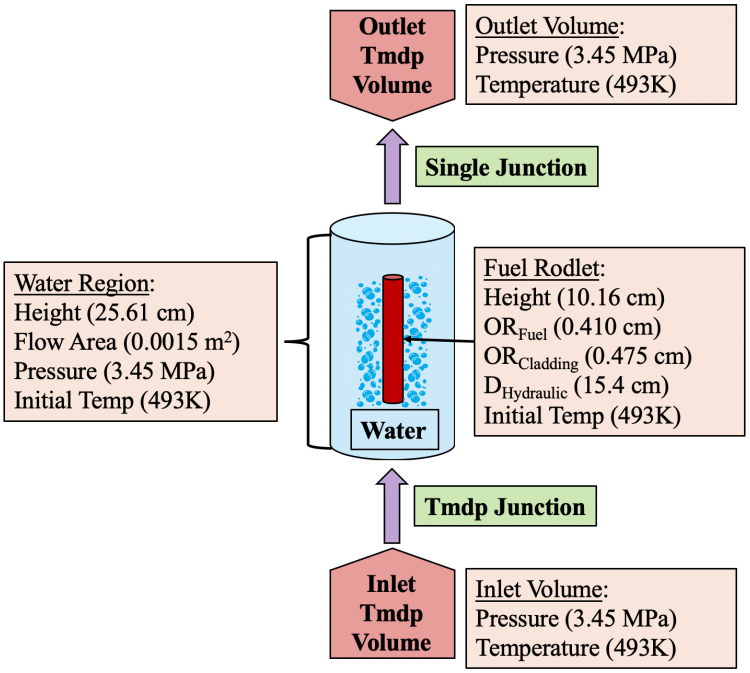

Figure 31. RELAP-3D model used to represent the experimental PWR rodlets within the test section of a flow boiling TREAT loop system.

the importance of various input metrics in regard to the sensitivity and uncertainty of a given output, regardless of whether the system response is linear [122]. However, the computational requirements increase in proportion to increases in the non-linearity and discontinuity of an output's system response curve, and the input parameters must be uniformly distributed as well as independent of the output [122]. To determine the variance's proportional significance to each individual parameter in terms of the overall variance of the output, Sobol indices are calculated for each input parameter. Sobol methods allow the user to not only capture the *main Sobol indices effect* (Equation 11) (i.e., an input's individual influence on the desired output) of each parameter, but also the *total Sobol index effect* (Equation 12) (i.e., the pair-wise interactions between input metrics) of each parameter:

$$S_i = \frac{V_{X_i}\left(E_{X_{\sim i}}(Y|X_i)\right)}{V(Y)} \text{ (Eq. 11)} \qquad S_{Ti} = \frac{E_{X_{\sim i}}\left(V_{X_i}(Y|X_{\sim i})\right)}{V(Y)} \text{ (Eq. 12)}$$

where $V(Y)$ is the total output variance resulting from the main effects of all the individual input parameters. The numerator in Equation (7) is the variance contribution of input parameter X_i to the output. The summation of the first-order main effect, S_i, of all input parameters is equal to 1.0. The numerator in Equation (8) is the total output variance due to input parameter X_i, along with any additional variance contributions from interactions between this parameter and other inputs. The summation of the total effects, S_{Ti}, of all parameters is at least 1.0, but this can be exceeded depending on how correlated the input parameters are in generating the output. As was mentioned, RAVEN utilizes an adaptive Sobol sampling method that creates subsets within the desired input space. Subsets upon which the targeted output is not dependent are skipped, greatly reducing the number of samples needed to converge the Sobol indices [9]. This method also uses an adaptive sparse grid sampling technique based on the least-squares support vector regression model

described in [123], that does not require 'uniformly-distributed' input parameters to generate accurate Sobol indices. This is referred to as a "ROM," and its accuracy begins to dip when the output response is non-linear or discontinuous. For this study, convergence of these Sobol indices in RAVEN was verified by plotting the number of samples vs. the total Sobol index [S_{Ti}] for each input parameter, and the convergence was considered reached when the S_{Ti} remained mostly unchanged despite an increasing sample number. DAKOTA does not use a ROM to conduct Sobol decomposition analysis, necessitating a much higher number of samples for converging the Sobol indices. But DAKOTA's application is not limited to highly continuous and linear response curves, and convergence is determined when the summation of the main Sobol indices [S_i] is close to or reaches 1.0 [10].

6.1.3 Sobol Sensitivity Study Approach

To study the effects of the DNB phenomenon under pool and flow boiling conditions on the two different PWR fuel/cladding integral designs during RIA testing in TREAT, the maximum fuel centerline and outer cladding temperatures were identified as the key FoMs in the HTTC Sobol sensitivity analysis. The considered input parameters were those thermophysical properties used to describe the HTTC for the UO_2/Zircaloy and UO_2/FeCrAl fuel rodlets; namely, the thermal conductivity of the Zircaloy/FeCrAl cladding materials ($k_{FeCrAl/Zirc}$) and that of the fuel material (k_{UO_2}) and helium gap region (k_{Helium}), the volumetric heat capacity of the fuel ($\rho c_{p_{UO_2}}$), and the HTC multipliers of the coolant, including the natural convection (NC_F), nucleate boiling (NB_F), transition boiling (TB_F), and film boiling (FB_F) factors. In addition, the CHF multiplier (CHF_F) was included to investigate how occurrence of the DNB event (as well as considering DNB and non-DNB cases separately) impact the rankings of these HTTC input parameters in terms of the importance of the output of the two key FoMs. Further, for the flow boiling cases the mass flow

rate (MFR) was included as an input parameter because it influences the cladding-to-coolant heat transfer coefficient. The time of CHF was identified as the key FoM in a subsequent sensitivity analysis that considered DNB cases only. Lastly, because during a transient power pulse the fuel region is expected to expand and thereby decrease the thickness of the gap region, the sensitivity analysis also included this physical parameter as an input variable, (Gap_T), when studying the maximum fuel centerline and outer cladding temperatures as well as the time at which CHF occurs for the DNB cases only.

The thermophysical material properties of the UO_2 fuel [124], and helium gap [125], along with both the Zircaloy [126] and FeCrAl [127] cladding options, were taken from the literature. Specifically, the Zircaloy-2 and Fe-13Cr-5Al variants were considered in this study. Although both cladding options have similar thermal conductivity values, the volumetric heat capacity of Zircaloy as function of temperature is about half that of FeCrAl [126,127]. Maintaining a constant thickness for both cladding materials caused comparative changes in thermal responsiveness—and thus the HTTC impacts—of these systems. When substantiating the chosen variation range of each input for the Sobol analysis, measurement and modeling uncertainties were taken into consideration. Measurement uncertainties result from discrepancies in the different experimental results that are found in the literature and used to generate data on the thermophysical properties of the materials. For example, the range of uncertainty in UO_2's heat capacity values is about $\pm$13% at up to 1800 K, and as much as $\pm$20% in its thermal conductivity values [124]. The FeCrAl cladding's uncertainty of about $\pm$7% for thermal conductivity results from experimental fluctuations in other thermal properties of this material [127]. Uncertainties in the heat capacity data on the Zircaloy material is about $\pm$3% at low temperatures. But this increases to around $\pm$10% at temperatures of 1300–1600 K, and up to $\pm$30% for temperatures higher than 1600K [127].

Modeling uncertainties include geometrical discrepancies with real-world experiments and uncertainties in correlations used to estimate CHF. Using a conservative approach that accounts for all the uncertainties discussed above, a range of parameter variation of $\pm$20 % was chosen for all HTTC thermophysical parameters for the fuel/cladding systems and surrounding coolant. The MFR input variation range was determined based on prototypic PWR flow rate conditions achievable by the current TWERL design specifications. Found in a published status report for the TWERL, the range variation for the prototypic PWR fluid velocities were between 4-5.5 m/s [40]. In addition, as discussed in section 2.3.7, Bessiron [82,83] used the out-of-pile Patricia facility in France to conduct significant pool-and-flow-boiling CHF experiments that replicated conditions found in the Nuclear Safety Research Reactor in Japan, and noticed an increase in the CHF value by a factor of up to between 5 and 6 when comparing steady-state and transient heating conditions. RELAP5-3D does not account for this heating rate effect when calculating the value of CHF due to the usage of steady state CHF correlations. Therefore, this uncertainty was accounted for by varying the CHF_F between 0.5 and 5.0 in the occurrence-of-CHF study. When studying DNB and non-DNB cases separately, the CHF_F range considered was decreased to 0.5–1.5. Lastly, the sensitivity of the gap region for DNB cases was studied, along with the time of CHF. The range considered for this input was between 0 cm and the default value of 0.008 cm to account for CHF experiments in which the fuel expanded to completely eliminate the gap region during a transient power pulse in TREAT. A summary of the ranges for the considered input parameters, along with their mathematical relationship to the HTTC in Table 13.

Table 13. Summary of the variation ranges for the input parameters considered in this study and their mathematical relationship with the HTTC.

		Column 1		Column 2	
Parameter Multipliers	**HTTC Relationship**	**Occurrence of DNB**		**DNB/non-DNB Time of CHF* Gap Effects***	
		Lower Bound	Upper Bound	Lower Bound	Upper Bound
Volumetric Heat Capacity Fuel $\rho c_{p_{UO_2}}$	Inverse	0.8	1.2	0.8	1.2
Thermal Conductivity of Fuel k_{UO_2}	Proportional	0.8	1.2	0.8	1.2
Thermal Conductivity of Gap k_{Helium}	Proportional	0.8	1.2	0.8	1.2
Thermal Conductivity of Cladding $k_{cladding}$	Proportional	0.8	1.2	0.8	1.2
Natural Convection Multiplier (NC_F)	Proportional	0.8	1.2	0.8	1.2
Nucleate Boiling Multiplier (NB_F)	Proportional	0.8	1.2	0.8	1.2
Transition boiling Multiplier (TB_F)	Proportional	0.8	1.2	0.8	1.2
Film Boiling Multiplier (FB_F)	Proportional	0.8	1.2	0.8	1.2
CHF Multiplier (CHF_F)	N/A	0.5	5.0	0.5	1.5
Gap Thickness (Gap_T)*	N/A	N/A	N/A	0.0 cm	0.008 cm

*Gap thickness only a parameter for time of CHF and gap effects.

6.2 Sensitivity and Uncertainty Analysis of Heat Transfer Time Constant Effects of TREAT Experimental Rodlets.

The results of the HTTC Sobol sensitivity analysis of the effects of DNB occurrences on the heat transfer mechanisms of the UO_2/Zircaloy and UO_2/FeCrAl fuel systems are presented here. This analysis focused on determining how manifestation of a DNB event impacts the relative importance of the HTTC input parameters in regard to the output of the maximum fuel centerline and outer cladding temperatures of these rodlets, as well as the time at which the CHF is exceeded. The POCT and maximum fuel centerline temperature are particularly important measurable quantities during TREAT fuel experiments, capable of describing the fuel-to-coolant thermal behavior transition resulting from the thermophysical properties of the different components used in the fuel/cladding system. Further, these two FoMs can be used to characterize fuel safety limits, predict pellet-to-cladding mechanical interaction (PCMI) behavior, analyze cladding tube failure modes, and characterize the CHF limit for a fuel/cladding design. Thus, these were chosen as key FoMs in the subsequent sensitivity studies with the purpose of exploring what HTTC related input parameters will generate the most uncertainties during rapid heating testing in TREAT under flow and pool boiling conditions. The time of CHF was chosen as the third key FoM to investigate how different HTTCs, achieved through the two fuel/cladding designs involved, as well as a thermomechanical effects of the changing fuel-to-cladding gap region impact the manifestation of this event. The initial section of this results segment involves an analysis of combined DNB and non-DNB cases only under pool boiling conditions, achieved using RELAP5-3D/DAKOTA coupling, because these findings are not expected to change under flow boiling conditions. This initial sensitivity study alone is the result of a total of about **121,000** RELAP5-3D/DAKOTA sample runs. Following, DNB and non-DNB cases are studied separately under both flow and pool

boiling conditions which takes advantage of the much-reduced computational requirements of the adaptive Sobol sampling achieved through coupling of RELAP5-3D/RAVEN. The adaptive Sobol sampling method is highly effective in reducing the number of sample runs needed to achieved converged, when the variance of data points is decreased [9]; this was achieved by separating DNB and non-DNB cases. A total of eight separate sensitivity studies were conducted, with about **48,000** RELAP5-3D/RAVEN sample runs to investigate DNB and non-DNB cases separately, as well as thermomechanical effects of the gap thickness variation effects and the time-occurrence-of-CHF.

Validation of the Sobol indices results for each of the subsequent sensitivity runs in this section was performed through convergence studies with respect to the number of samples. For the RELAP5-3D/DAKOTA runs, simulation cases were conducted until the main Sobol indices summated to 1.0, and there were no negative Sobol index values for any of the considered input parameters. For the RELAP5-3D/RAVEN sensitivity runs, the Sobol index of the input parameters were plotted as a function of number of samples as shown in the example in Figure 32. This specific example required around 1,000 cases for the Sobol indices to converge. All of the sensitivity studies performed using RAVEN involved 1,500 simulations; for which all achieved converged Sobol indices. Further, an important assumption of variance based Sobol sensitivity analysis is the independency of the input parameters with respect to the targeted output. Here, the considered thermophysical properties of the fuel/cladding systems are dependent on temperature; which happens to be the output. To avoid the interdependency of these parameters for the subsequent sensitivity studies, multipliers were established for the temperature-dependent basis functions of these thermophysical properties in RELAP5-3D, as shown in Table 13, These which were then varied independent of temperature as input parameters.

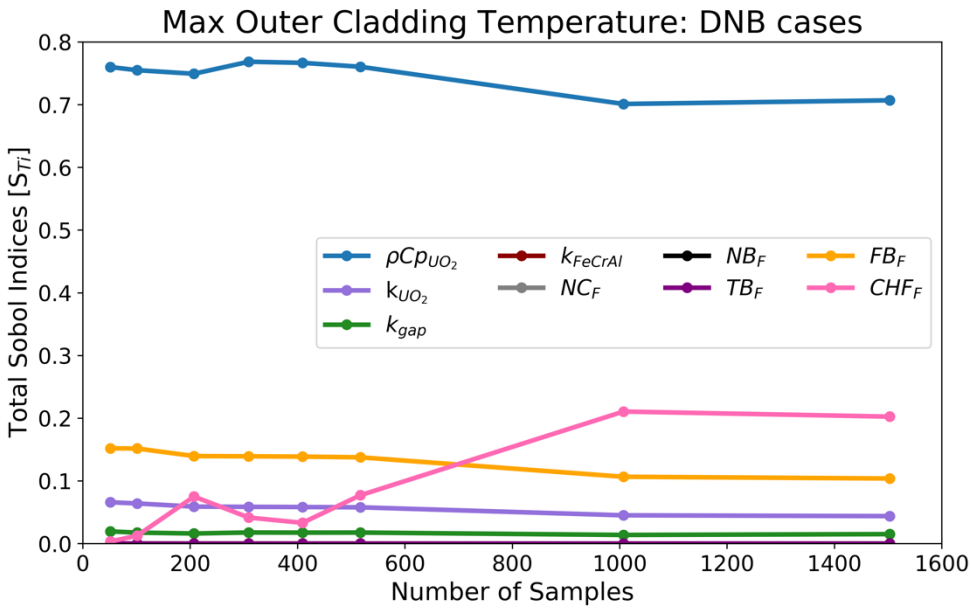

Figure 32. Convergence study of Sobol indices as a function of number of samples in RAVEN.

These validation studies were conducted for each of the sensitivity studies in this section.

6.2.1 Occurrence of DNB

We begin by analyzing how the occurrence of DNB impacts on the heat transfer characteristics of the UO_2/Zircaloy and UO_2/FeCrAl fuel designs under transient heating conditions represented by using a TREAT power pulse. This part of the study included both DNB and non-DNB cases under pool boiling conditions only. The two identified key FoMs were the maximum fuel centerline and outer cladding temperatures, because the former relates to fuel melting and the latter influences the DNB event. The HTTC range of parameters utilized here is found in Table 13 under the "Occurrence of DNB" column. The CHF_F input multiplier feature in RELAP5-3D was increased by up to 500% to eventually inhibit the DNB event, and include non-DNB cases for this analysis. The total Sobol indices, which can exceed a value of 1.0 for the maximum fuel centerline temperatures for both cladding/fuel rodlets are shown in Figure 33. As expected, the results clearly show that the only important HTTC parameter dictating the evolution of this FoM is the volumetric heat capacity of the fuel, and that manifestation of DNB does not impact this metric. Furthermore, volume and surface thermal resistances do not noticeably impact the peak fuel centerline temperature during a fast-heating event such as an RIA. This is because the maximum fuel temperature occurs during the initial quasi-adiabatic phase of the transient power pulse, during which the energy deposition occurs so rapidly that the heat has not had time to transfer out of the center of the rod. This results in equal maximum fuel temperatures for both rodlet designs, as shown in Figure 34, which displays the sensitivity of the peak fuel temperature as a function of fuel volumetric heat capacity. Figure 34 also supports the Sobol index data from Figure *33*, due to a lack of peak fuel temperature value ranges for each $\rho c_{p_{UO_2}}$ input data point present; which means this latter parameter is overwhelmingly dominant and the output is independent of all other considered inputs in Table 13. Note that, as the $\rho c_{p_{UO_2}}$ value decreases,

the maximum fuel centerline temperature increases, since less energy is needed to raise the temperature of this material by one degree per unit volume. Nevertheless, it was found that the long-term thermal behavior of the energy in the fuel is impacted by the characteristics of the HTTC and the DNB event, but this study was focused on understanding the main sources of parametric influence on predictions of the peak centerline fuel temperature during the transient pulse in TREAT. Because this data clearly shows that this FoM strongly depends on this particular HTTC parameter, the focus of the remainder of the studies was shifted towards the maximum outer cladding temperature metric.

The total Sobol indices for the POCTs are shown in Figure 35 and Figure 36 regarding the UO_2/Zircaloy and the UO_2/FeCrAl rodlets, respectively. The CHF multiplier was overwhelmingly the most dominant parameter. For that reason, regardless of the different thermophysical properties of the cladding materials, manifestation of the DNB event dominates the HTTC effects of these rodlet designs when determining the POCT. This is because, as shown in Figure 37, the CHF_F is responsible for a large variance in predicted cladding surface temperatures, according to whether the DNB event manifested. When the CHF is exceeded under pool boiling conditions, the convective heat transfer coefficient at the cladding-to-coolant heat transfer interface suddenly decreases due to the formation of a vapor layer. During rapid heating as in the TREAT testing, this vapor layer most likely forms through the coalescence of a large number of tiny bubbles that form on the heated surface as described by the Rohsenow bubble interference method [45]. This effectively results in thermal insulation of the fuel rodlet, leading to very high POCTs not otherwise observed under non-DNB conditions. The CHF_F input in RELAP5-3D can essentially inhibit/manifest the occurrence of the CHF phenomenon, and this is attributable to the large variance and discontinuity in outer cladding temperatures.

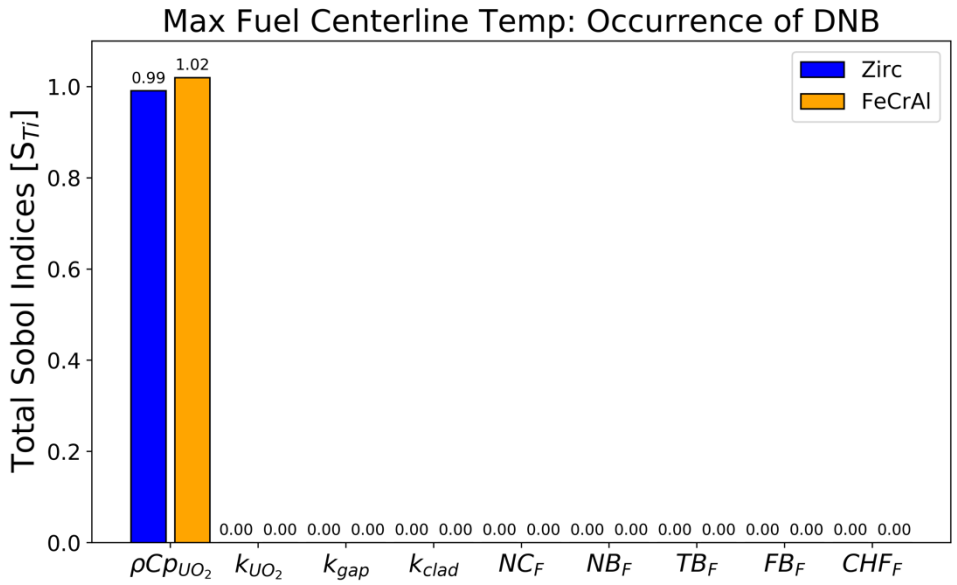

Figure 33. Total Sobol indices for the fuel centerline temperature of the HTTC input parameters of the FeCrAl and Zircaloy cladding systems including both DNB and non-DNB cases.

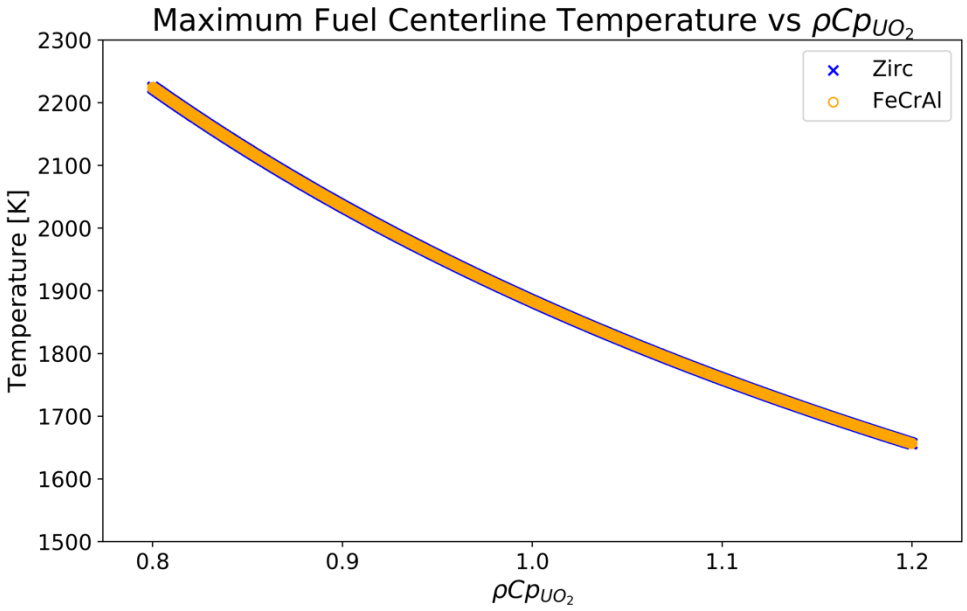

Figure 34. Maximum fuel temperature as a function of the volumetric heat capacity of the UO_2 fuel.

The main influence of the HTTC parameters can be observed when comparing the way in which POCTs vary between DNB and non-DNB pool boiling cases. In DNB cases, variations in the HTTC variables cause much larger deviation in values than observed in non-DNB cases see Figure 37. Thus, the HTTC is important in determining the POCT for cases in which the CHF is exceeded. The Sobol analysis results for the HTTC parameters that include both DNB and non-DNB cases can be seen in Figure 35 and Figure 36. The most important HTTC parameter is the volumetric heat capacity of the fuel, with noticeable contributions from the thermal conductivity of the fuel and gap materials. Because of the relatively small radius-to-height ratio of typical PWR fuel rods, the thermal responsiveness of these designs, is dominated by the volumetric heat capacity of the fuel material and not by thermal resistances. This is consistent with the data from the Sobol sensitivity analysis discussed here. Furthermore, the HTTC cladding-to-coolant convective coefficient input parameters only negligibly impacted the variance in the POCT output, most likely because the CHF_F is the dominant fluid parameter for the occurrence-of-DNB study. To better study how the HTTC parameters affect the POCT metric, sensitivity studies on both DNB and non-DNB cases were conducted separately under pool and flow boiling thermal-hydraulic conditions to limit the influence of the CHF_F.

Another topic of discussion is how the effects of the CHF_F vary as a function of cladding temperature. When maintaining a constant variation range for the values of this parameter, the impact of the CHF_F decreases as the maximum outer cladding temperature increases, since a higher CHF_F multiplier is needed to achieve the same impact. A higher POCT can be achieved through a larger rodlet energy deposition, a lower coolant degree of subcooling, or a lower volumetric heat capacity, as is the case in this study. From Figure 37 it can be seen that, because of the lower volumetric heat capacity of the Zircaloy cladding material, UO_2/FeCrAl sample runs reach

maximum outer cladding temperatures about 100 K lower. This results in a slightly lower CHF_F total Sobol index for the Zircaloy results shown in Figure 34, since this input is less impactful. Meaning, a higher CHF multiplier is needed before non-DNB cases begin to manifest, and DNB cases extended into a higher range of CHF_F values. This can be seen from the POCT data in Figure 37, and it leads to the HTTC parameters being slightly more significant in the UO_2/Zircaloy fuel rodlet when studying the occurrence of CHF as per this sensitivity analysis.

6.2.2 Sensitivity Study of DNB/non-DNB Cases

Pool and flow boiling thermal-hydraulic conditions, as well as experimental systematic parameters can heavily impact POCT predictions during transient fuel testing in the TREAT facility. In RELAP5-3D, these can include hydrodynamic characteristics such as coolant mass flow rate, temperature and pressure, total energy deposition and heating rate in the rodlet, and the systematic value of CHF. When these are held constant, the POCT becomes strongly dependent on the fuel system thermophysical parameters that make up the HTTC. By separating DNB and non-DNB cases for this analysis, we achieve a better understanding of how the HTTC parameters of the considered fuel/cladding rodlet designs impact the cladding-to-coolant heat transfer mechanism under both pool and flow boiling TREAT fuel tests. Effectively, this achieves a decreased influence of the CHF_F input, which was dominant when including both DNB and non-DNB cases in the previous analysis. For this part of the sensitivity analysis in this study, the range of variations chosen can be found under Column 2 in Table 13. Note that there are several differences in parameter variations from what was reported in section 6.2.1. Firstly, the range of the CHF multiplier is limited to 0.5–1.5. Furthermore, this analysis studied both pool and flow boiling conditions for the fuel/cladding systems, and thus, a MFR input parameter was included (see Table 13). Lastly, the rodlet energy deposition was increased for the flow boiling cases so that

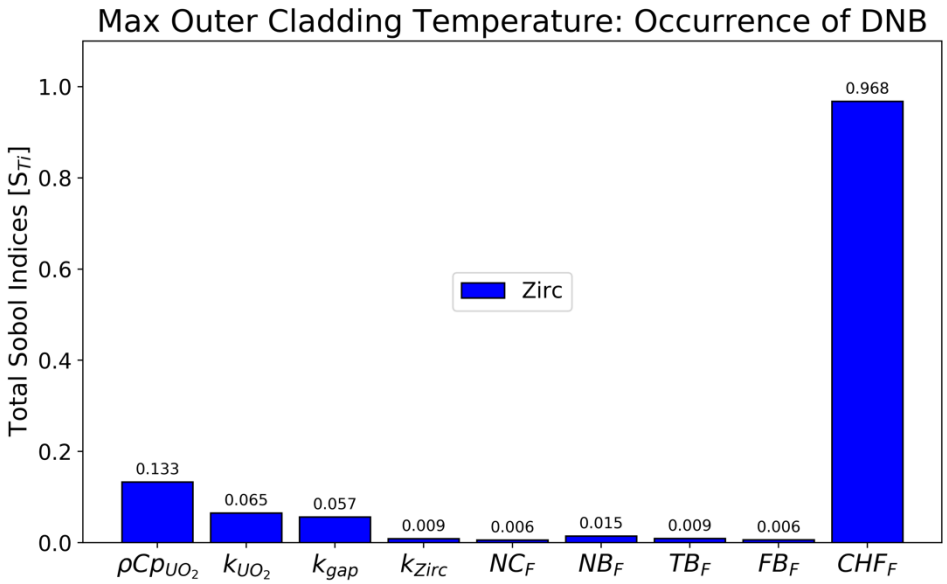

Figure 35. Total Sobol indices for the maximum outer cladding temperature of the HTTC input parameters for the UO_2/Zircaloy fuel rodlet including both DNB and non-DNB cases.

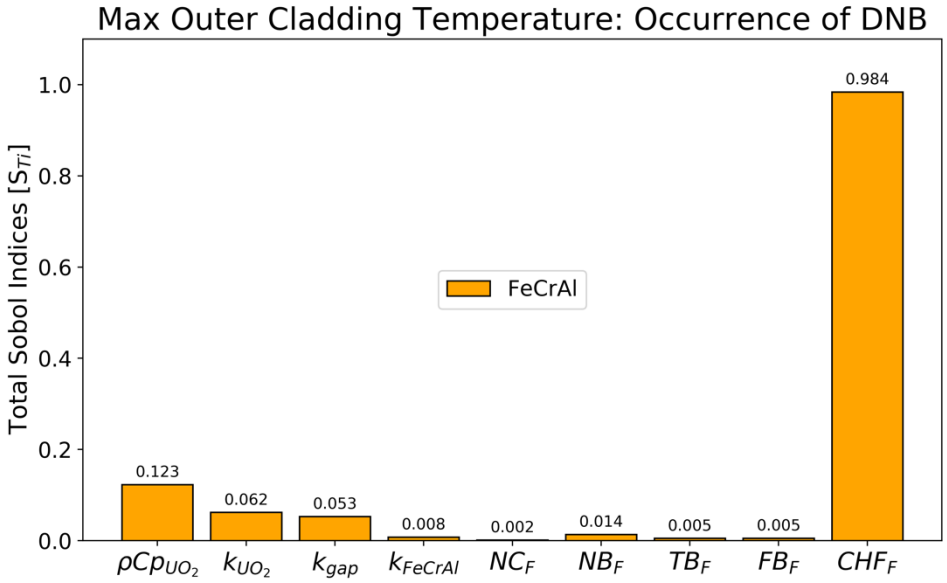

Figure 36. Total Sobol indices for the maximum outer cladding temperature of the HTTC input parameters for the UO_2/FeCrAl rodlet design including both DNB and non-DNB cases.

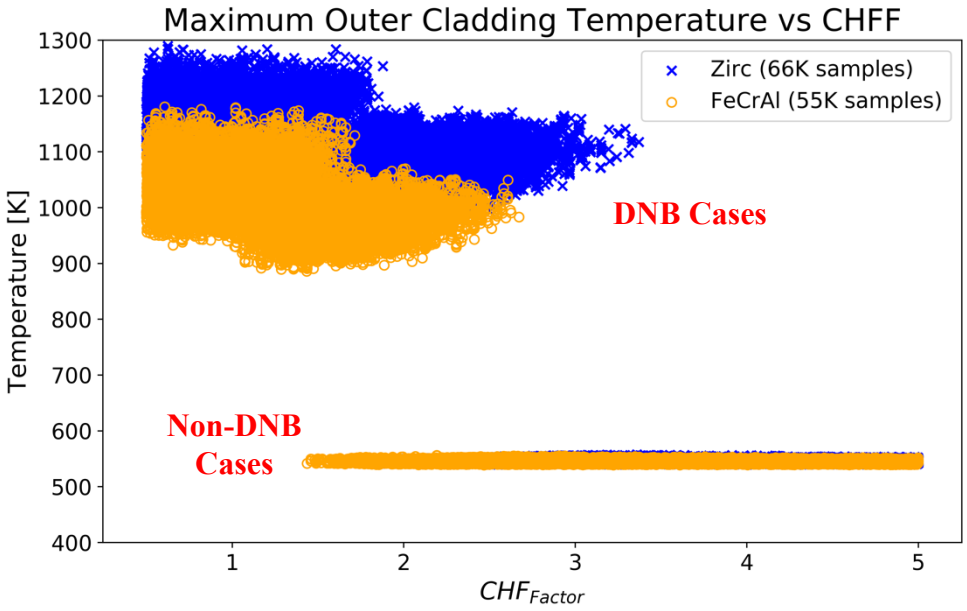

Figure 37. Maximum outer cladding temperature versus CHF_F. Both DNB and non-DNB sample runs included.

the range of DNB cases occurred within CHF_F values between 0.5 to 1.5, and was decreased for the non-DNB cases to ensure that the CHF was not exceeded. The increased energy deposition for flow boiling cases was needed due to RELAP5-3D taking into account the MFR hydrodynamic parameter when predicting the systematic value of CHF (see Table 14).

The total Sobol index effect of the HTTC parameters in the sample runs involving only DNB cases can be found in Figure 38 and Figure 39 for the UO_2/Zircaloy and UO_2/FeCrAl rodlets, respectively for both pool and flow boiling experimental environments for the TREAT fuel test representative models. In all instances, the volumetric heat capacity of the UO_2 fuel was observed to be the dominating parameter in calculating the POCT values. Furthermore, the importance of this fuel thermophysical property towards the POCT output increased slightly under flow boiling conditions as a result of the higher fuel energy deposition needed to cause DNB under this environment. For the pool boiling UO_2/Zircaloy design, the FB_F was the second most influential parameter, with noticeable contributions from the thermal conductivity of the UO_2 fuel and gap region, as well as the CHF_F. Whereas for the pool boiling UO_2/FeCrAl rodlet, the CHF_F was the second most important input variable, followed by notable contributions from the FB_F as well as the thermal conductivities of the fuel and gap region. Likewise, under a flow boiling environment the second most influential parameter towards the POCT is the FB_F for both fuel/cladding systems. Note that the impact of the CHF_F does not manifest for the flow boiling cases, as a result of the high post-DNB POCTs diminishing the impact of this input parameter. The FB_F becomes an influential fluid HTC because, after the CHF is exceeded, the cladding-to-coolant heat transfer mode during which the POCT occurs is characterized by the film boiling region of the boiling curve. To support this discussion, Figure 40 and Figure 41 displays the sensitivity of the POCT values to the four most dominant parameters in the Sobol analysis results for the DNB cases. For

these Figures, the horizontal based variations in POCT values are a function of the x-axis labeled input. Whereas, vertical variations in POCT values are a function of a constant value for the x-axis labeled input parameter, with variations of all other considered input parameters. Thus, a large slope in the plotted response of these data points equates to that specific x-axis labeled input parameter having a significant influence on the chosen output. Using this, Figure 40 and Figure 41 show that the peak cladding surface temperature value is most sensitive to the fuel's volumetric heat capacity, and that the FB_F has significant impact under both thermal-hydraulic conditions (pool and flow boiling). Lastly, in the case of the flow boiling environment, the MFR input parameter was shown to have no significant impact for the POCT predictions of the DNB cases. The increased heat transfer efficiency due to increments in the MFR is observed mainly under the single-phase heat transfer regime– which has a short duration under the modeled TREAT transient experiments– and the advantages of this enhancement are less impactful under nucleate boiling two-phase flow during which induced convection resulting from vapor generation in the surrounding coolant becomes more significant. As a result of this, the MFR range of values considered for this study has no significant effect on the POCT predictions. Another reason behind the lack of influence of the MFR on the POCTs is found in Table 14. Although there is a large increase in the CHF value between the pool and flow boiling conditions, this effect saturates as the MFR is increased for the representative RELAP5-3D models. We can see that for the considered range of MFR values, between 3-5.5 m/s, there is no significant difference in the predicted RELAP5-3D values of CHF. Note that the results in Table 14, utilize the Groeneveld 2006 steady-state CHF LUT correlation in RELAP5-3D and does not take into account rapid heating effects [29].

Table 14. Predicted RELAP5-3D values of the CHF as a function of the coolant MFR.

Fluid Velocity [m/s]	**Mass Flow Rate [Kg/s]**	**Predicted RELAP5-3D CHF Value [MW/m^2]**
0.00	0.00	2.14
1.00	0.97	4.05
3.00	2.90	4.46
5.50	5.31	4.64

Several observations can be made from the results of the sensitivity analysis conducted here on the representative experimental TREAT fuel tests RELAP5-3D models. From the total Sobol indices shown in Figure 38 and Figure 39, it can be seen that the thermophysical properties of the fuel rodlet components are vastly more important collectively than those of the coolant and CHF_F, implying that fuel-to-coolant heat transfer mechanisms under DNB conditions are mostly dominated by the fuel/cladding rodlet component aspects of the HTTC for both pool and flow boiling conditions. Furthermore, the summation of the total Sobol effects of the fluid HTCs and the CHF_F is higher in the UO_2/FeCrAl rodlet compared to the UO_2/Zircaloy design. This points to the importance of not only the CHF_F, but also the thermophysical properties of the coolant decreasing as peak outer cladding temperature increases. As shown in Figure 40 and Figure 41 for all pool and flow boiling sample runs, the POCTs reach higher values in the UO_2/Zircaloy rodlet, leading to increased dependence of the HTTC on the thermophysical properties of the fuel components. Furthermore, the POCTs are between 300-400K higher under flow boiling DNB conditions due to the larger energy deposition needed to exceed the systematic value of CHF for this environment. Thus, flow boiling conditions provided an additional CHF safety margin during an RIA in relation to that observed under pool boiling conditions. Note that the HTTC multiplier is inversely related to the fuel's volumetric heat capacity values. The final observation made from the results of the Sobol analysis of DNB cases only also supports the conclusion reached in section 6.2.1; namely, the impact of the CHF_F decreases with increased peak cladding temperature, as expected. This is evident under flow boiling conditions, for which the effect of this parameter is non-existent for both fuel/cladding systems due to large POCTs. Furthermore, under pool boiling conditions the CHF_F Sobol index of the UO_2/FeCrAl system is higher than that of the Zircaloy cladding rodlet. This is because the effects of the CHF_F input are observed to have an increased

impact on the variance of the POCTs in the FeCrAl case at a value of around 1.2–1.3, due to the higher volumetric heat capacity of this cladding material. Whereas, in the Zircaloy rodlet, noticeable effects on the calculation of the POCTs begin to manifest later, once the CHF_F value rises above 1.45 or so (see Figure 40). Overall, the Sobol sensitivity studies for DNB cases display similar HTTC dependencies for both flow and pool boiling thermal hydraulic conditions.

The total Sobol indices for the pool and flow boiling cases that did not exceed the CHF during the TREAT transient application can be found in Figure 42 and Figure 43 for the UO_2/Zircaloy and UO_2/FeCrAl rodlets, respectively. For pool boiling cases in both fuel/cladding designs, the volumetric heat capacity of the fuel remains the most influential parameter regarding the output of the POCTs. Whereas, under flow conditions the volumetric heat capacity of the fuel is one of the most important parameters, and the coolant input parameters have increased importance due to the MFR within the flow channel for these experimental conditions. The nucleate boiling regime now characterizes the cladding-to-coolant heat transfer, and the multiplier for this input becomes highly influential for both flow and pool boiling environments, indicating that the POCT now strongly depends on the surface thermal resistance of the surrounding coolant. Further, the thermal conductivity of the gap region significantly affects the predicted outer cladding surface values, making it the third most influential parameter in the total Sobol indices. Because of the higher cladding-to-coolant HTC experienced during the nucleate boiling regime, the gap region becomes a critical parameter due to the low thermal conductance in this region limiting heat transference from the fuel into the cladding.

Under flow conditions the MFR becomes a noticeable parameter towards predictions of the POCTs for non-DNB cases. Although it manifests differently, the influence of the MFR for both of these fuel/cladding systems are similar. In the UO_2/Zircaloy case, the increase in MFR

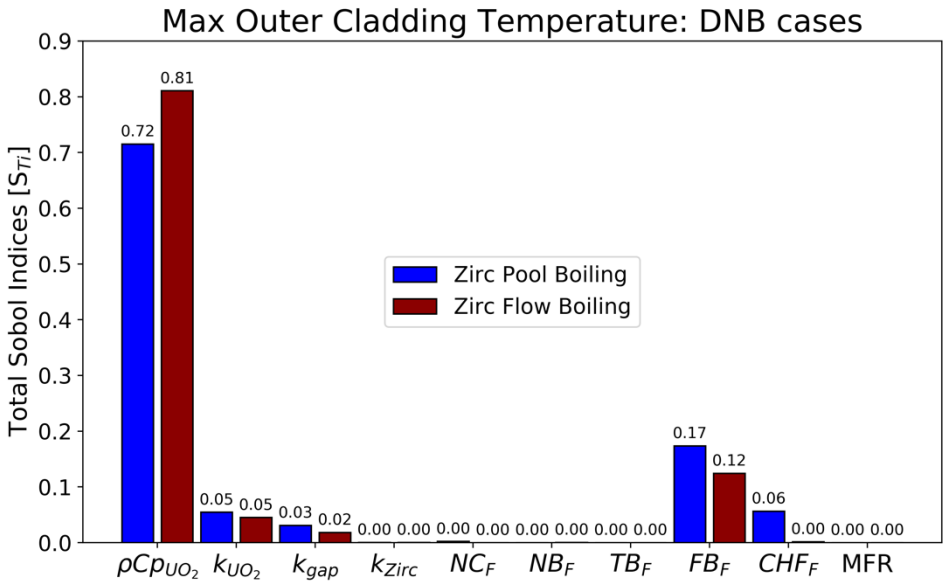

Figure 38. Total Sobol indices for the POCTs of the UO_2/Zircaloy rodlet under pool and flow boiling conditions. The DNB event manifested for all cases.

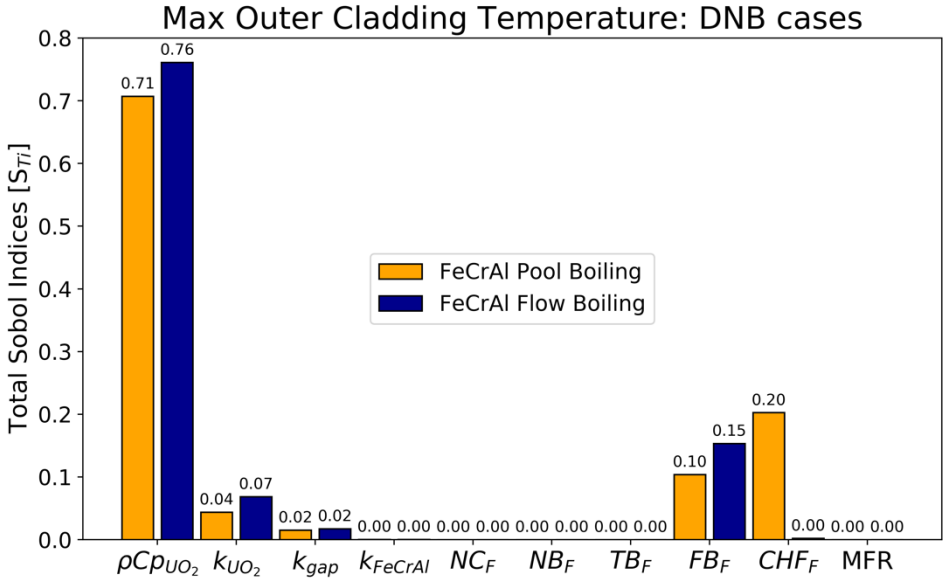

Figure 39. Total Sobol indices for the POCTs of the UO_2/FeCrAl rodlet under pool and flow boiling conditions. The DNB event manifested for all cases.

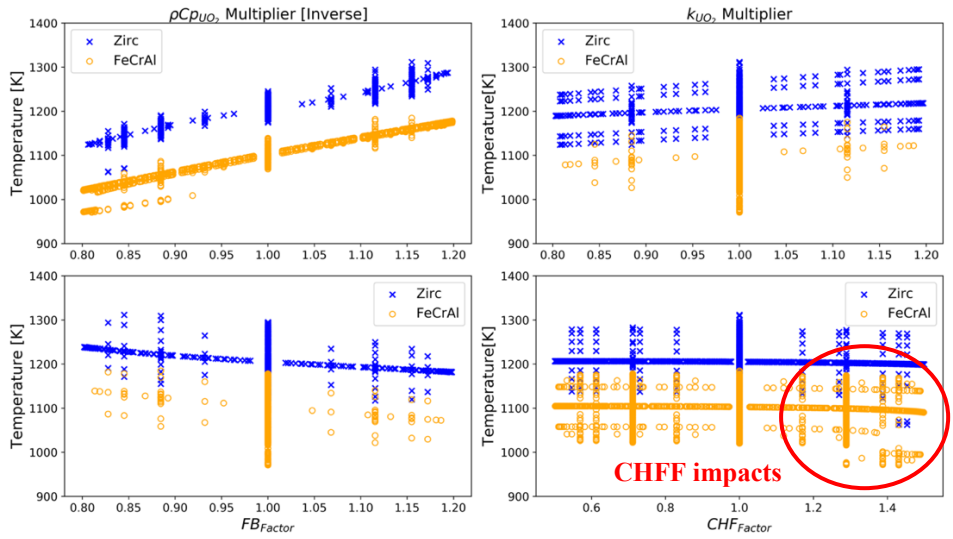

Figure 40. Sensitivity of the maximum surface cladding temperatures to various identified HTTC parameters and the CHF multiplier under pool boiling conditions (for DNB cases only).

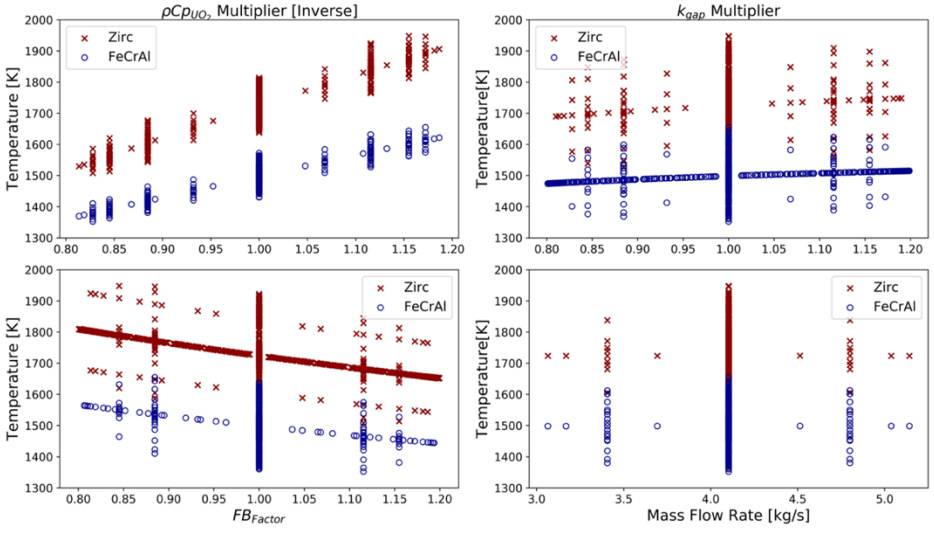

Figure 41. Sensitivity of the maximum surface cladding temperatures to various identified HTTC parameters and the CHF multiplier under flow boiling conditions (for DNB cases only).

represents itself through a more impactful NB_F. For the FeCrAl case, this is observed for the MFR input with almost a 20% influence on the predicted POCT values. The MFR has a significant impact for these cases during which CHF was not exceeded, because no significant vapor is generated within the flow channel under these circumstances as observed during DNB cases. Therefore, the heat transfer enhancements associated with increments in MFR under single-phase and two-phase nucleate boiling regimes are more impactful due to a reduction in boiling induced convective heat transfer. The HTTC analysis places about the same overall importance on the fuel components as it does the fluid HTCs for all cases. But, as seen in Figure 37 and Figure 44 for pool and flow boiling respectively, the total variance experienced for the non-DNB cases of both fuel/cladding designs is relatively small. This means that the effects of the HTTC on the fuel-to-coolant heat transfer mechanisms are not as important in cases that do not exceed the CHF. The volume and surface thermal resistances collectively surpass the importance of the fuel's heat capacity material properties when it comes to the POCT output; and because the CHF phenomenon does not manifest itself, the CHF_F input parameter has no impact—as seen from Figure 42 and Figure 43. Overall, the results are similar for both fuel/cladding systems and thermal-hydraulic conditions. When comparing pool and flow boiling Sobol sensitivity study results under non-DNB cases, one conclusion that can be drawn pertains to the slight decreased importance of the thermophysical properties of the fuel system, due to the mass flux of the coolant enhancing heat transfer efficiency.

6.2.3 Sensitivity Study of Gap Effects

The motivation behind this part of the study was to explore the coupling of thermomechanical and thermal hydraulic effects of TREAT fuel experiments during fast transient testing. As UO_2 is

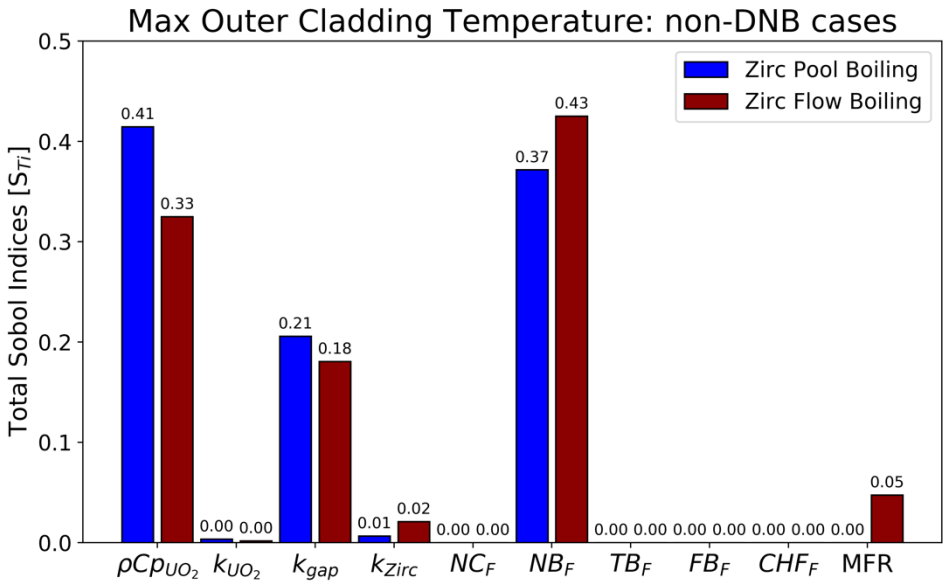

Figure 42. Total Sobol indices for the maximum cladding surface temperature of the UO_2/Zircaloy rodlet for both pool and flow boiling conditions. The DNB event did not manifest for all cases.

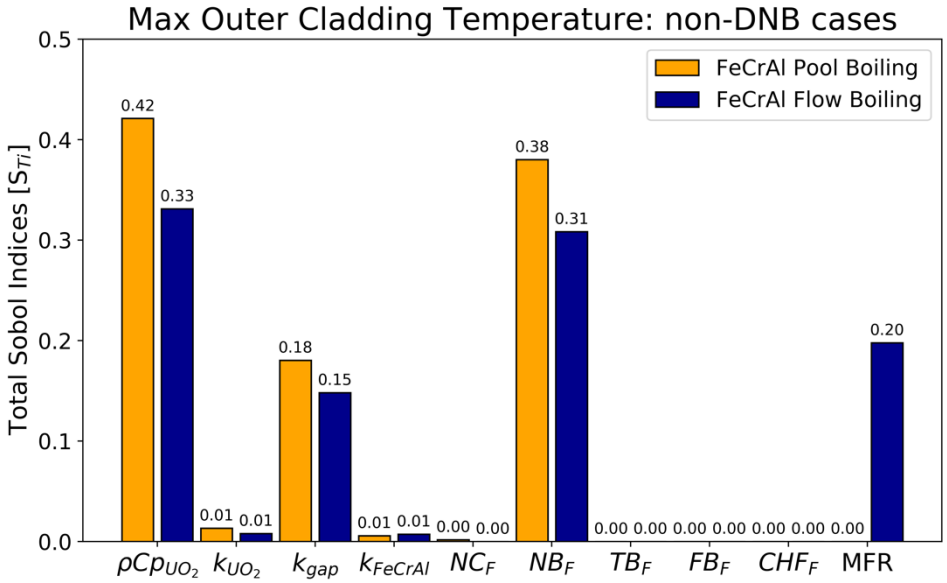

Figure 43. Total Sobol indices for the maximum cladding surface temperature of the UO_2/FeCrAl rodlet for the sample runs that did not experience a DNB occurrence.

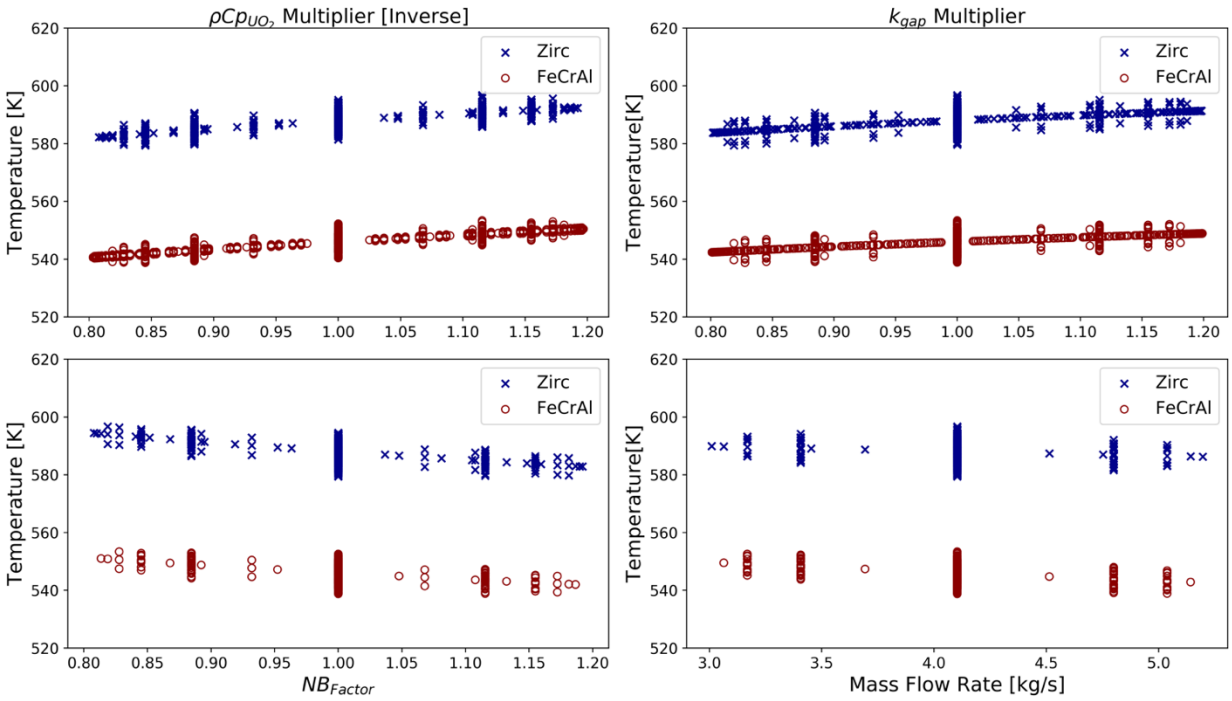

Figure 44. Sensitivity of the POCT temperature for the non-DNB flow boiling cases to chosen input HTTC parameters from the Sobol sensitivity study.

heated, this material thermally expands faster than both the FeCrAl and Zircaloy cladding materials due to its ceramic properties. In addition, the volumetric swelling rate of this component increases with temperature, and, as a result, the gap thickness of the experimental rodlet will decrease during application of a transient power pulse in TREAT [13]. Here, the ensuing impacts on the heat transfer of these rodlet systems are analyzed using two different sensitivity study methodologies that only considered those cases that experienced DNB conditions under pool and flow boiling conditions. In both methodologies, the fuel radius was gradually increased to model the swelling of this material during the application of a power pulse. This resulted in slightly lower maximum fuel temperatures as the gap thickness decreased, since energy deposition was held constant as the total fuel volume increased. The initial approach studied the sensitivity of the thickness of the gap region as an input parameter, along with the HTTC variables, over the range of chosen variations, as shown in Column 2 of Table 13. The total Sobol indices in Figure 45 and Figure 46—for the UO_2/Zircaloy and UO_2/FeCrAl rodlets, respectively—indicate that the volumetric heat capacity of the fuel is still the dominant parameter influencing the variance of the POCT output under pool and flow boiling conditions. Further, the width of the gap region is the second most important parameter in the Zircaloy case and the third most in the FeCrAl case. Lastly, the thermal conductivity of the fuel and the film boiling multiplier of the coolant also show significant influence on the POCT calculations. For the flow boiling cases, the gap thickness parameter is slightly less influential than in pool boiling. This is a result of larger energy deposition introduced into the flow boiling model to cause CHF, slightly increasing the influence of the volumetric heat capacity of the fuel while drawing away from the gap thickness effects. Figure 47 displays the sensitivity of gap variations on the maximum outer cladding temperature for both

thermal-hydraulic environments studied—as expected, the latter increases as the former decreases, due to increased thermal conductance within this region.

The analysis using this approach can be summarized through several observations. For both pool and flow boiling cases, the total Sobol index for the gap width is higher in the Zircaloy case, due to the lower volumetric heat capacity of this material. This implies that the POCT becomes more dependent on the gap thickness as the average cladding temperature value increases, thus offering an advantage—from a safety perspective—to the UO_2/FeCrAl design in the event of an RIA. Furthermore, when compared to the DNB cases in section 6.2.2, it is seen that the influence of the CHF_F is no longer present in these results. As shown in Table 15, the average and maximum cladding temperatures of the sample runs increase when gap thickness is included as an input variable. Essentially, the decreasing gap width causes an increase in the HTTC value for these rodlet systems. This leads to a decrease in the effects of the CHF_F, both because of the rise in POCT as well the similar impacts on the time at which CHF occurs for the CHF_F and the gap thickness—for which the latter parameter is dominant. This is discussed in more detail in section 6.2.4. The influence thermal conductivity of the gap region is also no longer present in the Sobol results in Figure 45 and Figure 46, due to the thermomechanical effects of the gap thickness having the most controlling effect on the thermal conductance within this region. Overall, the influence of the HTTC parameters, the CHFF, and the MFR was similar regardless of the pool or flow boiling environments for the UO_2/Zircaloy and UO_2/FeCrAl cases.

The second approach used to study these effects was to sample the HTTC Sobol indices for the considered range, using different gap thickness data points under DNB pool and flow boiling conditions. Sobol analysis is shown in Figure 48 and Figure 49 for the UO_2/Zircaloy and

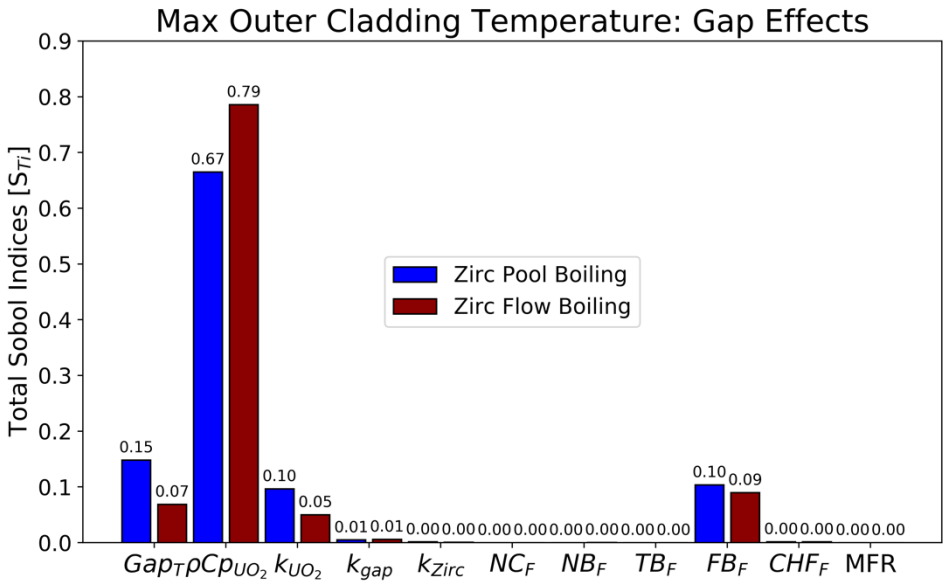

Figure 45. Total Sobol indices for the UO_2/Zircaloy gap sensitivity study under flow and pool boiling conditions. All cases experienced DNB.

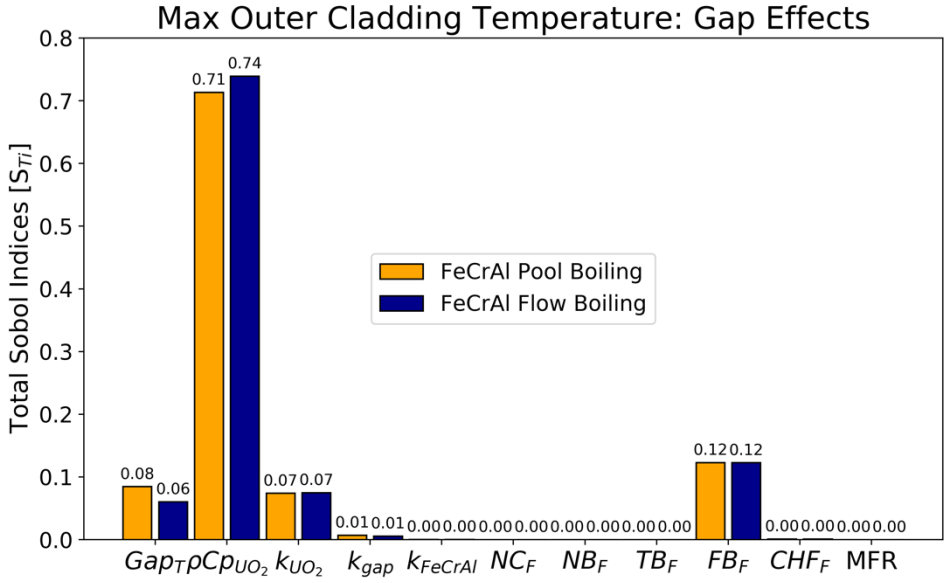

Figure 46. Total Sobol indices for the UO_2/FeCrAl gap sensitivity study. All cases experienced DNB under flow and pool boiling conditions.

Table 15. Dependence of the gap effects on the mean and maximum outer cladding temperature values for the DNB cases.

Rodlet System	Including Gap Effects		Excluding Gap Effects	
	Average	Maximum	Average	Maximum
UO_2/Zircaloy POCT (pool)	1235 K	1360 K	1203 K	1311 K
UO_2/Zircaloy POCT (flow)	1777.1K	2019.7K	1719.5K	1948.5K
UO_2/FeCrAl POCT (pool)	1125 K	1214 K	1094 K	1185 K
UO_2/FeCrAl POCT (flow)	1533.2K	1701.5K	1495.1K	1654.8K

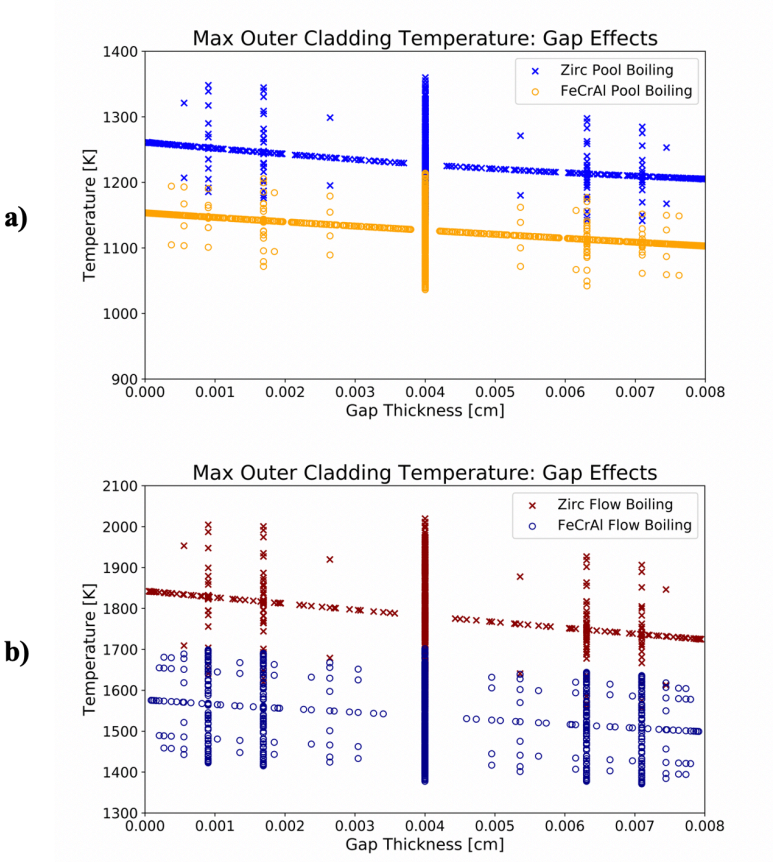

Figure 47. Maximum outer cladding temperature relationship to gap thickness in the Zircaloy and FeCrAl rodlets under a) pool boiling and b) flow boiling conditions. All cases experienced DNB.

UO_2/FeCrAl designs, respectively. In both cases, the impacts of the volumetric heat capacity and thermal conductivity of the UO_2 fuel on the POCTs increase as the gap thickness decreases. This is due to the fuel expanding into the gap region during an RIA. As this continues to progress, the total Sobol effect of the gap's thermal conductivity diminishes. It can also be seen that the influence of the CHF_F in pool boiling cases manifests itself only for the highest default (0.008 cm) gap thickness data point, due to the increasing POCT as the gap conductance increases. Further, the MFR and the CHF_F input parameter for the flow boiling cases has no impact on the POCT predictions throughout the considered gap thickness variation range. Lastly, the HTTC becomes less influenced by the fluid thermophysical properties as the fuel region expands. Meaning that the fuel-to-coolant heat transfer mechanisms become more dependent on the thermal responsiveness within the volume of these fuel rodlets. The work shown in this section highlights the importance the coupling of thermomechanical and thermal hydraulic effects of the gap region when studying the HTTC of nuclear fuel designs under rapid heating pool and flow boiling conditions. The behavior of the HTTC shown here displays differences compared to what is observed in the sensitivity analysis conducted only on DNB cases and excluding the width of the gap region as a parameter. These differences included a decreased dependence in fluid properties and an increased importance of the fuel region, regardless of the different thermophysical properties of the two considered cladding options.

6.2.4 Time of CHF

The third key FoM studied via sensitivity analysis methods was the time at which the CHF is exceeded for the experimental TREAT fuel systems. Heat transfer characteristics in nuclear fuel systems are directly responsible for determining when a DNB event occurs. Time of occurrence is

a)

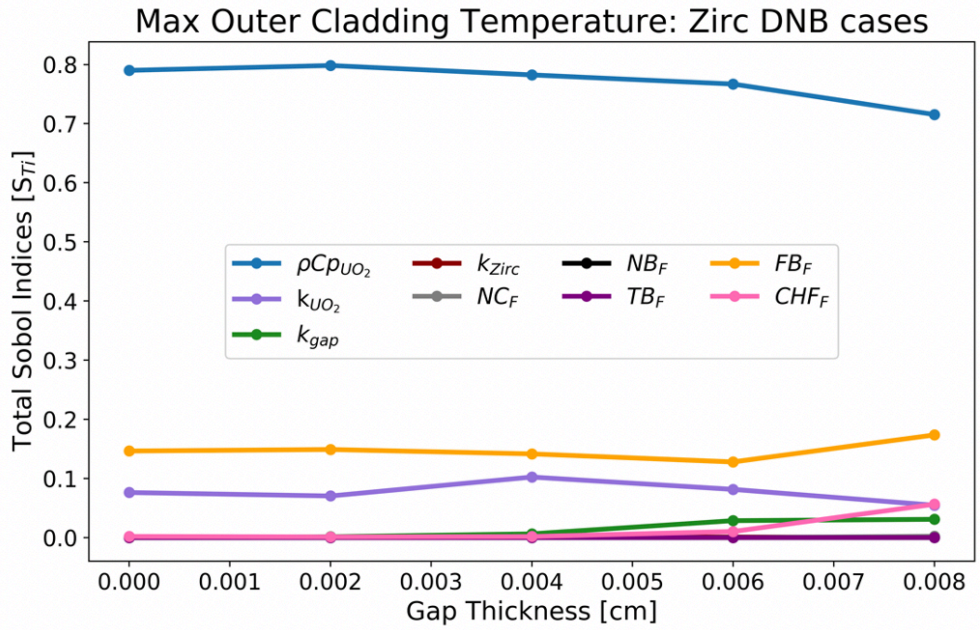

b)

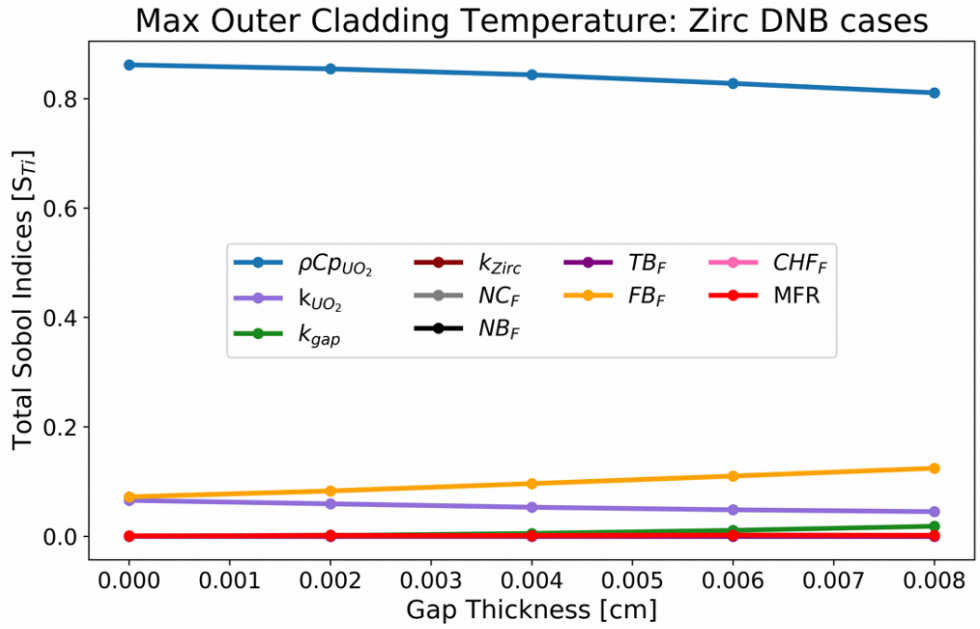

Figure 48. Gap thickness thermomechanical effects on POCT Sobol indices of the UO_2/Zircaloy HTTC parameters for all cases experiencing DNB under a) pool boiling and b) flow boiling conditions.

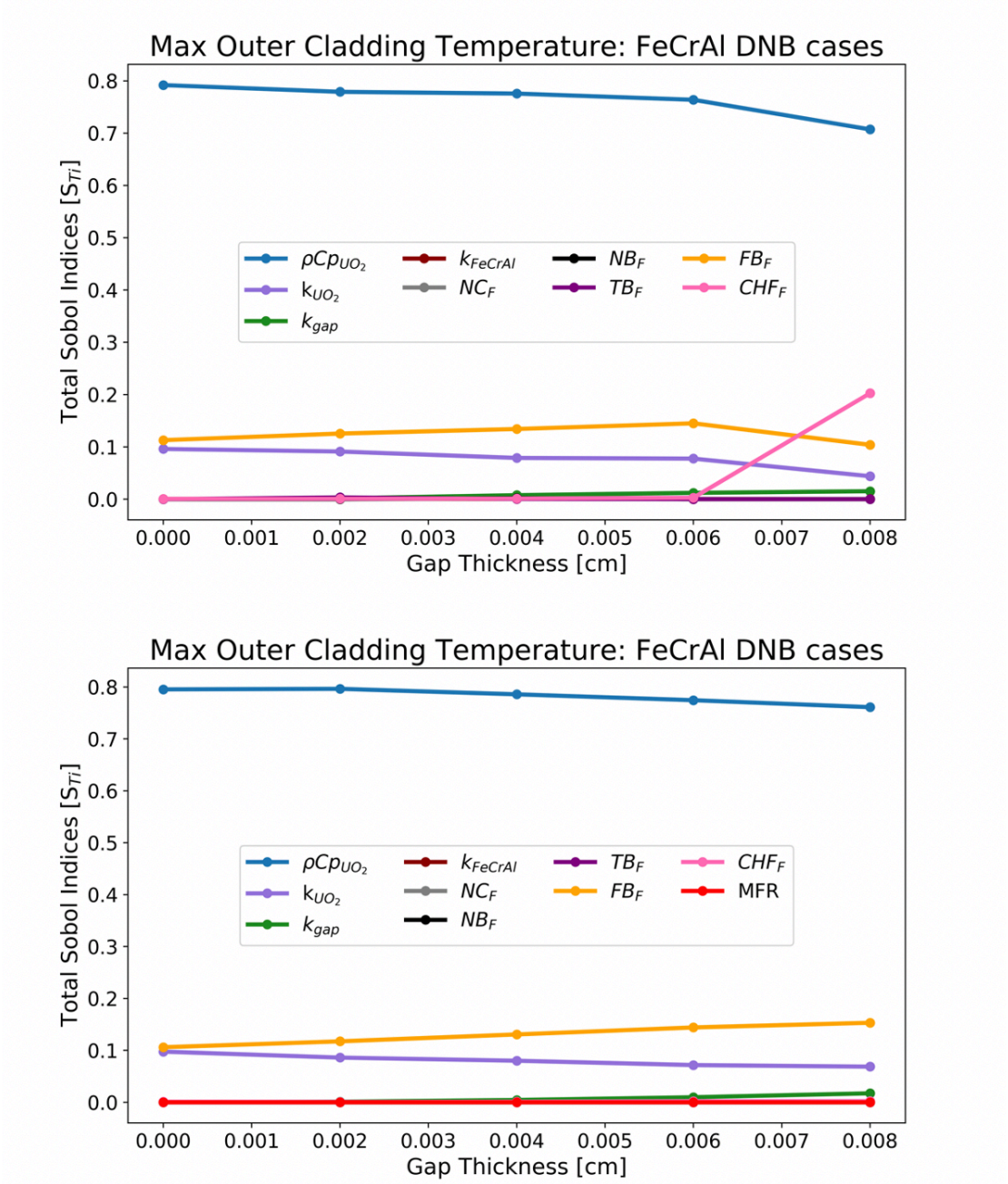

Figure 49. Gap thickness thermomechanical effects on POCT Sobol indices of the UO_2/FeCrAl HTTC parameters for all cases experiencing DNB under a) pool boiling and b) flow boiling conditions.

also important for determining the maximum outer cladding temperature of a fuel rodlet during an RIA, which can be correlated to accident progression such as cladding ballooning, bursting and/or melting [12, 13]. For a given fixed energy deposition, the POCT will be higher in fuel systems in which the DNB crisis occurs more rapidly. This is because less energy escapes via convective heat transfer into the coolant before the rodlet becomes effectively insulated due to post-DNB conditions. Here, we study the effects of the fuel-to-coolant heat transfer characteristics of the two fuel/cladding designs by means of the HTTC. The set of parameters used and their range of values can be found in Column 2 of Table 13. Since the time of CHF is being analyzed, only sample runs in which DNB pool and flow boiling conditions occurred are included.

The total Sobol indices for the time of CHF of the UO_2/Zircaloy and UO_2/FeCrAl fuel systems are shown in Figure 50 and Figure 51, respectively. The RELAP5-3D time of CHF was calculated by determining when the cladding-to-coolant heat transfer mode switched over to the transition boiling regime [8]. The data shows that under pool boiling conditions variations in the gap thickness region are the most important parameter for determining when a DNB event will occur for both fuel/cladding systems. The CHF_F has the second highest Sobol index, because this parameter can accelerate/delay the time of CHF. Under flow boiling conditions these observations also hold true, but there is an increased importance in the CHF_F multiplier. This is due to a higher systematic value of CHF under flow boiling conditions, relative to pool boiling, resulting in variations in this parameter being more important. Noticeable contributions can be observed from several thermophysical fuel system properties that comprise the HTTC, including the fuel's volumetric heat capacity as well as the gap and cladding thermal conductivities. The lower volumetric heat capacity of the Zircaloy material causes this fuel system to have a higher wall superheat than experienced in the UO_2/FeCrAl case. For this reason, DNB occurs faster in this fuel

design, as seen from Figure 52 and Figure 53. These figures display the sensitivity of the time-occurrence-of-CHF to the four chosen parameters shown. Horizontal variations in time values are a result of the chosen x-axis input. Whereas, vertical variations in time values in Figure 52 and Figure 53, are due to a combination of the chosen value of the input and combinations of values for the other considered HTTC parameters. Note that, because RELAP5-3D only takes into account hydrodynamic characteristics, these results do not consider other pool-and-flow-boiling-CHF-impacting parameters that could vary the time occurrence of this phenomenon, such as the wettability of the surface in contact with the fluid, rapid heating effects, and reactivity-induced surface activation CHF enhancements. Nevertheless, these results demonstrate how the thermophysical properties of the FeCrAl material can delay the time of CHF and alter the HTTC effects of this fuel design, thus demonstrating another safety advantage of this fuel system over conventional PWR Zircaloy fuel rods. Overall, both fuel/cladding systems behaved similarly regardless of the mass flux rate of the surrounding coolant.

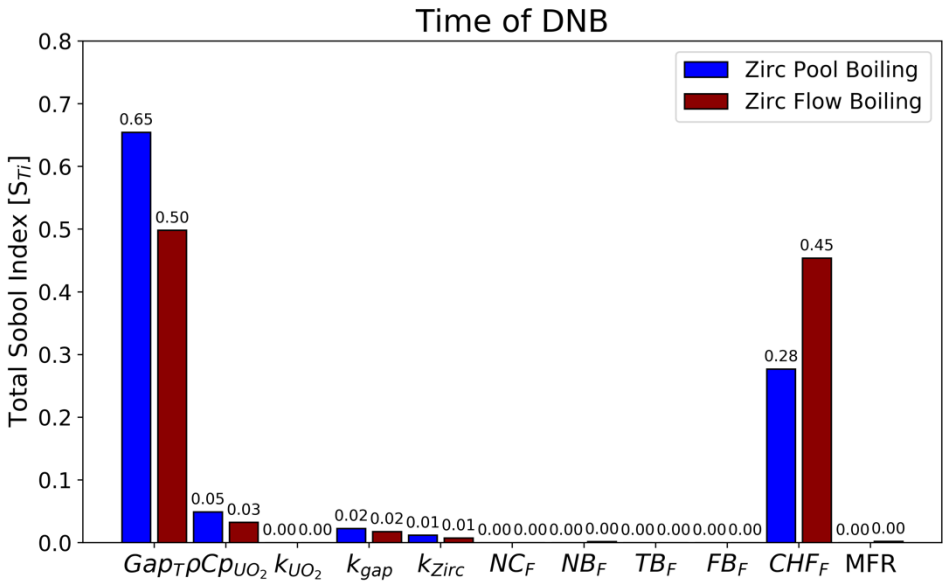

Figure 50. Total Sobol indices for the UO_2/Zircaloy time-of-CHF study for both pool and flow boiling DNB conditions.

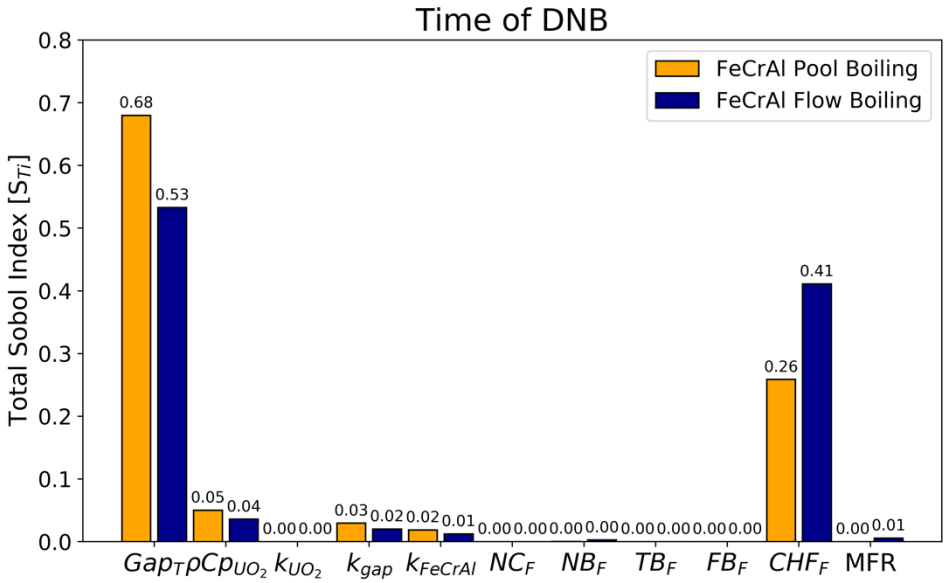

Figure 51. Total Sobol indices for the UO_2/FeCrAl time-of-CHF study. All cases experienced DNB for both pool and flow boiling conditions.

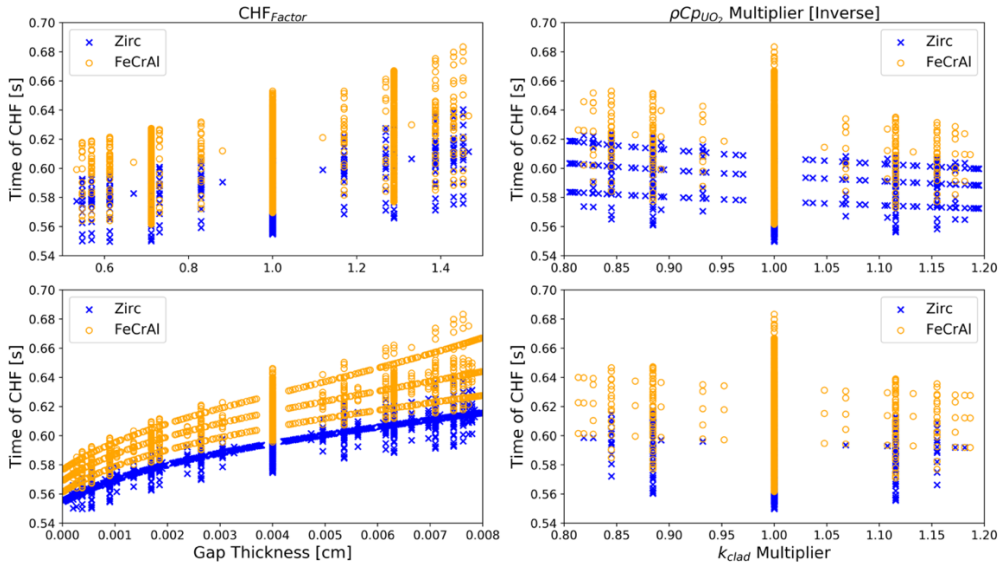

Figure 52. Time of CHF as a function of the CHF_F, gap thickness, volumetric heat capacity of UO_2, and the thermal conductivities of the Zircaloy and FeCrAl cladding for pool boiling.

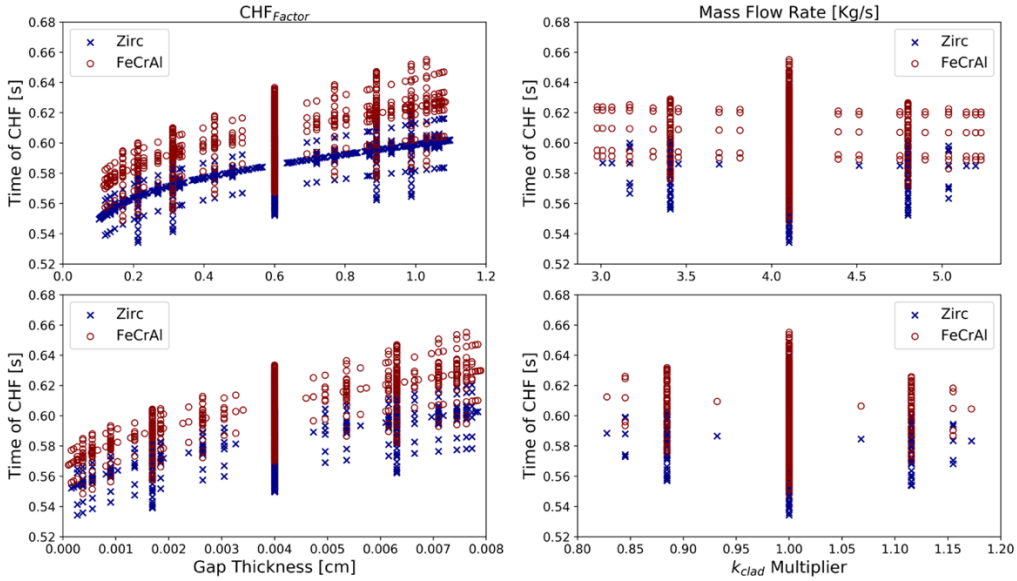

Figure 53. Time of CHF as a function of the CHF_F, gap thickness, MFR, and the thermal conductivities of the Zircaloy and FeCrAl cladding for flow boiling conditions.

CHAPTER 7

HIGHLIGHTING OTHER CONTRIBUTIONS

The purpose of this chapter is to highlight additional research contributions to the literature that are not part of the dissertation related work covered in the previous chapters. My contributions of the work in this chapter include two studies related to the advanced fuels campaign (AFC). The first research work discussed in section 7.1, conducted a reactor and fuel cycle performance of LWR fuel with ^{235}U enrichments between 4-7%. Cycle length, reactivity coefficients, as well as radial burnup, fission gas and plutonium content distribution were investigated. My direct contributions to this study included development of the study methodology, as well as modeling and analysis of the fuel cycle evaluation. The end result of the data generated in this study was published in a journal and can be found in the following reference [128].

The work in the second study investigated the use of high packing fraction fully ceramic micro-encapsulated fuel (FCM), and metal matrix micro-encapsulated (M3) fuel in LWRs. My direct contributions to the literature and knowledge related to this work, was the development of the necessary neutronics models, as well as the entire analysis that led to the development of a manuscript which was then submitted to a journal article for publication.

7.1 Reactor and Fuel Cycle Performance of LWR Fuel with ^{235}U Enrichments Above 5%

The objective of this section is to highlight the main contributions to the literature as a result of the work presented here investigating high-assay low enriched uranium (HALEU) fueled PWRs. The motivation behind conducting this study is a result of the development of accident tolerant fuels capable of elongating the duration of the fuel cycle length of current PWRs, as a result of advantageous features such as reduced cladding oxidation rates [129, 130]. The development of advanced small modular reactor (SMR) technologies have also led to the increased

interest in HALEU fueled, with potential benefits of such systems including increased flexibility, inherent safety and improved reliability [131]. The objective of this study was to conduct a pin-cell level neutronics investigation to investigate reactor performance parameters such as discharge fuel burnup, as well as radial pin analysis of burnup, fission gas production and plutonium production to determine whether increasing fuel above 5% impacted any of these parameters. Lastly, the investigation compared several metrics from the department of energy (DOE) fuel cycle evaluation and screening (E&S) study which classifies all fuel cycles within 40 evaluation groups [132]. Several high-level performance metrics were evaluated including natural resource utilization, spent fuel activity as well as environmental impacts. The methodology approach was to conduct neutronics evaluation of a PWR pin cell with ^{235}U enrichments between 4-7%. A 2-D model of the UO_2/Zircaloy pellet was developed using the SCALE code package, and the overall geometrical specifications were based on a 17x17 Westinghouse fuel pin. To conduct the radial analysis, the fuel pin was split into 20 radial regions, and depletion calculations were conducted using the T-DEPL feature of SCALE. Following, the linear reactivity model (LRM) was used to predict the single-batch cycle length, due to the assumption of a linear decay in reactivity for PWR cores. The 3-batch discharge burnup was then predicted for all of the considered fuel enrichment cases.

The initial reactor performance analysis resulted in discharge burnups ranging from 43.2 MWd/KgU for the 4% enrichment case, up to 75.8 MWd/KgU discharge burnup for the 7% enrichment case. These resulted in a discharge burnup dependence with enrichment of 10.9 MWd/kgU/%. Following, the beginning and end of life neutron spectrum was evaluated as shown in Figure 54 and Figure 55.

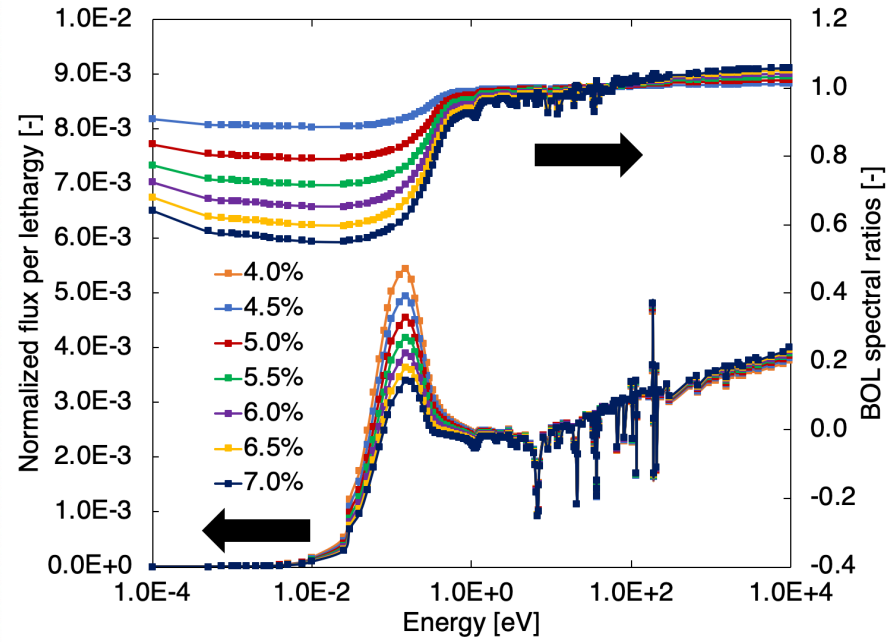

Figure 54. BOL neutron flux and spectral ratios of all enrichment cases for thermal and intermediate neutron energies.

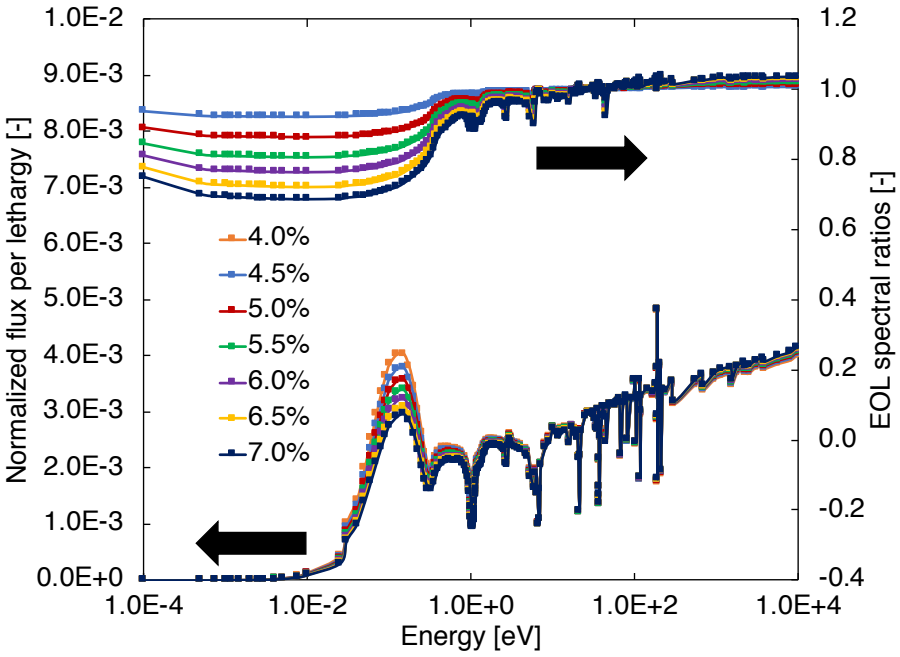

Figure 55. EOL neutron flux and spectral ratios of all enrichment cases for thermal and intermediate neutron energies.

Lastly, the reactor performance analysis also studied the impacts of changing enrichment on the fuel temperature coefficient (FTC), moderator temperature coefficient (MTC), the soluble boron coefficient (SBC) and the borated MTC. When it came to the FTC, the main takeaway is that although this reactivity coefficient became more positive with increasing reactivity, it remained sufficiently negative through the entire fuel cycle length. In the case of the MTC, this reactivity coefficient became slightly more positive with increasing enrichment, but once again remained negative enough throughout the entire fuel cycle length. The SBC and the moderated MTC also remained negative through the entire cycle length. Radial periphery burnup increased with increasing enrichment due to an increasing self-shielding effect as a result of more readily available ^{235}U atoms in the fuel material. This also resulted in an increment in fission gas content and plutonium yield near the outer periphery of the fuel pin. The main takeaway of the reactor performance analysis of increasing fuel enrichment above 5%, is that in regards to reactivity coefficients, and radial distribution of fission gas and plutonium content, these all behave similar for the considered enrichment cases, and the reactivity coefficients are maintained within the required safety constraints.

Next, a fuel cycle evaluation was conducted to investigate how increasing enrichment above 5%, impacts natural resource utilization, spent fuel activity, as well as environmental impacts. Starting with the front-end of the fuel cycle, the NRU normalized to a GWe-yr was evaluated. The results show that while the higher enrichment fuel is more efficient once it is loaded into the reactor as evidenced by a longer achievable fuel residence time, greater feedstock quantity is required to reach these enrichments in the first place. This is shown by the continuous increase in NRU needed to sustain the fuel cycle as enrichment is increased. The back end of the fuel cycle waste management metrics was evaluated for the three different radioactivity waste types. The

results show that the LLW is expected to increase as fuel enrichment is increased due to the higher separative work (SW) needed during the enrichment process of fuel production. Another major contribution to the amount of generated LLW is the operational requirements of the fuel cycle, which were assumed to be similar to that of a PWR. The highest amount of greater than class C (GTCC) waste production is also created during these normal cycle operations. The LLW generated for all the enrichment cases studied would have been classified under the "C" bin in the E&S study. The amount of the disposed DU+RU is the remaining mass after the required fuel cycle NRU has been deducted from the mass flow usable fuel amount of the system. Because more natural resources are needed to fabricate fuel with higher enrichment levels, the mass of the DU+RU increases with enrichment.

Finally, this effort analyzed the environmental impacts resulting from the operation of the fuel cycle within the range of enrichment cases considered. This evaluation focused on the land and water use, as well as CO2 emissions normalized to a GWe-yr. These environmental impacts were assumed to be similar to those of a PWR system on a per energy basis. The majority of the land and water use requirements come from the normal reactor operational requirements of the fuel cycle. The small variations are a result of the front- and back-end cycle demands. The higher enrichment cases needed more contributions from the front end of the fuel cycle to fabricate fuel, resulting in slightly higher land and water use. On the other hand, the slightly higher 100-year activity of the SNF+HLW in the lower enrichment range of this study required higher land and water use for spent fuel storage applications. Nevertheless, the performance of these two criteria for these enrichment cases were very similar. The greatest difference in CO2 emissions for all the cases analyzed came from the mass flow requirements of the fuel cycle. The data of these results is summarized in Table 16.

Table 16. Summary of evaluated fuel cycle performance parameters and performance bins for all fuel enrichment cases considered in this study. Performance bins range from A (best) to E (worst) [132].

Criterion	Metrics	Enrichment cases (%)						
		4.0	4.5	5.0	5.5	6.0	6.5	7.0
Nuclear Waste Management	Mass of SNF+HLW disposed, t/GWe-yr	25.61 (E)	22.60 (E)	20.23 (E)	18.44 (E)	16.93 (E)	15.69 (E)	14.6 (E)
	Activity of SNF+HLW (@100 yr), MCi/GWe-yr	1.403 (C)	1.400 (C)	1.397 (C)	1.396 (C)	1.395 (C)	1.394 (C)	1.393 (C)
	Activity of SNF+HLW (@100,000 yr), 10^{-4} MCi/GWe-yr	17.35 (C)	17.20 (C)	17.13 (C)	17.12 (C)	17.08 (C)	17.12 (C)	17.19 (C)
	Mass of DU+RU disposed, t/GWe-yr	182.31 (E)	185.36 (E)	187.8 (E)	191.18 (E)	193.85 (E)	196.56 (E)	198.7 (E)
	Volume of LLW, m^3/GWe-yr	406.46 (C)	407.17 (C)	407.87 (C)	409.15 (C)	410.22 (C)	411.37 (C)	412.33 (C)
Resource Utilization	Natural U required per energy generated, t/GWe-yr	207.93 (D)	207.97 (D)	208.03 (D)	209.62 (D)	210.78 (D)	212.25 (D)	213.29 (D)
Environmental Impact	Land use per energy generated, km^2/GWe-yr	0.186 (B)	0.183 (B)	0.181 (B)	0.18 (B)	0.18 (B)	0.179 (B)	0.178 (B)
	Water use per energy generated, ML/GWe-yr	23906 (B)	23906 (B)	23906 (B)	23907 (B)	23908 (B)	23909 (B)	23910 (B)
	Carbon emission - CO_2 released per energy generated, kt CO_2/GWe-yr	48.2 (B)	47.0 (B)	46.1 (B)	45.7 (B)	45.2 (B)	45 (B)	44.7 (B)

7.2 Investigation of High Packing Fraction FCM/M3 fuel in PWRs

Presented in this section is a neutronics investigation that was conducted using the Serpent monte carlo neutronics code, to investigate the implementation of high packing fraction FCM and M3 fuel in PWRs. These two micro-encapsulated matrix fuels have been of high interest to the ATF program, because they offer several safety advantages over conventional PWR pellet fuel including additional barriers preventing the release of fission products, the elimination of PCMIs and fuel swelling during an accident event, higher density and increased burnup fuel, as well as enhanced thermal properties [133,134,135]. The main challenge associated with the deployment of these fuels in PWRs is a decreased initial heavy metal (IHM) fuel load, which can be mitigated by increasing the ^{235}U fuel enrichment of the fuel, employing fuel kernel options with higher Urania density relative to UO_2 fuel, as well as employing higher packing fractions which is defined as the TRISO volume over the total volume of the TRISO and the matrix materials for the FCM/M3 fuels considered.

The objective of this study was then to conduct an assembly level neutronics investigation of PWRs loaded with high packing fraction FCM/M3 fuels. For the scope of the study, packing fractions between 40-74% were considered in a conventional 17x17 AP-1000 Westinghouse fuel assembly with ^{235}U enrichments between 10.0-19.75%. Three different fuel kernel options were considered; uranium mononitride (UN), uranium carbide (UC) and uranium oxycarbide (UCO). One of the novelties of the work presented here in the literature, is the development of body-centered cubic (BCC) and face-centered cubic (FCC) TRISO lattices needed to achieve the high packing fractions needed for this study. The overall methodology of the investigation consisted of development and validation of the AP-1000 fuel assembly baseline Serpent models for the study, followed by the development of BCC and FCC models, a fuel cycle length parametric study

involving packing fraction versus enrichment, and the development of realistic cases that did not include particle cutoffs for the FCM/M3 fuels for which a fuel cycle evaluation and calculations of reactivity coefficients was conducted. Verification of PF fractions in the models was performed through a stochastic monte carlo “checkvols” feature of Serpent.

As in the methodology approach, the first step was to develop and validate baseline Serpent neutronics models, which would then be used to conduct the subsequent burnup and depletion calculations for this investigation of high packing fraction FCM/M3 fueled PWRs. The baseline assembly model was based on a 17 x17 AP-1000 Westinghouse with 157 fuel assemblies, with an active core height of 14 ft and total core power of 3400 MW_{th}. The model, shown in Figure 56, utilized reflective boundary conditions and was depleted for 1500 effective full power days (EFPDs). To conduct the verification and validation study, the fuel cycle length in EFPDs of the fuel assembly Serpent model shown in Figure 56 with 19.75% enriched UN fuel kernels in an FCM matrix was compared with results from the following reference [133]. The comparison was made for two TRISO packing fractions, 0.40 and 0.55, using both hexagonal and square TRISO particle lattices. The fuel pin geometry, shown in Figure 57, had an outer FCM radius of 0.41 cm, and an outer cladding radius of 0.475 cm. Whereas, the TRISO particles had an outer UN kernel radius of 0.425 cm and an outer TRISO radius of 0.058 cm. These geometrical configurations were congruent with those in the reference used to validate the baseline models [133]. The results were agreeable with each other when comparing the expected k-effective trend behavior as well as the fuel discharge burnup for both packing fractions. Minor differences in fuel discharge burnup were attributed to particle cutoffs of the TRISO particles near the edges as a result of the geometry of the fuel pin (see Figure 57).

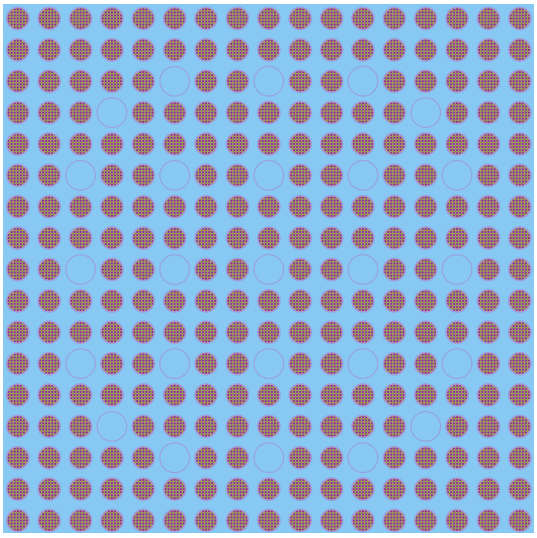

Figure 56. AP-1000 fuel assembly model used in the verification and validation study.

Table 1
FCM fuel particle configuration.

Material	Layer	Radius (cm)	Δ (cm)	ρ (g/cc)
UN	Kernel	0.0425	0.0425	14.31
C	Buffer	0.0475	0.0050	1.05
C	PyC layer	0.0510	0.0035	1.90
SiC	SiC layer	0.0545	0.0035	3.18
C	PyC layer	0.0580	0.0035	1.90

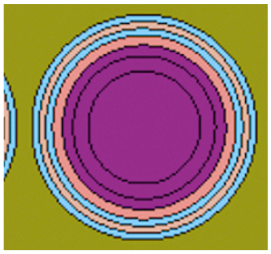

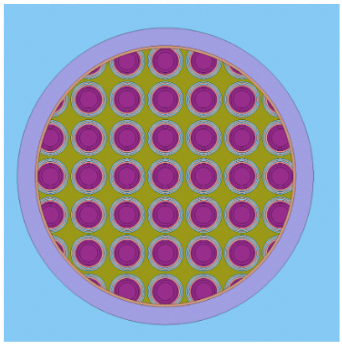

Table 2
FCM pellet configuration.

	Radius (cm)	Material
Pellet radius	0.4095	SiC matrix/FCM fuel
Gas gap radius	0.4180	Helium
Clad radius	0.4750	SiC
Pitch	1.2600	Water

Figure 57. Geometrical specifications of fuel pin and TRISO particles for the verification study.

This information was taken from the following reference [133].

Following, the baseline modes were used to conduct a parametric of study of cycle length, including both BCC and FCC lattices, with packing fractions ranging from 0.44 to 0.74. The scope of the parametric study consisted of calculating the fuel cycle length for an FCM fueled UN fuel assembly utilizing BCC and FCC lattices for the considered PFs, with three difference ^{235}U enrichments (10.0%, 15.0%, 19.9%). With the data from this parametric study, a scoping matrix of fuel cycle lengths vs PF/enrichment was developed which aided when choosing a realistic case for both the FCM and M3 fuels, that eliminated particle cutoff as shown in Figure 58. The realistic cases chosen all utilized 19.75% enriched ^{235}U fuel with UN, UC and UCO fuel kernels. The fuel cycle length evaluation is shown in Figure 59. Due to higher fuel content in UN, there is a" cross-over" in k-infinite factor of UCO and UC resulting in shorter fuel cycle for these two. Furthermore, both UC/UCO have initial higher excess reactivity due to higher parasitic neutron absorption in UN fuel.

Using the discharge burnup results for these realistic cases, a fuel cycle evaluation was then conducted following the guidelines of the DOE-NE fuel cycle E&S study. Three E&S study performance metrics were included in this analysis and compared the EG01 reference PWR case; the natural resource utilization, the waste management and the environmental impacts resulting from the operation of PWRs with these matrix based TRISO fuels. The results can be summarized as follows. For the natural resource utilization, all fuels behaved similarly with UC being marginally better at utilizing natural uranium. Further, all of the cases marginally underperformed the EG01 reference case of a conventional PWR with UO_2 pellet fuel. The spent fuel activity at 100 and 100,000 years both performed better than the reference EG01 case. Furthermore, the environmental impact metrics performed similar to the EG01 case; both are summarized in Figure 60 and Figure 61.

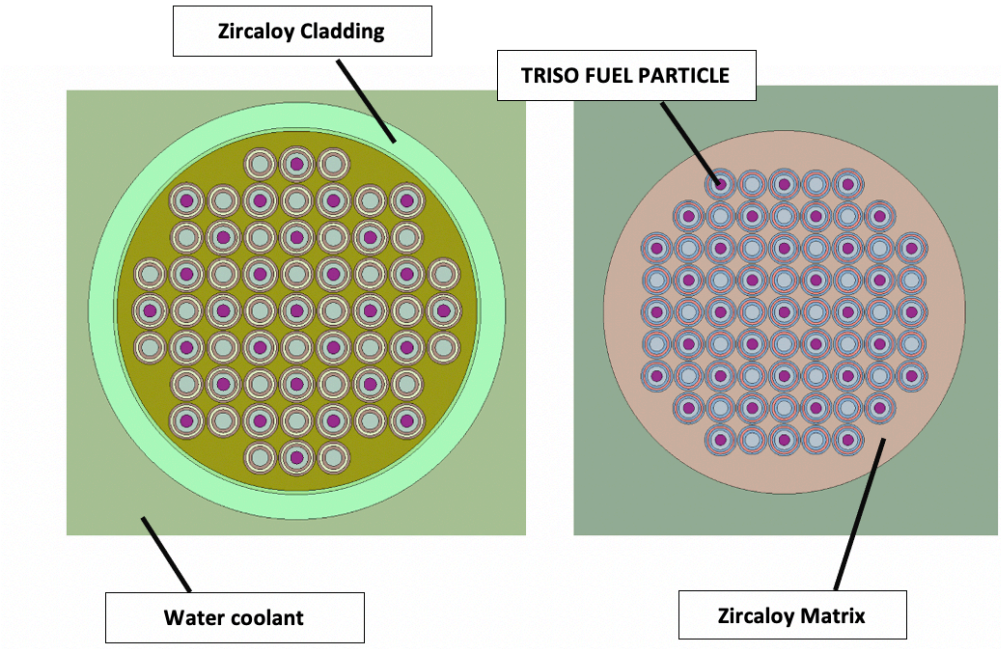

Figure 58. Cross-sectional view of the FCM (left) and M3 (right) configurations for the fuel pin region of the AP-1000 assembly model.

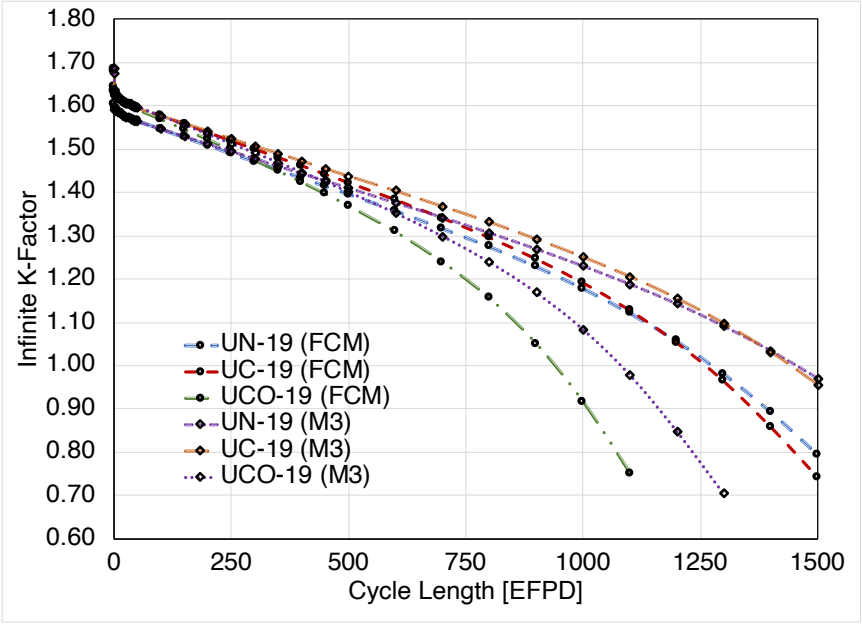

Figure 59. Fuel cycle burnup in EFPDs for both FCM and M3 fuels with three different TRISO fuel kernels (UN, UC, UCO).

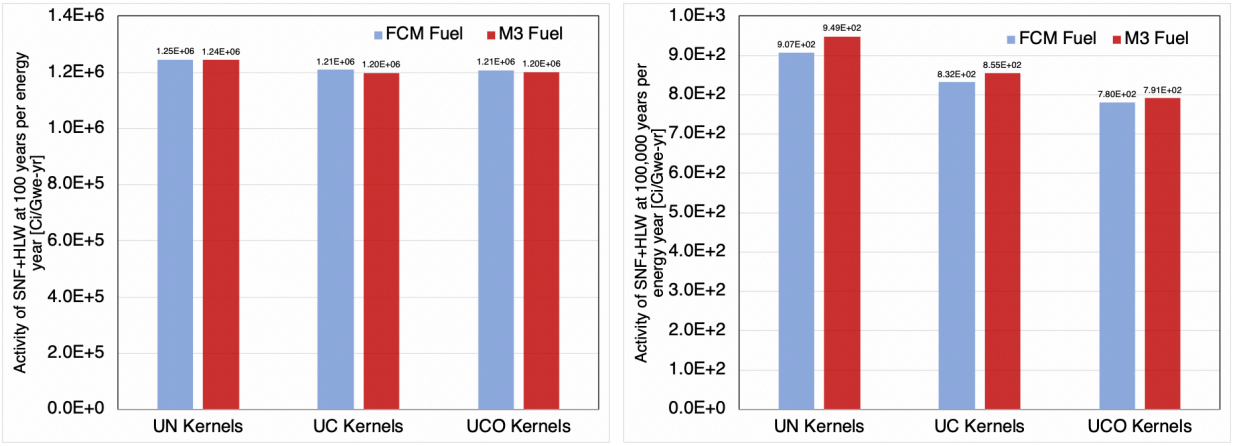

Figure 60. Spent fuel activity metrics at 100 and 100,000 years for all considered TRISO fuel options for the realistic cases.

Table 17. Environmental impact evaluation of all TRISO kernel fuel options for FCM/M3, along with categorization of metrics performance in the E&S study.

METRIC	FCM FUEL			M3 FUEL			EG01
	UN	UC	UCO	UN	UC	UCO	Reference
LAND USE - (km2/GWe-yr)	0.162/B	0.160/B	0.161/B	0.162/B	0.159/B	0.159/B	0.175/B
WATER USE - (ML/GWe-yr)	23896/B	23891/B	23893/B	23895/B	23888/B	23890/B	23891/B
CO2 EMISSIONS - (kt/GWe-yr)	39.2/B	38.5/B	38.8/B	39.0/B	38.1/B	38.3/B	44.1/B
WORKER RAD - (person-Sv/GWe-yr)	1.081/B	1.075/B	1.079/B	1.082/B	1.070/B	1.073/B	1.1/B

CHAPTER 8

CONCLUSION

8.1 Summary

The contents of this dissertation discusses the unique contributions provided by myself in support of an INL led project studying the effects of CHF-impacting parameters on this phenomenon. The overall objective of this work is to present the neutronics and thermal hydraulics design process of a TREAT borated heater rodlet CHF test device. Further, understanding the fuel-to-coolant heat transfer mechanisms of PWR-like test apparatuses under the fast-transient heating irradiation conditions within the TREAT facility is explored. The overarching goal of these heater apparatuses is to develop a pathway towards studying the comparison of the onset of the CHF phenomenon between accident tolerant cladding candidates and current Zircaloy-based materials, as well as improving current CHF correlations used in advanced computational tools. The topics discussed in Chapter 2, are crucial in establishing the basis of the work in this dissertation; mainly the reactivity-initiated accidents, as well as the effects of rapid heating and the thermal time constant definition.

The initial analysis covered in Chapter 3, discussed unique contributions in the neutronics design process of the TREAT borated test device in support of developing the technical requirements for the INL led project. This investigation took advantage of a full core TREAT model using the Serpent code. Originally, a solid borated heater rodlet was considered but the self-shielding study conducted determined that a tube apparatus can be used with minimal heat loss penalties. For the most limiting case, less than 15% of the heat generation occurred within the inner ~2mm of the borated rodlet. This is a result of the strong self-shielding effects of the borated material with a high thermal neutron cross section, and thus allowed instrumentation of the center

region for improved data gathering during TREAT experimentation. Following, a conservative analysis of the heat generation response expected for different boron concentrations was determined. A PCF was assigned to each boron concentration within a database spanning from 0.1-2.09 wt.%. These PCFs were utilized to couple the multi-physics approach of this design process. The neutronics results were independently validated using a full core TREAT model constructed using the MCNP code, and the results were within an agreeable range. The thermal hydraulics sensitivity analysis of the borated test device also covered in Chapter 3 of this dissertation, showed that the maximum energy deposition power pulse considered here, of about ~1400 MJ, is capable of inducing CHF in the water surrounding it with a considerable margin that could overcome the CHF enhancing effects experienced during rapid transient heating conditions. In addition, this is margin is important to account for systematic uncertainties between computer simulation models and real-life experimental conditions. Because the TREAT has a maximum capability of about ~2500MJ, this margin can be further expanded with a greater pulse energy deposition.

Chapter 4 covered the design analysis of radial and axial boron gradients manufactured into the borated heater device, and showed the possibility of these in shaping its axial and radial power curve. Furthermore, the axial transient behavior of the power curve was determined to be highly dependent on the occurrence of the CHF phenomenon. The goal is to ensure that the maximum heat flux values occur near the axial center of the rodlet, which is where most of the instrumentation will be located during TREAT experimentation. In addition, Chapter 5 covered a multiphysics capabilities validation study that compared experimental results with modeling predictions of several thermal heat transfer behaviors. The analysis showed that the RELAP5-3D code used in modeling the thermal hydraulics of these novel borated devices in TREAT

overpredicted peak cladding temperature, as well as post-DNB duration. A best fit model was also developed in Chapter 5 that vastly improved the peak cladding predictions, but nevertheless, this still showed differences between modeled and actual post-DNB behavior.

The work presented in Chapter 6 provide unique contributions that investigated the fuel-to-coolant heat transfer characteristics of two integral TREAT experimental fuel/cladding fuel designs consisting of UO_2/FeCrAl and UO_2/Zircaloy. The maximum fuel centerline temperature, the POCT, and the time of CHF were all analyzed for a transient power pulse application in TREAT using sensitivity analysis achieved using a RELAP5-3D model coupled with the RAVEN and DAKOTA codes. The first sensitivity study determined that the occurrence of the CHF phenomenon is the source of the highest uncertainty to the POCTs, but had no impact on the maximum fuel centerline temperature due to this occurring during the initial low-temperature adiabatic phase of the transient. The HTTC of the fuel systems, specifically the volumetric heat capacity of the fuel, had a dominant effect on the resolution of the maximum fuel centerline temperature. Furthermore, the HTTC was the major source of deviance in the POCT values when comparing cases for which the CHF was exceeded. Because the volumetric heat capacity of the fuel is the main driver of the thermal inertia of these TREAT experimental fuel designs, it was once again the dominant HTTC parameter towards the uncertainty of the POCT value. The thermal conductivity of the material components was shown to have minimal impact on the POCTs. The influence of the CHF multiplier was determined to decrease as a function of temperature, and thus it was more impactful for the UO_2/FeCrAl fuel system.

The thermomechanical effects of the changing gap thickness were studied using two different sensitivity study approaches. The first studied the sensitivity of the gap thickness as a parameter and determined that it was the second most important when determining the POCT.

Furthermore, the inclusion of the gap thickness in the sensitivity study eliminated any importance that the thermal conductivity of the gap had on the POCT. The second study approach conducted various sensitivity studies along different gap thickness reference points to observe how the impact of the HTTC parameters changed over the considered thickness. The data showed that the importance of the thermophysical properties of the fuel on the POCT increased with a decrease in gap thickness. Furthermore, a decreasing gap width also resulted in a decrement in the impacts of the coolant HTCs on the POCT. The gap thickness was also determined to be the most impacting parameter determining the time of when the CHF was exceeded in the TREAT fuel system test devices. The CHF multiplier was second most impactful towards the time of CHF occurrence, and the thermophysical material properties of the fuel/cladding components were shown to have minimal impact. These studies highlighted the importance of coupling the thermomechanical and thermal hydraulic effects of the gap region during RIA testing in TREAT.

8.2 Evaluation of Hypothesis

In this section we review the hypothesis that were established in section 1.2.3 as result of the work presented in this dissertation.

1. *The strong self-shielding effects of the borated material of the test device will allow the utilization of a tube design, instead of a solid heater rodlet, with beneficial instrumentational capabilities at its center region.*

   This proved to be true as it was shown in the work in this dissertation. Less than 15% of the heat generated in the solid borated rodlets occurred in the inner ~2mm center region. The self-shielding effect was strong enough due to the high thermal neutron absorption cross section of ^{10}B which is in the order of around 3840 barns. The self-shielding effects also increased with and increment in the boron content, due to a higher packing density of boron.

2. *The heating capabilities of the borated material coupled with the transient pulse capabilities in TREAT will provide a large margin that could potentially overcome the transient heating effects on the CHF manifestation.*

   This statement is true based on the results shown in this work. The 2.00 wt.% natural boron rodlet analyzed here using the 1407 MJ energy deposition TREAT power pulse, with a coolant degree of subcooling of 0 °C was determined to surpass the predicted RELAP5-3D value by a factor of 7.8. This was determining by varying the CHF multiplier feature. If this margin is proven to not be large enough, the TREAT has capabilities of power pulses up to ~2500 MJ, and thus this margin can be further extended.

3. *The thermophysical properties of the experimental PWR fuel rodlet systems will be a significant contributing factor for the maximum outer cladding temperature under DNB conditions.*

   This was proven to be true using the sensitivity analysis studying cases that exceeded CHF only. The HTTC thermophysical material component parameters, such as volumetric heat capacity and thermal conductivity, within the fuel/cladding systems proved to be the determining factor that predicts how high the POCT will increase during the post-CHF condition. This included the duration of the transition and film boiling phases.

4. *Due to numerous sources of uncertainties, large discrepancies between experimental data and modeling prediction will exist when validating the developed multiphysics capabilities.*

   This hypothesis was studied in Chapter 5, and proved to be true when comparing peak cladding temperature, post-DNB behavior and the temperature change in the thermal equilibrium of the system. A best fit model was develop that vastly decreased the discrepancies in peak cladding

temperature, but nevertheless large discrepancies remained due to the conservative nature of the developed multiphysics capabilities.

5. *The decreasing gap thickness that could be experienced during the application of a transient power pulse in TREAT, will result in an increased important in the fuel material properties of the TREAT experimental PWR fuel systems.*

   This statement is true, and the volumetric heat capacity and thermal conductivity of the fuel material was observed to increase as the width of the gap decreased. This is a result of two factors including the increased volume of the fuel pellet as well as the elimination of the influence of the thermal conductivity of the gap variable.

6. *The time of CHF will be significantly impacted by the thermal time constant of the PWR fuel systems, as well as the thermomechanical effects of the gap region.*

   The sensitivity study conducted in this dissertation to address this hypothesis showed that the changing gap region is in fact the most important parameter in deviations of the time occurrence of CHF. The CHF multiplier, although a feature of RELAP5-3D, is the second most important. This multiplier represents parameters that could change the systematic value of CHF and thus it is not an HTTC parameter. The thermophysical material and fluid properties used to represent the HTTC were found to have minimal impacts on the time of CHF relative to the gap effects and CHF multiplier.

8.3 Path Forward

The intended purpose of this section is to discuss some of the next steps as a follow up to the work that has been presented in the chapters of my dissertation. Mainly, these steps are associated with how the value of this work can provide a path forward to understanding where the limitations of current predictive computational tools exists and how these can be improved to allow for better representation of real life physical phenomena. The approach will be to identify what the limitations are, followed by a discussion of how these can be addressed.

For example, one of the main drawbacks of the RELAP5-3D program used for the thermal hydraulics work in my dissertation, is it inability to accurately model transient CHF behavior due to a lack of experimental data needed to develop these capabilities for these advanced codes. In order to predict the value of CHF, as well as other thermal behaviors, the RELAP5-3D utilizes steady state empirical correlations for the different phases of the boiling curve, as well as the steady state Groeneveld LUT to predict CHF. These have been shown to be accurate under steady state conditions because such have been developed through steady state heating experiments. Furthermore, RELAP5-3D also does not capture the holistic multiphysics needed to accurately predict the value of CHF, needed to include additional impacting parameters such as in-pile RISA effects. These limitations are the sources of large discrepancies between actual experimental results and the predictive capabilities of current computational tools, as such was the case in section 5.2.

There are several ways in which such limitations of these predictive tools can be addressed; mainly through the process of generation of experimental data to generate improved transient heating correlations that capture the thermal hydraulics physics under these conditions. For example, under steady state conditions the CHF phenomenon has been shown to occur as a result

of hydrodynamic instabilities of vapor columns leading to a formation of a vapor film. Whereas, under fast transient conditions bubble formation is better described by a spontaneous nucleation process which leads to the CHF phenomenon as a result of bubbles coalescing to form vapor blanket regions. Thus, the integration of models that are capable of improving correlations to include spontaneous nucleation is one approach to improve current predictive tools. Other promising approaches to improve predictive CHF capabilities of modern computational tools can be found in the literature. One approach by Zhao [136], presents a mechanistic transient model utilizing two liquid sublayer theory based correlations that were validated for several transients. Although the paper highlights that the model still under estimates the value of CHF for very fast transients [136]. Another proposed method by Zhao [137], utilizes physics-informed machine learning to better predict CHF under transient conditions for rod fuel bundles. Other promising approaches to developing improved predictive computational tools, are reimagining how the physics behind the onset of the CHF phenomenon is described to better capture the multiphysics phenomenon of this event. For example, in the dissertation work of Demarly [138] the microhydrodynamic effects of the DNB manifestation event are studied using data from infrared thermometry experiments to more holistically capture the mutiphysics effects in a high pressure environment, as well as for surface characteristics for which current capabilities in predictive models aren't suitable. Furthermore, the work is this dissertation is aimed at capturing the multiphysics effects of combining several CHF impacting parameters so that better predictions can be achieve using current tools. The main takeaway of this path forward section, is that better implementation of the multiphysics of transient CHF is needed to accurately predict this phenomenon using current computational tools, and these efforts need to be continued to be supported through experimental efforts such as the work in this dissertation.

LIST OF REFERENCES

[1] Carmack, J., Goldner, F., Bragg-Sitton, S. M., & Snead, L. L. (september 2013). Overview of the U.S. DOE Accident Tolerant Fuel Development Program. *Top Fuels 2013*. doi:INL/CON-13-29288

[2] Yamamoto, Y., Pint, B. A., Terrani, K. A., Field, K. G., Yang, Y., Snead, L. L., "Development and property evaluation of nuclear grade wrought FeCrAl fuel cladding for light water reactors," *J. Nucl. Mater.*, 467 pp. 703-716, 2015.

[3] Field, K. G., Snead, M. A., Yamamoto, Y., Terrani, K. A., (2017). Handbook on the Material Properties of FeCrAl Alloys for Nuclear Power Production Applications. ORNL/TM-2017/186.

[4] Terrani, K. A., Karlsen, T. M., Yamamoto, Y., (2016). Input Correlations for Irradiation Creep of FeCrAl and SiC Based on In-Pile Halden Test Results. ORNL/TM-2016/191.

[5] OECD NEA, "RIA Fuel Codes Benchmark", Vol 1. NEA/CSNI/R(2013)/7.

[6] Marchand, O., Zhang, J., and Cherubini, M., "Reactivity Initiated Accident (RIA) Fuel Codes Benchmark Phase-II: Uncertainty and Sensitivity Analyses," Report NEA/CSNI/R(2017)1, Nuclear Energy Agency, Organisation for Economic Co- operation and Development (OECD), 2017.

[7] J. Leppänen. *Serpent – a Continuous-energy Monte Carlo Reactor Physics Burnup Calculation Code*. VTT Technical Research Centre of Finland. (June 18, 2015).

[8] Idaho National Laboratory, "RELAP5-3D Code Manuals, Volumes I, II, III, IV, V, and Appendix A, Revision 4.3," Idaho National Laboratory, INEEL-EXT 98-00834, 2015.

[9] Rabiti, C., ET AL., 2017. RAVEN User Manual. INL/EXT-15-34123.

[10] Adams, B.M., Bohnhoff, W.J., Dalbey, K.R., Ebeida, M.S., Eddy, J.P., Eldred, M.S., Geraci, G., Hooper, R.W., Hough, P.D., Hu, K.T., Jakeman, J.D., Khalil, M., Maupin, K.A., Monschke, J.A., Ridgway, E.M., Rushdi, A.A., Stephens, J.A., Swiler, L.P., Vigil, D.M., Wildey, T.M., and Winokur, J.G., "Dakota, A Multilevel Parallel Object-Oriented Framework for Design Optimization, Parameter Estimation, Uncertainty Quantification, and Sensitivity Analysis: Version 6.11 User's Manual," Sandia Technical Report SAND2014-4633, July 2014; updated November 2019.

[11] J. Desquines, D. A. Koss, A. T. Motta, B. Cazalis and M. Petit, "The issue of stress state during mechanical tests to asses cladding performance during a reactivity-initiated accident (RIA)," Journal of Nuclear Materials, vol. 412, pp.250-267, 2011.

[12] Kim, Sun-Ki. "Behaviors of Nuclear Fuel Cladding During RIA." *Advances in Nuclear Fuel*, 2012, doi:10.5772/34091.

[13] OECD NEA, "Nuclear Fuel Behaviour Under Reactivity-Initiated Accident". ISBN 978-92-64-99113-2. www.oecd-nea.org/nsd/reports/2010/nea6847-behaviour-RIA.pdf. (2010).

[14] Ott, Karl O., and Winfred A. Bezella. *Introductory Nuclear Reactor Statics*. American Nuclear Society, 1989.

[15] Schmitz, F., & Papin, J. (1999). High burnup effects on fuel behaviour under accident conditions: The tests CABRI REP-Na. *Journal of Nuclear Materials, 270*(1-2), 55-64. doi:10.1016/s0022-3115(98)00895-2

[16] Lorenz, R., & Parker, G. (1972). Final Report On The Second Fuel Rod Failure Transient Test Of A Zircaloy- Clad Fuel Rod Cluster In Treat. doi:10.2172/4691610

[17] Lorenz, R., Hobson, D., & Parker, G. (1971). Final Report On The First Fuel Rod Failure Transient Test Of A Zircaloy- Clad Fuel Rod Cluster In Treat. doi:10.2172/4018010

[18] Lorenz, R. A., Hobson, D. O., & Parker, G. W. (1971). Fuel Rod Failure Under Loss-of-Coolant Conditions in Treat. *Nuclear Technology, 11*(4), 502-520. doi:10.13182/nt71-a30847

[19] Fuketa, T., Sasajima, H., Mori, Y., & Ishijima, K. (1997). Fuel failure and fission gas release in high burnup PWR fuels under RIA conditions. *Journal of Nuclear Materials, 248*, 249-256. doi:10.1016/s0022-3115(97)00173-6
[20] Fuketa, T., Ishijima, K., & Mori, Y. (1996). New results from the NSRR experiments with high burnup fuel. doi:10.2172/269705
[21]"NRC Regulations Title 10, Code of Federal Regulations." *United States Nuclear Regulatory Commission - Protecting People and the Environment*, https://www.nrc.gov/reading-rm/doc-collections/cfr/.
[22] Rudling, P., & Jernkvist, L. O. (december 2016). Nuclear Fuel Behaviour under RIA Conditions. *Advanced Nuclear Technology International*.
[23] Reyes, Jose. "Natural Circulation in Water Cooled Nuclear Power Plants Phenomena, Models, and Methodology for System Reliability Assessments." *IAEA-TECDOC-1474*, 2005, doi:10.2172/836896.
[24] Rosenthal, M. W., "An Experimental Study of Transient Boiling," *Nucl. Sci. Eng.*, 2, 640, 1957.
[25] Serizawa, A., "Theoretical prediction of maximum heat flux in power transients," *Int. J. Heat Mass Transfer*, vol. 26, p.921, 1983.
[26] Pasamehmetoglu, K. O., Nelson, R. A., Gunnerson, F. S., "Critical Heat Flux Modeling in Pool Boiling for Steady-State and Power Transients," *Journal of Heat Transfer* 112 (4), pp. 1048-1057, 1990.
[27] Chang, S. H., Lee, K. W., Groeneveld, D. C., "Transient-effects modeling of critical heat flux," *Nucl. Eng. Des.*, 133, pp. 51-57, 1989.
[28] Kossolapov, A., "Transient flow boiling CHF under exponentially escalating heat inputs," Massachusetts Institute of Technology (2018).
[29] Groeneveld, D.c., et al. "The 2006 CHF Look-up Table." *Nuclear Engineering and Design*, vol. 237, no. 15-17, 2007, pp. 1909–1922., doi:10.1016/j.nucengdes.2007.02.014.
[30] Groeneveld, D. C., et al. "The 1995 Look-up Table for Critical Heat Flux in Tubes." *Nuclear Engineering and Design*, vol. 163, no. 1-2, 1996, pp. 1–23., doi:10.2172/111418.
[31] Bess, J. D. and DeHart, M. D., "Baseline assessment of TREAT for modeling and analysis needs," Report INL/EXT-15-35372, Idaho National Laboratory, 2015.
[32] Woolstenhulme, N. E., et al. "Capabilities Development for Transient Testing of Advanced Nuclear Fuels at TREAT." *Top Fuel 2016*, Sept. 2016, INL/CON-16-37608.
[33] Pope, Chad L., et al. "Transient Reactor Test (TREAT) Facility Design and Experiment Capability." *Nuclear Technology*, vol. 205, no. 10, June 2019, pp. 1378–1386., doi:10.1080/00295450.2019.1599615.
[34] Mccoy, Frank. "Final Report for the Contractor Readiness Assessment of the Transient Reactor Test Facility Resumption of Transient Testing Activity at the Idaho National Laboratory." June 2017, doi:10.2172/1468428.
[35] Woolstenhulme, N. E., et al. "Capabilities Development for Transient Testing of Advanced Nuclear Fuels at TREAT." *Top Fuels 2016*. doi:INL/CON-16-37608
[36] Bess, John D., et al. "Narrowing Transient Testing Pulse Widths to Enhance LWR RIA Experiment Design in the TREAT Facility." *Annals of Nuclear Energy*, vol. 124, 2019, pp. 548–571., doi:10.1016/j.anucene.2018.10.030.
[37] Woolstenhulme, Nicolas, et al. "Development of Irradiation Test Devices for Transient Testing." *Nuclear Technology*, vol. 205, no. 10, 2019, pp. 1251–1265., doi:10.1080/00295450.2019.1590072.

[38] Woolstenhulme, N., Baker C., Chapman D., Hill C., Papesh C., Rosvall E. and Snow S. "Conceptual Report for the Minimal Activation Retrievable Capsule Holder Irradiation Vehicle System." *INL/INT-17-43170*, Sept. 2017.
[39] Bess, J. D., & Woolstenhulme, N. E. (n.d.). TREAT Neutronics Analysis and Design Support, Part I: Multi-SERTTA. *Top Fuels 2016*. doi:INL/CON-16-37589
[40] Woolstenhulme, N. E., & Epiney, A. S. (2019). Status Report on Development of TREAT Water Loop. doi:10.2172/1572404
[41] Zuber, Novak. "Hydrodynamic Aspects of Boiling Heat Transfer (Thesis)." 1959, doi:10.2172/4175511.
[42] Zuber, N., and M. Tribus. "Further remarks on the stability of boiling heat transfer. Report 58-5." 1958, doi:10.2172/4332326.
[43] Kutateladze, S. S. "Hydromechanical Model of Heat Transfer Crisis in Pool Liquid Boiling." *Journal of Technical Physics*, vol. 20, 1950, pp. 1389–1392.
[44] Kutateladze, S. S., and L. L. Schneiderman. "Experimental Study of Influence of Temperature of Liquid on Change in the Rate of Boiling." *U.S Atomic Energy Commission Report*, 1953. USAEC Report, AECtr. 3405, pp. 95–100.
[45] Rohsenow, W. M., Griffith, P. "Correlation of Maximum Heat Flux Data for Boiling of Saturated Liquids." *The Office of Naval Research*, 13 Mar. 1955. Contract N5ori-07827.
[46] Liang, G. and Mudawar, I. "Pool Boiling Critical Heat Flux (CHF) – Part 1: Review of Mechanisms, Models, and Correlations." *International Journal of Heat and Mass Transfer*, vol. 117, 2018, pp. 1352–1367., doi:10.1016/j.ijheatmasstransfer.2017.09.134.
[47] N. ZUBER, M. TRIBUS and J. W. WESTWATER, "The hydrodynamic crisis in the pool boiling of saturated and subcooled liquids". Proc. Znt. Heat Transfer Conference, Boulder, Colorado, 1961, Part 2, pp. 224-229 (1961).
[48] Ponter, A.b., and C.p. Haigh. "The Boiling Crisis in Saturated and Subcooled Pool Boiling at Reduced Pressures." *International Journal of Heat and Mass Transfer*, vol. 12, no. 4, 1969, pp. 429–437., doi:10.1016/0017-9310(69)90138-0.
[49] Inoue, T., et al. "Effect of Subcooling on Critical Heat Flux during Pool Boiling on a Horizontal Heated Wire." *Heat and Mass Transfer*, vol. 33, no. 5-6, 1998, pp. 481–488., doi:10.1007/s002310050219.
[50] Elkassabgi, Y., and J. H. Lienhard. "Influences of Subcooling on Burnout of Horizontal Cylindrical Heaters." *Journal of Heat Transfer*, vol. 110, no. 2, 1988, p. 479., doi:10.1115/1.3250511.
[51] Sakurai, A. "Mechanisms of Transitions to Film Boiling at CHFs in Subcooled and Pressurized Liquids Due to Steady and Increasing Heat Inputs." *Nuclear Engineering and Design*, vol. 197, no. 3, 2000, pp. 301–356., doi:10.1016/s0029-5493(99)00314-3.
[52] Jun, Seongchul, et al. "Effect of Subcooling on Pool Boiling of Water from Sintered Copper Microporous Coating at Different Orientations." *Science and Technology of Nuclear Installations*, vol. 2018, 2018, pp. 1–9., doi:10.1155/2018/8623985.
[53] Katto, Y. "Critical Heat Flux." *Int. J. Multiphase Flow*, vol. 20, 13 Feb. 1994, pp. 53–90.
[54] Kirichenko, Yu. A., and P. S. Chernyakov. "Determination of the First Critical Thermal Flux on Flat Heaters." *Journal of Engineering Physics*, vol. 20, no. 6, 1971, pp. 699–703., doi:10.1007/bf01122589.
[55] Sakashita, Hiroto. "Critical Heat Flux on a Vertical Surface in Saturated Pool Boiling at High Pressures." *Journal of Thermal Science and Technology*, vol. 11, no. 2, 2016, doi:10.1299/jtst.2016jtst0020.

[56] Stelute, E., et al. “Roughness Effects on Nucleate Boiling Heat Transfer from Cylindrical Surfaces To Refrigerant R-134a.” *Boiling*, 2006, doi:10.1615/ihtc13.p28.180.
[57] Kunito, Okuyama, et al. “Transient Boiling Heat Transfer Characteristics of R113 at Large Stepwise Power Generation.” *International Journal of Heat and Mass Transfer*, vol. 31, no. 10, 1988, pp. 2161–2174., doi:10.1016/0017-9310(88)90125-1.
[58] Dahariya, Smreeti, and Amy R. Betz. “High Pressure Pool Boiling: Mechanisms for Heat Transfer Enhancement and Comparison to Existing Models.” *International Journal of Heat and Mass Transfer*, vol. 141, 2019, pp. 696–706., doi:10.1016/j.ijheatmasstransfer.2019.07.016.
[59] Derewnicki, K.p. “Experimental Studies of Heat Transfer and Vapour Formation in Fast Transient Boiling.” *International Journal of Heat and Mass Transfer*, vol. 28, no. 11, 1985, pp. 2085–2092., doi:10.1016/0017-9310(85)90102-4.
[60] Stock, B.j. “Observations on Transition Boiling Heat Transfer Phenomena.” 1960, doi:10.2172/4171499.
[61] Chowdhury, S. K., and R. H.S. Winterton. “Surface Effects in Pool Boiling.” *International Journal of Heat and Mass Transfer*, vol. 28, no. 10, 6 May 1985, pp. 1881–1889.
[62] Maracy, M., and R.h.s. Winterton. “Hysteresis and Contact Angle Effects in Transition Pool Boiling of Water.” *International Journal of Heat and Mass Transfer*, vol. 31, no. 7, 1988, pp. 1443–1449., doi:10.1016/0017-9310(88)90253-0.
[63] O'Hanley, Harry, et al. “Separate Effects of Surface Roughness, Wettability, and Porosity on the Boiling Critical Heat Flux.” *Applied Physics Letters 103*, 2013, htts://doi.org/10.1063/1.4813450.
[64] Liaw, Shih-Pin, and Dean Vijay K. Dhir. “Effect of Surface Wettability On Transition Boiling Heat Transfer From A Vertical Surface.” *Proceeding of International Heat Transfer Conference 8*, 1986, doi:10.1615/ihtc8.3980.
[65] Kandlikar, Satish G. “A Theoretical Model to Predict Pool Boiling CHF Incorporating Effects of Contact Angle and Orientation.” *Journal of Heat Transfer*, vol. 123, no. 6, 2001, p. 1071., doi:10.1115/1.1409265.
[66] Kang, Myeong-Gie. “Effect of Surface Roughness on Pool Boiling Heat Transfer.” *International Journal of Heat and Mass Transfer*, vol. 43, no. 22, 2000, pp. 4073–4085., doi:10.1016/s0017-9310(00)00043-0.
[67] Pioro I.L., Rohsenow W., Doerffer S.S., ‘Nucleate Pool-Boiling Heat Transfer, 1: Review of Parametric Effects of Boiling Surface’, IJHMT 47 (23) (2004) 5033–5044.
[68] Ferjancic, Klemen, and Iztok Golobic. “Surface Effects on Pool Boiling CHF.” *Experimental Thermal and Fluid Science*, 23 Oct. 2001, pp. 565–571.
[69] Lienhard, John H. “Transition Boiling Heat Transfer and the Film Transition Regime” *Journal of Heat Transfer*, vol. 111, no. 2, 1989, p. 248., doi:10.1115/1.3250670.
[70] Lee, Chi Young, et al. “Pool Boiling Heat Transfer with Nano-Porous Surface.” *International Journal of Heat and Mass Transfer*, vol. 53, 16 May 2010, pp. 4274–4279.
[71] Rioux, Russell P., et al. “A Systematic Study of Pool Boiling Heat Transfer on Structured Porous Surfaces: From Nanoscale through Microscale to Macroscale.” *AIP Advances*, vol. 4, no. 11, 2014, p. 117133., doi:10.1063/1.4902343.
[72] Tachibana, Fujio, and Mamoru Akiyama. “Non-Hydrodynamic Aspects of Pool Boiling Burnout.” *Journal of Nuclear Science and Technology*, vol. 4, no. 3, 1967, pp. 121–130., doi:10.3327/jnst.4.121.
[73] Lee, Chi Young, et al. “Critical Heat Flux of Oxidized Zircaloy Surface in Saturated Water Pool Boiling.” *Journal of Nuclear Science and Technology*, 2014, pp. 1–11., doi:10.1080/00223131.2014.956830.

[74] Otsuka, Teppei, et al. “On the Wettability Change of Oxidized and Gamma Irradiated Zircaloy.” *INIS Database*, vol. 37, no. 46, 2005.
[75] Svanholm, K, et al. “Halden Reactors IFA-511.2 and IFA-54x: Experimental Series under Adverse Core Cooling Conditions.” *Experimental Thermal and Fluid Science*, vol. 11, no. 1, 1995, pp. 77–100., doi:10.1016/0894-1777(94)00138-x.
[76] Sugiyama, Tomoyuki, and Toyoshi Fuketa. “Effect of Cladding Surface Pre-Oxidation on Rod Coolability under Reactivity Initiated Accident Conditions.” *Journal of Nuclear Science and Technology*, vol. 41, no. 11, 2004, pp. 1083–1090., doi:10.1080/18811248.2004.9726333.
[77] Georgenthum, V., et al, “Synthesis and Interpretation of Fuel Cladding Temperature Evolution under Reactivity Initiated Accident in NSRR Reactor.” *Proc. WRFPM 2014, Sendai, Japan,* Sept. 14-17, 2014.
[78] Kano, Sho, et al. “Investigation of Radiation-Induced Surface Activation Effect in Austenitic Stainless Steel under Ultraviolet and γ-Ray Irradiations.” *Journal of Nuclear Science and Technology*, vol. 56, no. 3, 2019, pp. 300–309., doi:10.1080/00223131.2019.1571451.
[79] Takamasa, T., et al. “Radiation Induced Surface Activation on Leidenfrost and Quenching Phenomena.” *Experimental Thermal and Fluid Science*, vol. 29, no. 3, 2005, pp. 267–274., doi:10.1016/j.expthermflusci.2004.05.014.
[80] Seshadri, Arunkumar, et al. “Towards Understanding the Effects of Irradiation on Quenching Heat Transfer.” *International Journal of Heat and Mass Transfer*, vol. 127, 2018, pp. 1087–1095., doi:10.1016/j.ijheatmasstransfer.2018.07.144.
[81] Auracher, Hein, and Wolfgang Marquardt. “Experimental Studies of Boiling Mechanisms in All Boiling Regimes under Steady-State and Transient Conditions.” *International Journal of Thermal Sciences*, vol. 41, no. 7, 2002, pp. 586–598., doi:10.1016/s1290-0729(02)01352-2.
[82] Bessiron, Vincent. “Modelling of Clad-to-Coolant Heat Transfer for RIA Applications.” *Journal of Nuclear Science and Technology*, vol. 44, no. 2, 2007, pp. 211–221., doi:10.3327/jnst.44.211.
[83] Bessiron, Vincent, Tomoyuki Sugiyama and Toyoshi Fuketa. “Clad-to-Coolant Heat Transfer in NSRR Experiments.” *Journal of Nuclear Science and Technology*, vol. 44, no. 5, 2007, pp. 723–732., doi:10.3327/jnst.44.723.
[84] Hata, K., Shiotsu, M., & Noda, N. (2006). Influence of Test Tube Material on Subcooled Flow Boiling Critical Heat Flux in Short Vertical Tube. Volume 2: Thermal Hydraulics. doi:10.1115/icone14-89162
[85] Hata, K., & Masuzaki, S. (2009). Subcooled Boiling Heat Transfer for Turbulent Flow of Water in a Short Vertical Tube. Journal of Heat Transfer, 132(1). doi:10.1115/1.3194768
[86] Park, J., Fukuda, K., & Liu, Q. (2009). Transient Chf Phenomena Due To Exponentially Increasing Heat Inputs. Nuclear Engineering and Technology, 41(9), 1205-1214. doi:10.5516/net.2009.41.9.1205
[87] Bessiron, Vincent. “Modelling of Clad-to-Coolant Heat Transfer for RIA Applications.” *Journal of Nuclear Science and Technology*, vol. 44, no. 2, 2007, pp. 211–221., doi:10.3327/jnst.44.211.
[88] Isao, K., Akimi, S., & Akira, S. (1983). Transient boiling heat transfer under forced convection. International Journal of Heat and Mass Transfer, 26(4), 583-595. doi:10.1016/0017-9310(83)90009-1
[89] Unal, C., Daw, V., Nelson, R.A., “Unifying the controlling mechanisms for the critical heat flux and quenching: the ability of liquid to contact the hot surface,” *J. Heat Transf.*, 114, pp. 972-982, 1992.
[90] Golobič, I., Bergles, A.E., “Effects of heater-side factors on the saturated pool boiling critical heat flux,” *Exp. Therm. Fluid Sci.*, 15, pp. 43-51, 1997.

[91] Saylor, J.R., "An Experimental Study of the Size Effect in Pool Boiling Critical Heat Flux on Square Surfaces," University of Minnesota (1989).
[92] Arik, M., Bar-cohen, A., "Effusivity-based correlation of surface property effects in pool boiling CHF of dielectric liquids," *Int. J. Heat Mass Transf.*, 46, pp. 3755-3764, 2003.
[93] Lee, M.H., Heo, H., Bang, I.C., "Effect of thermal activity on critical heat flux enhancement in downward-hemispherical surface using graphene oxide coating," *Int. J. Heat Mass Transf.*, 127, pp. 1102-1111, 2018.
[94] Ho, J.Y., Wong, K.K., Leong, K.C., "Saturated pool boiling of FC-72 from enhanced surfaces produced by Selective Laser Melting," *Int. J. Heat Mass Transf.,* 99, pp. 107-121, 2016.
[95] Gogonin, I.I., "Influence of the thickness of a wall and of its thermophysical characteristics on the critical heat flux in boiling," *J. Eng. Phys. Thermophys.*, 82 (6), pp. 1175-1183, 2009.
[96] Raghupathi, P.A., Kandlikar, S.G., "Effect of thermophysical properties of the heater substrate on critical heat flux in pool boiling," *J. Heat Transf.*, 139, Article 111502, 2017.
[97] Staszel, C., Yarin, A.L., "Exponential vaporization fronts and critical heat flux in pool boiling," *Int. Commun. Heat Mass Transf.*, 98, pp. 171-176, 2018.
[98] Kam, D.H., Choi, Y.J., Jeong, Y.H., "Critical heat flux on downward-facing carbon steel flat plates under atmospheric condition," *Exp. Therm. Fluid Sci.*, 90, pp. 22-27, 2018.
[99] Pasamehmetoglu, K. O., Nelson, R. A., Investigation of the quasi-steady approach used in transient two. phase flow analysis, ASME/AIChE/ANS National Heat Transfer Conference, p.279, 1988.
[100] Hwang, D. H., Kim, S. J., Kwon, H., Seo, K. W., Lee, J. H., "Transient CHF in Rod Bundle under SMR Conditions," *Transactions of the Korean Nuclear Society Autumn Meeting*, Gyeongju, Korea, October 26-27, 2017.
[101] Brown, E., Yan, Y., Marcum, W. R., "A Novel Method for Predicting Power Transient CHF via the Heterogeneous Spontaneous Nucleation Trigger Mechanism," *Nuclear Technology*, 2020.
[102] Umekawa, H., Ozawa, M., Mitsunaga, T., Mishima, K., Hibiki, T., Saito, Y., "Scaling parameter of CHF under oscillatory flow conditions," *Heat Transfer-Asian Research*, 28 (6), 1999.
[103] Kandlikar, S. G. (1990). A General Correlation for Saturated Two-Phase Flow Boiling Heat Transfer Inside Horizontal and Vertical Tubes. Journal of Heat Transfer, 112(1), 219-228. doi:10.1115/1.2910348
[104] Lee, S. K., Liu, M., Brown, N. R., Terrani, K. A., Blandford, E. D., Ban, H., . . . Lee, Y. (2019). Comparison of steady and transient flow boiling critical heat flux for FeCrAl accident tolerant fuel cladding alloy, Zircaloy, and Inconel. International Journal of Heat and Mass Transfer, 132, 643-654. doi:10.1016/j.ijheatmasstransfer.2018.11.141
[105] Folsom, Charles P. "Fuel Performance Modeling of Reactivity-Initiated Accidents Using the Bison Code." 2017, doi:10.2172/1464773.
[106] OECD NEA, "RIA Fuel Codes Benchmark", Vol 1. NEA/CSNI/R(2013)/7.
[107] Marchand, O., Zhang, J., and Cherubini, M., "Reactivity Initiated Accident (RIA) Fuel Codes Benchmark Phase-II: Uncertainty and Sensitivity Analyses," Report NEA/CSNI/R(2017)1, Nuclear Energy Agency, Organisation for Economic Co- operation and Development (OECD), 2017.
[108] Ortensi, J., Et al. "Preliminary Serpent Model of the MARCH-SETH Experiment in TREAT." *INL/MIS-18-45938*.

[109] Woolstenhulme, N., Baker C., Chapman D., Hill C., Papesh C., Rosvall E. and Snow S. "Conceptual Report for the Minimal Activation Retrievable Capsule Holder Irradiation Vehicle System." *INL/INT-17-43170*, Sept. 2017.
[110] Bess J., Woolstenhulme N., Hill C., Jensen C., Snow S. "TREAT Neutronics Analysis and Design Support, Part I: Multi-SERTTA". INL/CON-16-37589, August 2016.
[111] Lamarsh J. R. and Baratta A. J., 2001. Introduction to Nuclear Engineering, 3rd edition. Prentice Hall, Upper Saddle River.
[112] Los Alamos Scientific Laboratory. Group X-6. MCNP: a General Monte Carlo Code for Neutron and Photon Transport. Los Alamos, N.M.: [Springfield, Va.]: Dept. of Energy, Los Alamos Scientific Laboratory; [for sale by the National Technical Information Service], 1979.
[113] Mandelli, D., Prescott S., Smith C., Alfonsi A., Rabiti C., Cogliati J. and Kinoshita R. "A Flooding Induced Station Blackout Analysis for a Pressurized Water Reactor Using the RISMC Toolkit." *Science and Technology of Nuclear Installations*, vol. 2015, no. 308163, 17 May 2015.
[114] Groeneveld, D.c., et al. "The 2006 CHF Look-up Table." *Nuclear Engineering and Design*, vol. 237, no. 15-17, 2007, pp. 1909–1922., doi:10.1016/j.nucengdes.2007.02.014.
[115] Groeneveld, D.c., et al. "The 2006 CHF Look-up Table." *Nuclear Engineering and Design*, vol. 237, no. 15-17, 2007, pp. 1909–1922., doi:10.1016/j.nucengdes.2007.02.014.
[116] Jensen, C. B., et al., "Preliminary Results from In-Pile Transient Boiling Experiments at the TREAT Facility" *Submitted to the 2020 ANS Annual Conference.*
[117] J.P. Gorton, S.K. Lee, Y. Lee, N.R. Brown, "Comparison of Experimental and Simulated Critical Heat Flux Tests with Various Cladding Alloys: Sensitivity of Iron-Chromium-Aluminum (FeCrAl) to Heat Transfer Coefficients and Material Properties," *Nuclear Engineering and Design*, vol. 353, p.110295, 2019.
[118] Lee, S. K., Liu, M., Brown, N. R., Terrani, K. A., Blandford, E. D., Ban, H., … Lee, Y. (2019). Comparison of steady and transient flow boiling critical heat flux for FeCrAl accident tolerant fuel cladding alloy, Zircaloy, and Inconel. *International Journal of Heat and Mass Transfer*, *132*, 643–654. doi: 10.1016/j.ijheatmasstransfer.2018.11.141.
[119] Weirs, V. Gregory & Kamm, James R. & Swiler, Laura P. & Tarantola, Stefano & Ratto, Marco & Adams, Brian M. & Rider, William J. & Eldred, Michael S., 2012. "Sensitivity analysis techniques applied to a system of hyperbolic conservation laws," Reliability Engineering and System Safety, Elsevier, vol. 107(C), pages 157-170.
[120] Hernandez, R., Folsom, C. P., Woolstenhulme, N. E., Jensen, C. B., Bess, J. D., Gorton, J. P., & Brown, N. R. (2020). Review of pool boiling critical heat flux (CHF) and heater rod design for CHF experiments in TREAT. *Progress in Nuclear Energy*, *123*, 103303. doi: 10.1016/j.pnucene.2020.103303.
[121] Sudret, B. (2008). Global sensitivity analysis using polynomial chaos expansions. *Reliability Engineering & System Safety, 93*(7), 964-979. doi:10.1016/j.ress.2007.04.002
[122] Sakurahara, T., Reihani, S., Kee, E., & Mohaghegh, Z. (2019). Global importance measure methodology for integrated probabilistic risk assessment. *Proceedings of the Institution of Mechanical Engineers, Part O: Journal of Risk and Reliability, 234*(2), 377-396. doi:10.1177/1748006x19879316
[123] Steiner, M., Bourinet, J. M., and Lahmer, T., 2019, "An Adaptive Sampling Method for Global Sensitivity Analysis Based on Least-Squares Support Vector Regression," Reliab. Eng. Syst. Saf., 183(November 2018), pp. 323–340.
[124] Popov, S. G., Carbajo, J. J., Ivanov, V. K., & Yoder, G. L. (2001). Thermophysical Properties of MOX and UO2 Fuels Including the Effects of Irradiation. doi: ORNL/TM-2000/351.

[125] Eric W. Lemmon, Mark O. McLinden and Daniel G. Friend, " Thermophysical Properties of Fluid Systems" in NIST Chemistry WebBook, NIST Standard Reference Database Number 69, Eds. P.J. Linstrom and W.G. Mallard, National Institute of Standards and Technology, Gaithersburg MD, 20899, https://doi.org/10.18434/T4D303.
[126] Thermophysical properties database of materials for light water reactors and heavy water reactors. *International Atomic Energy Agency*. IAEA-TECDOC-1496.
[127] Yamamoto, Y., Snead, M. A., Field, K. G., & Terrani, K. A. (2017). Handbook of the Materials Properties of FeCrAl Alloys For Nuclear Power Production Applications. *Nuclear Technology R&D Advanced Fuels Campaign*. doi: 10.2172/1400207.
[128] Burns, J., Hernandez, R., Terrani, K., Nelson, A. and Brown, N., 2020. Reactor and fuel cycle performance of light water reactor fuel with 235U enrichments above 5%. *Annals of Nuclear Energy*, 142, p.107423.
[129] Zinkle, S. J. et al. "Accident Tolerant Fuels for LWRs: A Perspective." *Journal of Nuclear Materials* 448 (2014) 420–435.
[130] He, S. et al. "Thermal hydraulic analysis of accident tolerant fuels for Reactivity-Initiated-Accident in PWR with different coolant channel geometries." *Nuclear Engineering and Design* 351 (2019) 131-142.
[131] Hernandez, R.; Todosow, M; Brown, N. R. "Micro heat pipe nuclear reactor concepts: Analysis of fuel cycle performance and environmental impacts." *Annals of Nuclear Energy* 126 (2019) 419-426.
[132] Wigeland, R., et al., 2014. "Nuclear fuel cycle evaluation and screening—final report," INL/EXT-14-31465 FCRD- FCO-2014-000106 (Idaho Falls, ID, Idaho National Laboratory, October 8, 2014).
[133] Brown, N. R., Ludewig, H., Aronson, A., Raitses, G., & Todosow, M. (2013). Neutronic evaluation of a PWR with fully ceramic microencapsulated fuel. Part I: Lattice benchmarking, cycle length, and reactivity coefficients. *Annals of Nuclear Energy, 62*, 538-547. doi:10.1016/j.anucene.2013.05.025
[134] Hakim, A. R., Harto, A. W., & Agung, A. (2019). Neutronic analysis of fuel assembly design in Small-PWR using uranium mononitride fully ceramic micro-encapsulated fuel using SCALE and Serpent codes. *Nuclear Engineering and Technology, 51*(1), 1-12. doi:10.1016/j.net.2018.08.007
[135] Fratoni, M., & Terrani, K. A. (2017). PWR core design with Metal Matrix Micro-encapsulated (M3) fuel. *Progress in Nuclear Energy, 100*, 419-426. doi:10.1016/j.pnucene.2017.07.009
[136] Zhao, X. G., Wysocki, A. J., Salko, R. K., & Shirvan, K. (2018). Mechanistic Modeling of Departure from Nucleate Boiling under Transient Scenarios. *International Congress on Advances in Nuclear Power Plants (ICAPP 2018) - Charlotte, North Carolina, United States of America*.
[137] Zhao, X., Salko, R. K., & Shirvan, K. (2021). Improved departure from nucleate boiling prediction in rod bundles using a physics-informed machine learning-aided framework. doi:10.31224/osf.io/hxut7
[138] Demarly, E. (2020). A new approach to predicting Departure from Nucleate Boiling (DNB) from direct representation of boiling heat transfer physics. *Submitted to the Department of Nuclear Science and Engineering in Partial Fulfillment of the Requirements for the Degree of Doctor of Philosophy in Nuclear Science and Engineering*.

VITA

Originally from Venezuela and a naturalized citizen of the United States, Richard Hernandez grew up in South Florida. After high school, he attended the Pennsylvania State University receiving a Bachelor's and Master Degree in Nuclear Engineering. Richard then chose to attend the University of Tennessee-Knoxville, to complete is doctorate degree in Nuclear Engineering. After graduation, Richard will immediately begin work for Kairos Power as a core design engineer in the development of the company's advanced reactor fluoride cooled concept.